NTNU – Trondheim
Norwegian University of
Science and Technology

Analysis and control of drilling riser dynamics in dual gradient drilling

Trygve Olav Fossum

Marine Technology
Submission date: June 2013
Supervisor: Asgeir Johan Sørensen, IMT
Co-supervisor: John Morten Godhavn, IPT
Svein Sævik, IMT
Anne Marthine Rustad, IMT

Norwegian University of Science and Technology
Department of Marine Technology

NTNU Trondheim
Norwegian University of Science and Technology
Department of Marine Technology

MASTER THESIS IN MARINE CYBERNETICS

SPRING 2013 FOR

STUD. TECH. Trygve Olav Fossum

Analysis and control of drilling riser dynamics in dual gradient drilling

Work description

Dual gradient drilling (DGD) is a method used in deep water wells to reduce the hydrostatic pressure, employing two separate fluid volumes. To separate these the riser must accommodate a device known as a rotating control device (RCD), located inline on the riser body about 300-600m below the sea surface. Using subsea pumps and a backpressure control system it is possible attain more control over the bottom hole pressure (BHP) in narrow pressure regions. By installing the subsea equipment inline with the riser, forces will at these locations be of vital importance to the operational window. These forces will be examined for the purpose of attaining a sense of the operating environment for the key components such as the sealing element. Based on this, preliminary control strategies to control the riser dynamics are proposed, where the control objective will be to minimize the riser response using the rig/vessel motion, tension and position. The main focus will be on reducing the response and equipment exhaustion at key locations around the RCD, while maintaining global riser integrity. The scope of the thesis is to investigate mathematical models and analyze behavior of the riser dynamics and control strategies for handling a dual gradient type drilling configuration.

Scope of work

- Review relevant literature on DGD systems, riser mechanics and control strategies for DP drilling operations.
- Describe the concept of the drilling setup and its main components.
- Analyze motions and crucial local forces for a modified drilling riser at a given water depth and sea environment inherit to the Gulf of Mexico using SIMA/RIFLEX.
- Modify the (2D) riser model in MATLAB/SIMULINK to incorporate rig/vessel motion and verify the model using SIMA/RIFLEX.
- Propose control strategies for the riser dynamics with the intent of reducing the response at intermediate locations along the riser.

The report shall be written in English and edited as a research report including literature survey, description of mathematical models, description of control strategies, simulation results, model test results, discussion and a conclusion including a proposal for further work. Source code should be provided on a CD with code listing enclosed in appendix. It is supposed that Department of Marine Technology, NTNU, can use the results freely in its research work, unless otherwise agreed upon, by referring to the student's work. The thesis should be submitted in two copies within June 10th.

Advisers: Professor Svein Sævik - NTNU, Adjunct Associate Professor Anne Marthine Rustad - NTNU and Professor II John Morten Godhavn - Statoil.

Professor Asgeir J. Sørensen
Supervisor

Abstract

The aim of this thesis is to investigate a dual gradient riser system, adapted for operations in the Gulf of Mexico and subjected to first- and second-order wave forces, current and rig/vessel motion.

Deep water drilling in narrow pressure zones pose several challenges for handling well pressure. Using two separate fluid volumes, in what is known as a dual gradient drilling (DGD) solution, the hydrostatic well pressure can be reduced by managing the return flow. To separate these volumes and control the mud return, the riser must accommodate a device known as a rotating control device (RCD). The RCD and the well pressure system extends the capabilities of conventional drilling schemes allowing for operations in deeper water and narrower pressure zones. The two volumes are closed off using a sealing element in the RCD, which holds the differential pressure created by the drilling system. The seal operate in a hostile environment resulting in extensive wear originating from abrasive particles, the rotating drillpipe and dynamic forces from the sheltering riser. The abrasion related to friction contact is strongly coupled with the riser and drillpipe contact and prompt the need for a closer analysis of the forces occurring between them. The riser system and RCD is therefore modelled in SIMA/RIFLEX and a dynamic analysis is carried out to obtain the lateral drillpipe/riser contact forces, indirectly finding the forces affecting the seal element. The analysis results indicate that the lateral force is below 4% of the seal element's clamp force. The force magnitude is modest and will most likely have no significant impact on the operation. However, local forces and vibrations associated with resonance can create undesirable effects, which over time can lead to fatigue damage of the RCD and its subcomponents.

Submerged equipment will be sensitive to range of resonance phenomena originating from the rig motions, second-order wave forces, current and vortex induced vibrations. This will encourage a review of the local dynamics and the potential use of riser control. Motivated by this, a finite element model is developed in Matlab/SIMULINK to study this in more detail. In order to detect resonance related vibrations, a modal decomposition model is formulated based on the finite element model. Using the modal model, a weighted estimate of the eigen frequencies active in the response can be provided to evaluate the resonance properties of the riser. To obtain a better understanding of the riser system and the control potential, a dynamic analysis of the models is carried out, focusing on low frequent rig/vessel motion. Both models are throughly verified using the commercial program RIFLEX, to ensure the sufficient accuracy. Inspired by the results from the analysis, control strategies based on manipulation of the resonance properties (modal control) of the riser are examined, applied to a riser management system framework. The purpose of modal control is to increase safety margins and the operational economy, e.g. by reducing the time spent suspended because of seal element exchange or the risk for well head fatigue. Four different strategies based on manipulation of tension and position are proposed. Followed by a qualitative evaluation of the practical aspects, indicating that setpoint chasing and tension control are the most effective and attainable strategies available.

The main contributions in this thesis are assessment of the lateral contact force associated with a deep water pipe-in-pipe dual gradient riser in the Gulf of Mexico, the development and verification of a extensive riser model using Matlab and SIMULINK, and the formulation of modal riser control for resonance vibrations in deep water drilling risers.

Sammendrag

Formålet med denne oppgaven er å studere kontroll og respons av en modifisert stigerørsløsning tilrettelagt for operasjoner i Mexico Gulfen, der krefter fra bølger, strøm og riggbevegelse opptrer.

Dypvannsboring i trange trykksoner er en stor utfordring. Ved å bruke to separate fluidvolumer i en såkalt "dual gradient-løsning" kan det hydrostatiske trykket i brønnen reduseres ved å manipulere den statiske borevæskesøylen. For å separere disse volumene trengs en spesiell type utstyr lokalisert på stigerøret dypt under havoverflaten, omtalt som et "rotating control device" eller RCD. Denne utvidelsen gjør at man kan borre på dypere vann og manøvrere nedihullstrykket på en mer forsvarlig måte. For å holde tett mellom væskesøylene brukes en stålforsterket gummiforsegling. Dette tetningselementet holder også på et diffrensialtrykk som brukes til å trykksette/trykkavlaste nedihullstrykket, i tillegg er elementet svært utsatt for slitasje og horisontale krefter. En modellering av stigerørssystemet er derfor blitt utført i programmet SIMA/RIFLEX, dernest er en kraftanalyse av RCD og tetningselementet gjennomført. Simuleringene indikerer at kreftene mindre enn 4% av den allerede påsatte forseglingskraften. Noe som antyder at kreftene ikke vil ha noen innflytelse på det operasjonelle plan. Det faktum at utstyret befinner seg på stigerøret i området 400m under havoverflaten gjør at resonansvibrasjoner kan oppstå.

Over tid kan kombinasjonen av krefter og vibrasjoner gi utmattingsskader, noe som tilsier at disse lokale bevegelsene og kontrollpotensialet må studeres nærmere. I denne hovedoppgaven er det derfor foreslått en konseptuell tilnærming for utvidelsen av stigerørssystemer til å detektere og kontrollere uønskede responser. En elementmodell og en modal dekomposisjonsmodell er utviklet i Matlab/SIMULINK for å se nærmere på dette. En sensitivitetsanalyse er gjennomført med modellene for å studere stigerørets følsomhet ovenfor resonans knyttet til lavfrekvent toppbevegelse av rigg på et 2500m stigerør. Ved å utnytte en spesiell egenskap hos den modale modellen er det mulig og estimere de aktive egensvingningsmodene i bevegelsen og bruke disse som vurderingsgrunnlag i kontrollsystemet. Ved å forandre resonansegenskapene til stigerøret, eller aktivt fjerne bevegelsene kan sikkerhetsmarginene økes og den operasjonelle effektiviteten holdes høy. Fire forskjellige kontrollstrategier er utviklet med dette som utgangspunkt. En kvalitativ evaluering av disse er gjennomført i lys av hva som er praktisk mulig og effektivt. Vurderingen peker på at dynamisk forfølgelse av optimal posisjon og kontroll av toppstrekk er de mest hensiktsmessige fremgangsmåtene.

Hovedbidragene i denne hovedoppgaven er fastsettelsen av kreftene som virker på tetningselementet, utviklingen av en ekstensiv stigerørsmodell i Matlab/SIMULINK, samt utviklingen av kontrollstrategier for håndtering av lokale bevegelser på stigerør brukt i dypvannsboring.

Acknowledgement

This report represents my master's thesis which has been carried out from January to June 2013 at the Department of Marine Technology at NTNU. The subject was put forward by John Morten Godhavn, Professor II at NTNU and Statoil ASA and Asgeir Sørensen, Professor at the Department of Marine Technology.

I would like to thank Asgeir J. Sørensen who has been an excellent supervisor throughout the project, and provided vital insight during the process. I would also like to thank my co-supervisors Anne Marthine Rustad, Svein Sœvik and John Morten Godhavn for discussion and important guidance. Thanks also to Andreas Amundsen have contributed with valuable feedback and specific advice on use of RIFLEX.

To all the friends I have made in Trondheim and the guys in office A 1.027, I want to thank you for the good times we have spent together.

Trygve Olav Fossum
Trondheim, June 10, 2013

Nomenclature

Abbreviations

ARA	Acoustic Riser Angle
BAB	Backarc Basin
BHA	Bottom Hole Assembly
BHP	Bottom Hole Pressure
BOP	Blowout Preventer
BPMPD	Back Pressure Managed Pressure Drilling
BPP	Back Pressure Pump
DP	Dynamic positioning
ERA	Electronic Riser Angle
FEM	Finite Element Method
FP	Fracture pressure
GOM	Gulf of Mexico
HSE	Health safety and environment
HTHP	High Temperature High Pressure
IOR	Increased Oil Recovery
MODU	Mobile Offshore Drilling Unit
MPD	Managed Pressure Drilling
NCS	Norwegian Continental Shelf
NPT	Non-Productive Time
PP	Pore pressure
PWD	Pressure While Drilling
RCD	Rotating Control Device
ROP	Rate Of Penetration
TD	Total Depth

TTR	Top Tensioned Riser
UBD	Under Balanced Drilling
VIV	Vortex Induced Vibrations

Greek Symbols

κ	Curvature
ν	Kinematic viscosity
ω_n,ω_{n_i}	Natural frequency
ρ	Density
ξ_i,ξ_{n_i}	Relative damping

Roman symbols

C_D,C_d	Drag coefficient
C_M	Added mass coefficient
C_{global}	Global damping matrix
E	Young's modulus of elasticity
EI	Bending stiffness
F	Force
f_0	Eigen frequency in still water
f_{sh}	Vortex shedding frequency
g_g,g	Gravitational constant
H_s	Significant wave height
I	Second moment of inertia
K_{bulk}	Bulk modulus for mud
K_{global}	Global stiffness matrix
k_{pip}	Spring contact stiffness for pipe-in-pipe
L,L_r	Riser length

m	Mass per unit length
M_m	Moment
M_{global}	Global mass matrix
n,N	Number of elements
p_0	Atmospheric pressure
Q	Shear force
q_i	Time dependent modal weighting parameter
Re	Reynolds number
St	Strouhal number
T	Tension (effective)
T_t	Top tension
T_{p_n}	Natural period
T_{sh}	Vortex shedding period
u	Horizontal displacement
V	Volume
$\mathbf{A}$	System matrix
$\mathbf{B}$	Input matrix

Contents

List of Figures

List of Tables

Chapter 1

Introduction

Estimates from the Norwegian Oil and Energy Department suggest that as much as 60% of the total oil and gas resources available on the Norwegian continental shelf (NCS) are still unexploited [32]. The level of activity in the Norwegian petroleum industry is high, with focus on improved oil recovery (IOR) from producing fields, development of newly discovered resources and exploration activity. The emphasis on IOR is growing with the demand for utilizing the remaining resources and maximizing the economic potential on the NCS. Operating in greater depth and harsher environments has become vital in order to confront the decline in production. New oil fields and environments give rise to new challenges, which only can be resolved trough determinated research and innovation. To reach reservoirs previously proved inaccessible or too expensive the development and implementation of new technologies must be the main ambition of the petroleum sector.

Innovative technological solutions and high standards have always been the competitive advantage for the Norwegian oil industry. New and exciting drilling schemes like dual gradient drilling (DGD) and managed pressure drilling (MPD), both which in the last decade has experienced great attention, can be part of this solution. Already used in Brazil and the Gulf of Mexico, these technologies are becoming relevant for application in the Norwegian petroleum sector. The prospective advantage can be substantial for handling complex pressure regimes in demanding fields. New technology solutions emerging from the basis of this drilling perspective will play a vital role in meeting the challenges of future.

1.1 Motivation

The riser stretches from the seafloor to the top joint connection on the rig and is the key to drilling in ultra deep water (Figure 1.1). In effect the riser extends the well head to the rig and is essential for the safety and integrity of the wellbore. Conventional drilling systems use equipment situated on the seafloor or topside. In the development of modern drilling schemes, new solutions utilize subsea equipment situated at intermediate locations along the drilling riser. Submerged equipment attached to the riser well below the surface will be sensitive to a range of resonance phenomena, originating from the rig/vessel motions, waves, current and vortex induced vibrations (VIV), leading to large motions along the riser. This poses a problem for fatigue life and riser integrity which can lead to costly repairs and increased non productive time (NPT). Riser stability at these locations are unexamined territory and prompt the need for both local and global control strategies to manage the associated dynamics at these locations. Extending the riser control to attenuate dynamic behaviour can help reduce damage and fatigue, and additionally increase the safety and operational margins. The available control domain is limited to rig/vessel position and top tension, calling for elegant solutions to be found.

Figure 1.1: Marine drilling riser deployment in the North Sea (statoil.com).

1.2 Previous work

Since the early days of offshore drilling, the dynamics of the drilling riser have been the subject of many research papers. The focus have largely been on monitoring and controlling the riser angle magnitudes in numerous applications, from shallow to deep water. The objective have largely been on increasing the time available for drilling and to maximize safety margins. Similar concepts have been studied in the field of pipe trenching, steel catenary risers and flexible risers. Commercial systems monitoring the riser response are available today, such as the Riser Management System (RMS) delivered from Kongsberg Oil and Gas Technologies (SeaFlex) [33].

In Ervik [10], analysis and monitoring of drilling risers on dynamic positioned (DP) vessels are studied. Investigating the drilling riser exposed to currents, waves and vessel motions using SIMA/RIFLEX, a software program developed at MARINTEK for static and dynamic analysis of slender marine structures [34]. Several environmental and operational cases are examined featuring different sea states, currents, vessel motions and extreme scenarios connected with DP drilling operations. The aim is to increase the operating window and avoid unnecessary disconnection.

Rustad [35] has thoroughly studied control of top tensioned risers (TTP), where the main focus have been on avoiding collisions between adjacent risers. A mathematical model of the riser system is developed in Matlab/SIMULINK and cross-referenced and verified with RIFLEX. The number of elements needed to maintain a desired level of accuracy is also investigated.

How, Ge and Choo in [20] has studied active control of flexible marine risers, and the reduction of forced vibrations under a time-varying distributed load, such as currents. They propose a robust control system, based on partial differential equations using boundary control. Numerical simulations have been carried out to verify the effectiveness of the approach presented.

Sørensen, Leira, Strand and Larsen in [47] present a hybrid dynamic positioning controller derived on the basis of the riser angle offset. The aim is to reduce the riser bending stress and angle magnitudes at the well head and the vessel connection point. Implementing optimal setpoint chasing, using specific key parameters, the target position is obtained as a function of these, surpassing the conventional control strategy based on manual setting the desired position. Reducing the dynamic response and improvement of the riser structural integrity is achieved.

Hoen and Moe in [18] has presented a general method for modal decomposition of time series in structural vibration response. The modal decomposition method is driven by the riser measurements and rig/vessel response data only, using no a priori FEM model. The method is applied to measurements of vortex induced vibrations of deep water risers in operation.

Toellefsen, in [49] gives a introduction to the general principles in managed pressure and dual gradient drilling. Additionally, pressure models, riderless mud returns, pressure control devices, choke and backpressure pumps are discussed. The economic aspects of drilling operations are also presented.

1.3 Main contributions

The main contributions found in this thesis are summarised here.

- In Chapter 3, a FEM and modal decomposition model for a riser system exposed to current and rig motion is developed, using Matlab and SIMULINK.
- A comprehensive pipe-in-pipe (PIP) model of a 2500m drilling riser is established in Chapter 5 using SIMA/RIFLEX, featuring a heave compensated wire-line vessel connection representation.
- Using the SIMA/RIFLEX model from Chapter 5 a dynamic analysis of the riser and drillpipe is carried out to evaluate the lateral contact forces between the riser wall and drillpipe. Using the result obtained in the dynamic analysis, the operational environment for the internal rise components are evaluated.
- The mathematical system model from Chapter 3 is verified both statically and dynamically by the commercial software SIMA/RIFLEX in Chapter 4. Additionally, a brief sensitivity analysis is conducted to investigate the effect of the number of elements on the model accuracy.

- Using the mathematical model verified in Chapter 4, an resonance analysis of the drilling riser is performed. Based on the simulation results, four different control strategies are formulated in Chapter 6, to incorporate control of the resonance properties of the riser, relevant for submerged equipment attached to the riser.

1.4 Outline of thesis

The outline of the thesis is as follows:

Chapter 2	describes the fundamentals of managed pressure drilling , dual gradient drilling and backpressure managed pressure drilling.
Chapter 3	focuses on the basic theory essential for implementing a mathematical model for a marine drilling riser. From the riser itself to the physical environment.
Chapter 4	covers the validation and sensitivity analysis of the mathematical model developed in Chapter 3 using SIMA/RIFLEX as the model verification software.
Chapter 5	includes the modelling and dynamic analysis of a pipe-in-pipe drilling riser model at a deep water location in the Gulf of Mexico using the commercial FEM software SIMA/RIFLEX.
Chapter 6	gives a brief introduction to riser dynamics, relevant for control application. The chapter also includes the simulation and evaluation of the mathematical model and cover a extension of a riser management system to incorporate control of the resonance properties of the riser.
Chapter 7	contains a finishing discussion of the completed work.
Appendix A	includes a simplified calculation of the lateral contact force between the riser and drillpipe.
Appendix B	shows the simulation results from the SIMA/RIFLEX simulation in Chapter 5
Appendix C	includes the supplementary harmonic simulation results from the low frequent dynamic simulation in Chapter 6.
Appendix D	gives an overview and description of the relevant result and model files associated with the SIMA/RIFLEX simulations.
Appendix E	covers use of the Matlab/SIMULINK code and the overview of the FEM and modal model files.

Chapter 2

MODU drilling systems

This chapter will give a shot introduction to a few modern drilling systems used on deep water mobile offshore drilling units (MODU), which typically include marine units like semi-submersibles and drillships.

As the oil industry is moving into greater water depths to access new resources, the operating scope of conventional methods needs to be expanded. Complex pressure regimes in the reservoirs, narrow pressure windows in combination with high temperatures, push towards more elaborate drilling schemes like dual gradient drilling (DGD) and managed pressure drilling (MPD). Both which in the last decade have gathered significantly more attention from the oil industry, due to complex challenges. Also the necessity for improved oil recovery (IOR) is growing with the demand for utilizing the remaining resources and maximising the economic potential. Performance, safety and increased operation time are also key elements in favour of implementing these systems. A wide range of complex processes today are controlled by automatic control systems, providing accuracy and safety. Drilling operations continue to get more intricate as the pressure margins decrease, due to reservoir depletion and depth. Fields previously considered unaccessible due to high pressure and high temperature (HPHT) are now becoming more workable, seeing that the technology can handle the practical problems connected to deep water and high precision pressure control. With increased focus on health safety and environment (HSE) operations on the drill floor have been entrusted to special robots controlled by the driller. The cost reduction aspect is also becoming more relevant as the labour cost on the Norwegian Continental Shelf (NCS) are, compared to other oil producing countries, more than 40 % higher [6]. The progress of automatisation will continue to strive towards more "intelligent drilling systems", and this includes more elaborate control systems for pressure handling.

2.1 Managed pressure drilling

Managed pressure drilling can be fully automated or partially operated by the driller, dependent on the operation and the required accuracy related to the bottom hole pressure (BHP). MPD control have largely been based on control of the choke to control well pressure [39]. Modern well control advance towards multivariable control of pumps, chokes and draw works to increase the precision of the control system. MPD systems control the hydrostatical pressure in the well, so that the pressure can be kept within a required operating window, that can be as small as $p_0 \pm 2.5$bar in extreme situations. Accuracy is vital, as the consequences of either loss, where mud is forced/lost into the formation, or a kick can be devastating. A kick is a term used to describe uncontrolled influx and incidental flow in the well. The primary objective of MPD is to reduce the drilling risks, cost, increase accuracy in narrow pressure margins and enhance drilling safety. Sensor quality and accuracy is important. Density measurements, pressure measurements and flow measurements are

transmitted back and used in hydraulic models predicting relevant parameters utilizing historical data, pressure model and statistical information. Transmissions from equipment located behind the drill bit, a part of the drillbit support package known as the bottom hole assembly (BHA) send crucial information using pulse telemetry, and is updated every 20-30 seconds. Transmission is dependent on the mud flow, and is not available at low and zero mud rate.

2.2 Dual gradient drilling

The International Association of Drilling Contractors (IADC) defines DGD as follows:

> *"Two or more pressure gradients within selected well sections to manage the well pressure profile."*

The first dual gradient technology was patented by Howell in 1975 [21], but it was not before 2001 a similar concept termed subsea mudlift drilling had its first successful field trial [40]. DGD can be classified as a tool to control the riser fluid level, and is considered a variation of managed pressure drilling. The ability to control the BHP as precise as possible within the "drilling window" and gain hydrostatic pressure allowance is the motivation for implementing these drilling arrangements. The "drilling window" is a term which is used to describe the supportable pressure zone in which drilling operations can proceed. This zone is defined by the pressure region between the pore pressure (PP) and fracture pressure (FP), which in Figure 2.2 can be seen as the region between the two "pressure lines". Exceeding the fracture pressure will often result in loss to the formation, meaning that drilling mud will be forced into the rock formation. Drilling with pressure below the pore pressure, often referred to as under balanced drilling (UBD), can result in a flow of material from the formation into the mud return channel. Safety and reliability are important factors, and vital to a successful drilling operation. The flexible attribute using two gradients allow the rig to reduce the influence of the static head present in a single gradient configuration. A gradient is the term used for the development of hydrostatic pressure in a given volume. The two gradients used in DGD are separated into two volumes using what is known as a rotating control device (RCD), more details about the RCD will be given in Section 2.3.

The gradient above the RCD contains a static riser fluid volume, typically water or base oil. This is illustrated in Figure 2.1 where we can see the difference between a single gradient versus a dual gradient setup. The static case operates with only one H, while the dual gradient case have one H_a for the static volume in the gradient above the subsea pump, and one H_b for the gradient containing the returning mud.

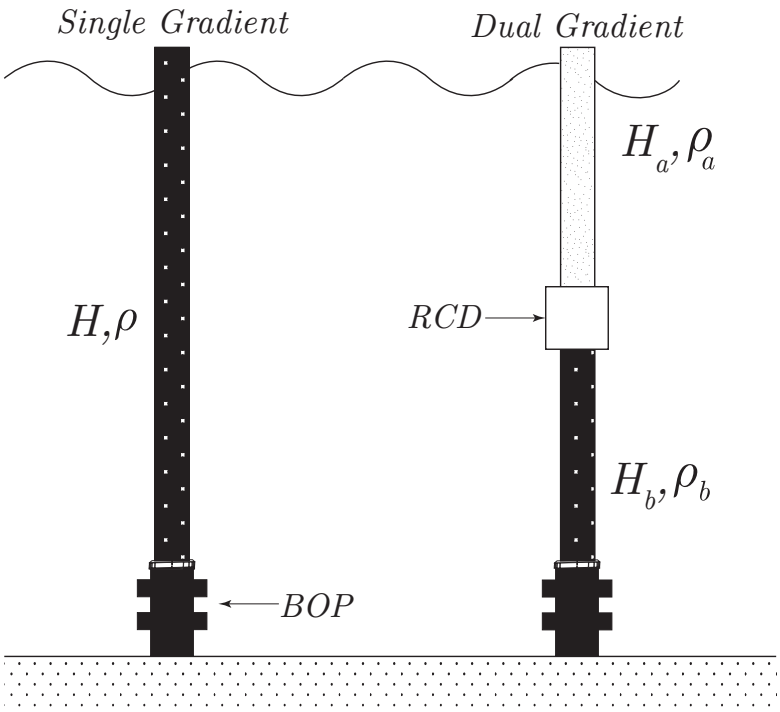

Figure 2.1: Single gradient and dual gradient configuration.

Two pressure formulations of the BHP are given based on the configuration in Figure 2.1.

$$\text{Single gradient BHP [Pa]} = (\rho g H), \tag{2.1}$$

$$\text{Dual gradient BHP [Pa]} = (\rho_a g H_a + \rho_b g H_b), \tag{2.2}$$

where ρ is the fluid density, g is the gravitational constant, H is the length of the well bore from the rig floor to the deepest point in the well, ρ_a is the first gradient fluid density, ρ_b is the second gradient fluid density, H_a is the first gradient volume height, and H_b the second gradient volume height. In (2.1) and (2.2) the expression for the hydrostatic contribution form the internal fluid to the BHP is established in a single and dual gradient well bore. The hydrostatic head imposed in the single gradient is less flexible compared to the dual gradient well.

The location of the gradient separation point, i.e. the location of the RCD, is based upon several requirements, one being that the "gained" pressure clearance is about 30-40bar. This correspond approximately to the friction pressure in the well, which is the pressure needed in order to a keep the mud volume in motion. Finding a suitable location for the RCD, given the operational requirements, is one of the questions this thesis will try to answer. Assuming a pressure increase of 0.1bar/m, portions a space designated for the dual gradient equipment 300 - 400m below the mean sea surface. However using more robust equipment, this region can be extended to 600m if necessary. Since the tools are attached to the drilling riser, considerations regarding the riser

dynamics and control prospects at these points has to be considered. Deeper water means higher hydrostatic pressure at the seabed resulting in a more compact sediment formation, due to the weight of the hydrostatic column of water. As a consequence, the pressure window is reduced. From a hydraulic perspective, dual gradient drilling effectively moves the rig closer to the mud line. The hydrostatic head imparted on the well by the mud and cuttings contained in the marine riser is more controllable. Illustrated in Figures 2.2 and 2.3, the effect of removing the hydrostatic water pressure is shown. In Figure 2.2, the hydrostatic pressure felt by the well (the red lines) stretch from the sea surface, while in Figure 2.3 the lines start from the sea floor, implying a smaller hydrostatic pressure column. Since the mud hydrostatic pressure is moved closer to the seabed in Figure 2.3 it is possible to use fewer casing sections, select a more suitable shoe location (the casing section end point) and have a more flexible mud program for the well. This will reduce the need for various casing sizes and different BHA - tools fitted for the section. Also the drilling window is "expanded", due to the fact that pressure and mud parameters can span a larger range, consequently making pressure navigation between the PP and FP more simple.

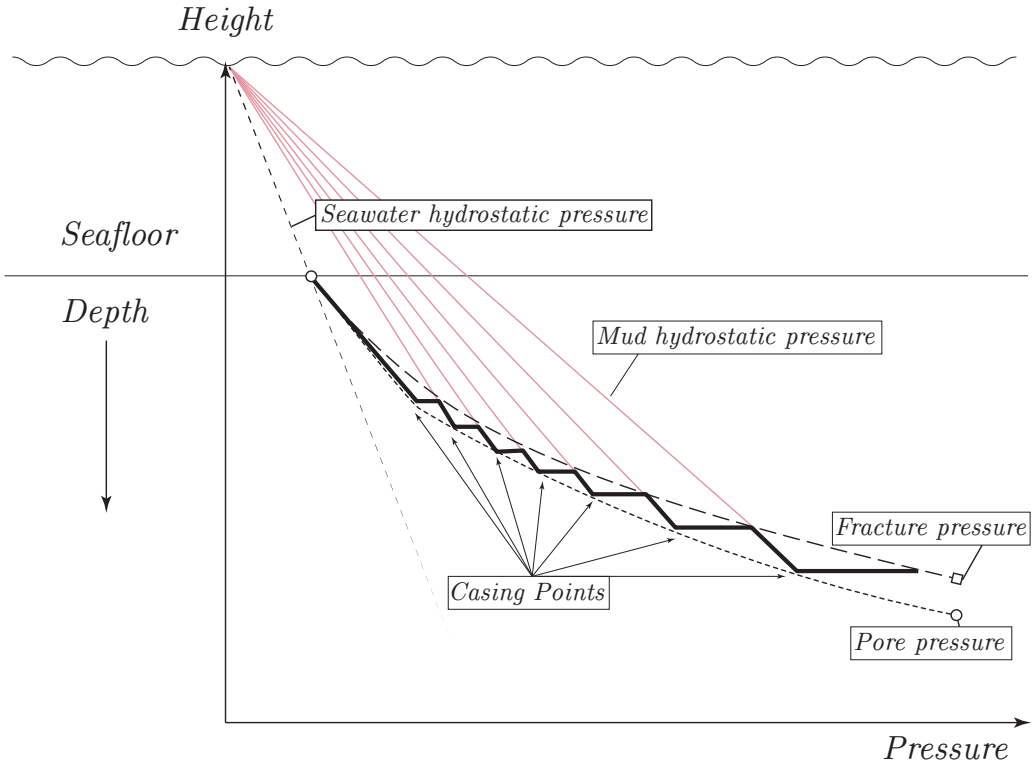

Figure 2.2: Single gradient wellbore.

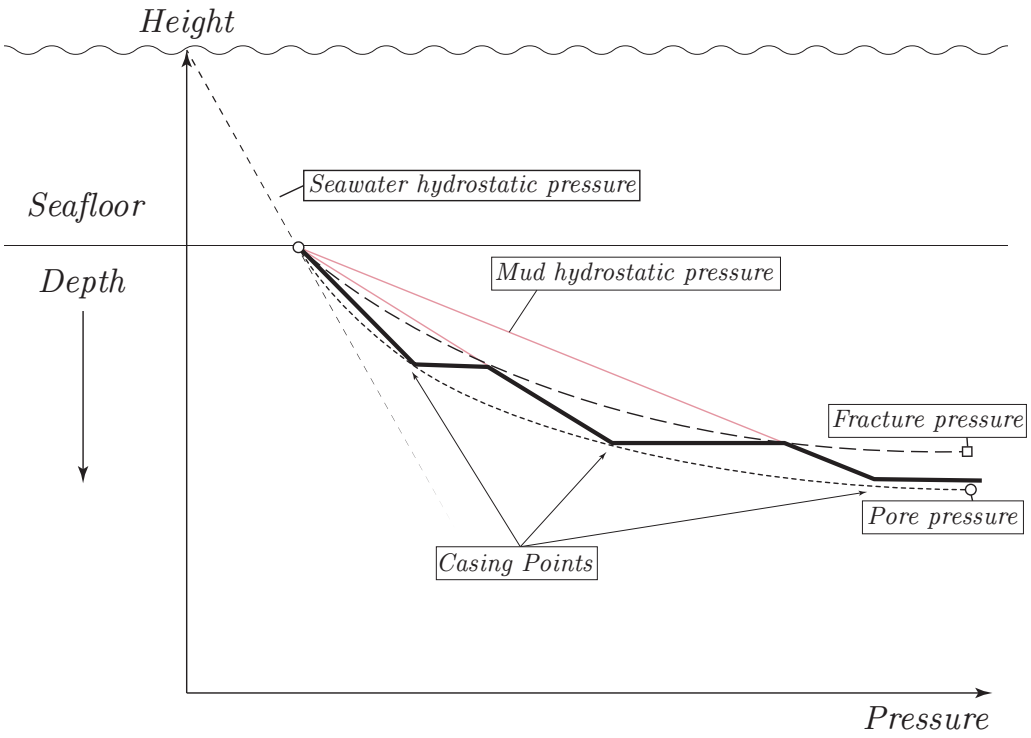

Figure 2.3: Dual gradient wellbore.

The consequence of implementing a dual gradient drilling scheme provides several advantages, extracted from [40]:

- Improved well construction.
- Fewer casing points and optimal shoe placement.
- Reduced mud volume, fewer mud density changes and steel consumption.
- Increased production.
- The possibility to utilize heavier mud and reduce the non productive time (NPT).
- Improve cuttings transport, hole cleaning and reduce issues related to wiper trips.
- Increased safety and cost.

Since the technology is relative new, there are several concepts not subjected to rigorous examination thus far, but the development have come a long way from the earliest concepts.

2.3 Backpressure managed pressure drilling

The drilling system concept used in this thesis is a combination of DGD and MPD and is known as "backpressure MPD" or BPMPD, but will for simplicity be referred to as just DGD in the remaining sections. The conceptual topography of the system is illustrated in Figure 2.4. BPMPD is founded on a dual gradient solution, where the riser volume is separated into two different gradients separated by a RCD. The first riser gradient is filled with a fluid derived from the present mud type, e.g. base oil or seawater, the second is the immediate drilling mud. One key concept here is that, in contrast to a conventional internal mud riser system, the arrangement have control over the differential pressure separating the gradients. The differential pressure is held in place by the seal element, a reinforces rubber component clamped around the drillpipe. Control of the pressure is handled by the MPD system, keeping the BHP constant subjected to an alternating wellbore (the drilled hole) environment. As a result the drilling window is more "open" with increased operating margins. This setup also features a separate mud return line operated using subsea mud handling equipment, this return line can be seen to the left in Figure 2.4. An important distinction from conventional drilling schemes is the circumstances related to connection operations (extending or shortening the current drillpipe assembly). During connection in conventional drilling the hydrostatic head is kept constant, but you will have a pressure drop since the circulation is halted. This pressure drop originates from the additional pressure associated with circulation friction. If the first riser gradient is unable to pressurize, the level in the riser must be filled to compensate for the lost pressure fall. The rig pump must therefore ramp down while the subsea pump ramps down faster in order to build up volume on the return side. This is time-consuming and may take about 15-20 minutes. The advantage with this modified scheme using a closed volume in the well below the RCD, is that the same pressure can be obtained in 1-2 minutes, owing to the fact of compressibility. The closed volume can be pressurised extremely fast, since the fluid is incompressible.

Not all BPMPD systems work the same way, either back pressure, circulation or other mud gradients can be controlled. A basic BPMPD system is designed to manage backpressure while keeping the BHP constant, requiring a rotating control device (RCD) and a choke valve [13]. An automated backpressure pump might be used to maintain controllability of the back pressure even when not circulating through the well. In addition to this, choke redundancy, flow meter for kick detection and mud gas separator are crucial components [13]. As long as the flow is large enough, the choke is the main tool for adjusting the pressure. However, in the opposite case, if the flow stops, the choke has to close. If the choke is not closed fast enough (in the case of a immediate loss), potential loss of backpressure can occur. This practical problem is solved by using a backpressure pump (BPP) capacity to recover control over the system.

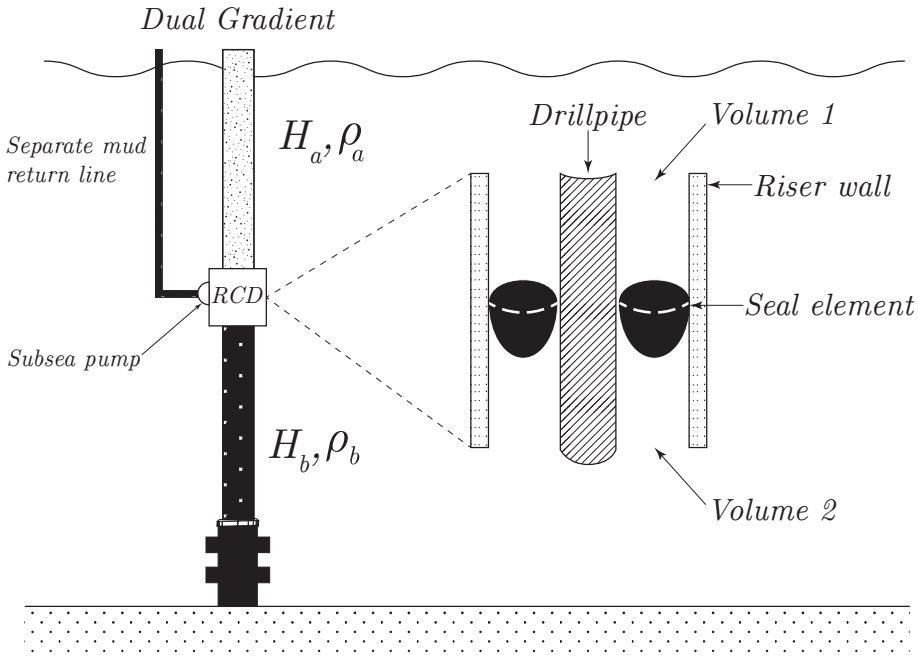

Figure 2.4: Dual gradient configuration with RCD.

2.4 Drilling system components

Dual gradient drilling and MPD require a set of components neither dimensioned nor present in a conventional drilling setup. Extensive requirements for subsea equipment with regard to durability and robustness, are important as the system will be subjected to substantial pressure, wear and temperature. Downtime will be expensive and repair will demand a comprehensive, dangerous and costly operations. Therefore such systems becomes complicated, and large investments are related to the design process and implementation operation.

2.4.1 Subsea rotating control device (RCD)

Rotating control devices have been used on land based rigs and at offshore platforms, their application on MODUs is limited, but similar systems have been used [49]. The RCD has two main tasks; function as a barrier between the two gradient sections, and secondly divert the returning mud flow. Both high- and low-pressure control devices exist. The DGD configuration used in this thesis uses a RCD located 300-400m below the mean sea surface inline with the riser. At the heart of the RCD sits a sealing element, which in Figure 2.5 is highlighted in red color. Figure 2.5 (a) show the drillpipe segment penetrating the seal with no joint, (b) show the drillpipe joint connection going through the seal, while (c) show the system topography. The seal have one job; serve as a pressure containing barrier that separates the static volume above the RCD and the volume containing return mud. Additionally, the seal supports the drillpipe in lateral direction,

maintaining it at the centre. The seal has to contain a substantial differential pressure between the two compartments while the drillpipe is rotating and tripping. Tripping is the act of pulling the drillpipe out of the hole or replacing it in the hole. Most vendors offer RCD units that holds about 344bar (5000psi) when the drillpipe is static and approximately 172bar (2500psi), when rotating [49]. Since the sealing element obviously is the part subjected to the most severe forces, the ability to change sealing elements without a complete rig down is an important feature. Estimates suggest that the seal may have to be changed as often as every day, depending on the operation [1]. There exist RCD designs with one or multiple sealing elements and with several pressure compartments [45]. The RCD used in this thesis accommodates one sealing element.

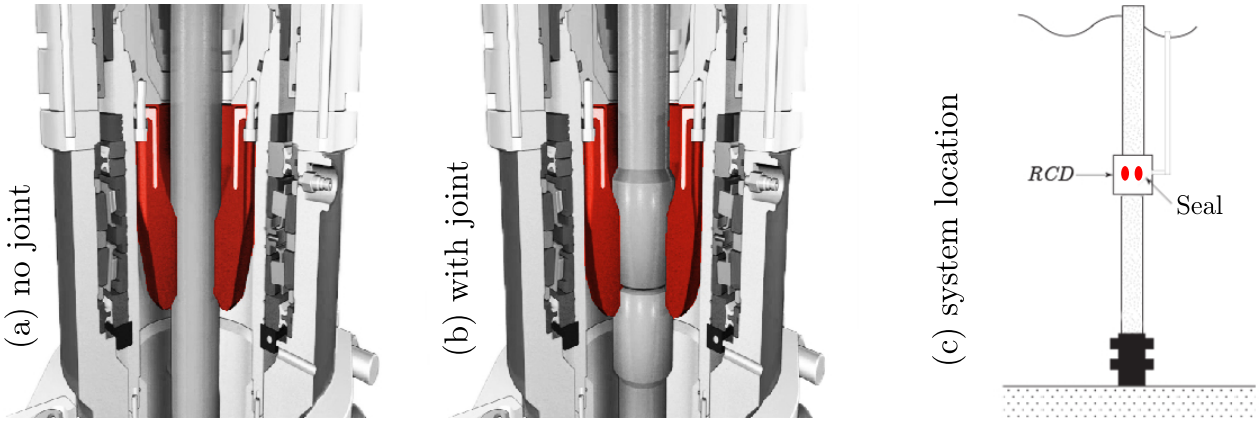

Figure 2.5: Rotating control device (RCD) with sealing element (Schlumberger 2012).

2.4.2 Subsea pump and choke manifold

In conventional drilling practice, the mud returns are transported up through the riser annulus using the rig pump at the topside. This implies that the pressure applied on top need to match the distance the mud has to be carried, counteracting the wellbore friction pressure. This "transport pressure" is consequently included in the BHP. This restricts the mud type and the casing program. By introducing an separate subsea mud return pump located either at the seabed or further up on the riser, the transport and the excess friction pressure can reduced, minimizing the load on the rig pump. The flow diverter, choke manifold and subsea pump have control over the return side of the mud system.

2.4.3 Pressure control system

In order to control the BHP a pressure control system is put into service, following the relation

$$BHP = \delta_1 g h_1 + \delta_2 g(h - h_1) + clq + \triangle P_{rcd}, \tag{2.3}$$

where g is the gravitational constant, h_1 is the distance from the drill floor to the RCD unit (indicating the end of the first gradient), h is the distance from the RCD to TD (total depth), c is

the friction coefficient, l is the length traveled by the fluid connected with friction pressure, q is the volume flow and $\triangle P_{rcd}$ is the differential pressure over the sealing element. The purpose of the control system is to keep the BHP as constant as possible, in extreme narrow banded operations fluctuations can be in the region of $p_0 \pm 2.5$bar.

The advantage with the modified scheme using a static volume and backpressure MPD, is that the same pressure can be obtained in 1-2 minutes, owing to the fact of compressibility. The subsea pump which is connected below the sealing element ramps down faster than the rig pump, but because we now have a closed volume the compression will allow us to gain the lost pressure faster. To illustrate this we can study the bulk modulus for typical mud types:

$$K_{bulk} = V\frac{dP}{dV} \tag{2.4}$$

where K_{bulk} is the bulk modulus, V is the volume of the fluid and $\frac{dP}{dV}$ is the pressure rate. For example, assume that the typical bulk modulus for standard mud is 10000bar. Using the relation above, taking $dP = 10$bar, an annulus volume of $V = 100m^3$ and solving for dV. It follows that, in order to increase pressure by 10bar it is necessary to add $0.1m^3$ to the annulus. Using a pump with a pump rate of 2000lpm (litres per minute), increasing the pressure 10bar will take about 3s. This example tries to illustrate the advantage of using a closed system in contrast to a "open" system, benefiting from compression to build pressure.

2.4.4 Sealing element

This thesis will study the lateral forces acting on the seal form the sheltering drilling riser, for that reason a brief introduction to the seal composition is provided.

Conventional seals are made of steel-reinforced rubber elements enclosing the drillpipe, allowing all of the annular well fluid to be diverted to the flow line or choke manifold [1]. The use of multiple rubber sealing elements provides redundant protection against a sudden large leak and allows a higher working pressure. A variety of rubber materials can be used to provide optimal protection for the fluid composition and temperature expected in the return flow. The shape of the sealing element can be selected to cause the closing forces pressing the seal against the drillpipe (clamp force) to be assisted by wellhead pressure [1]. Seals used in drilling operates exclusively in hostile environments containing fracturing rocks. Among all mechanisms, leading to eventual seal degradation, the clamp force and wear resulting from abrasive particles from the surrounding drilling fluid is considered the primary contribution factors in most cases. Therefore, to effectively improve seal durability, it is important to understand the seal abrasive wear process. The seal installed in the RCD, referring to Figure 2.5, will be subjected to a severe abrasive environment and need to be substituted regularly, and can be a major source of downtime. Since the seal is located inside the RCD, riser dynamics will play a role in determining how the seal will interact with the drillpipe. Obviously the abrasion related to friction contact will be minimal when the drillpipe is centred in the riser, where the lateral forces are smallest. This will be relevant for control systems, which may be used to reduce there forces.

Chapter 3

Riser model theory

This chapter will focus on the basic theory essential for implementing a mathematical model for a marine drilling riser, from the riser itself to the physical environment.

3.1 Riser types

Marine drilling risers can be subdivided into *low-pressure* and *high-pressure* drilling risers. Drilling risers differ from production risers in the sense that drilling risers are used for drilling and embody the rotating drill string. Production risers are for pipes transporting oil, and can be divided sub-types as bundled risers, flexible risers and top tensioned risers (TTR) [37]. The standard drilling riser today is the low-pressure drilling riser, open to atmospheric pressure at the top end. Thus, the internal pressure can never exceed that owing to the hydrostatic head created the drilling mud, visible in Figure 2.1. Drilling risers are made up of riser joints, typically $15 - 23$m long. The riser consists of one main tube, usually 21in diameter, and a number of peripheral lines running along the side. These lines are connected to the control panel of the blow out preventer (BOP), namely the kill, choke and boost lines. Buoyancy modules are added to the riser segments to reduce the weight in water. The top part and lower part of the riser line are left bare, to reduce the hydrodynamic loads and module cost, which increase with the depth due to the specific buoyancy material having to withstand more pressure [37]. The riser is connected to the vessel via the heave compensating system, the connection point is a ring suspended by steel wire cables. These cables keep the riser steady while the rig is moving, by adjusting the payout length (refer to Figure 3.1). The slip joint attend to the movement of the physical connection.

The riser used in this thesis is a standard a low-pressure marine drilling riser with parameters found in Table 5.2 Chapter 5. These specifications can vary depending on the design conditions used. E.g. the mud density is constantly changed during a drilling operation, but is assumed constant in this thesis.

3.2 Riser environment

The Gulf of Mexico (GoM) is chosen as the conceptual environment location for the drilling riser. The following sections will give a brief introduction to the structural riser theory, followed by a short summary of the local metocean factors important for deep water locations in the GoM.

3.2.1 Hydrodynamic forces

The riser is subjected to a time-varying distributed load due to subaquatic ocean current, resulting in forces acting on the slender body. These dynamic forces imply a time dependent solution and they introduce inertia loads throughout the structure. The current forces studied in this thesis are applied to the riser model through *Morison's Equation*. Hydrodynamic loads on small-diameter submerged objects such as risers are almost exclusively calculated using Morison's equation. Morison's equation is based on experimental results and is considered empirical. The horizontal force per unit length of the moving cylinder can, according to Morison's equation be written as given in [37] and [11]

$$F_{hydro} = \frac{1}{2}\rho C_D D_e |u - v|(u - v) + \rho A_{exposed}\dot{u} + (C_M - 1)\rho A_{exposed}(\dot{u} - \dot{v}). \tag{3.1}$$

where ρ is the fluid density, C_D is the drag coefficient ($C_D = 1$ for a circular cylinder), D_e is the effective diameter, in our case equal to the outer diameter D, C_m=(C_M-1) is the added-mass coefficient where C_M is typically close to 2, hence C_m is 1, $A_{exposed}$ is the external riser cross-sectional area, u is the current velocity and v is the cylinder velocity. The force is considered to be a resultant of three dynamic pressure fields; the static, the dynamic and the pressure filed resulting from the disturbed flow relative to the riser, found in the last term. Due to the slender structure the riser will gain speed faced with substantial current, and thus the relative speed becomes important, limiting the drag force. Vortex induced vibrations (VIV) may cause some variation for C_m [35], due to the induced structure oscillations. However, for application in this thesis such effects are considered to be insignificant.

3.2.2 Top tension and effective tension

The riser have no capacity to support its own weight. Therefore tension must be applied to help reduce the apparent weight felt by the riser structure. Since the perceived weight increases along the riser length the tension applied at the top will decrease accordingly. The top tension should therefore be larger than the effective weight of the riser, in order to avoid buckling. The heave compensation system is designed to keep the top tension constant and transfer the load from the risers to the platform. Heave compensators are usually divided into three groups; passive, active and a combination of these [35]. Most passive systems rely on pneumatic-hydraulic solutions, and do not require any input of energy during operation. There are two types of active heave compensators: Wire-line and N-line (pistons) tensioner systems [35]. The N-line system use cylinders connected in a ring and hydraulics to control the stroke. Wire-line connects to the tension ring with wires and control the length by extending auxiliary cylinders, an example of a wire line connection and tension ring can be seen in Figure 3.1. The tension ring is a massive steel ring connecting the riser to the rig. The ring is suspended using the heave compensation system, keeping the ring and riser still when the rig is moving vertically.

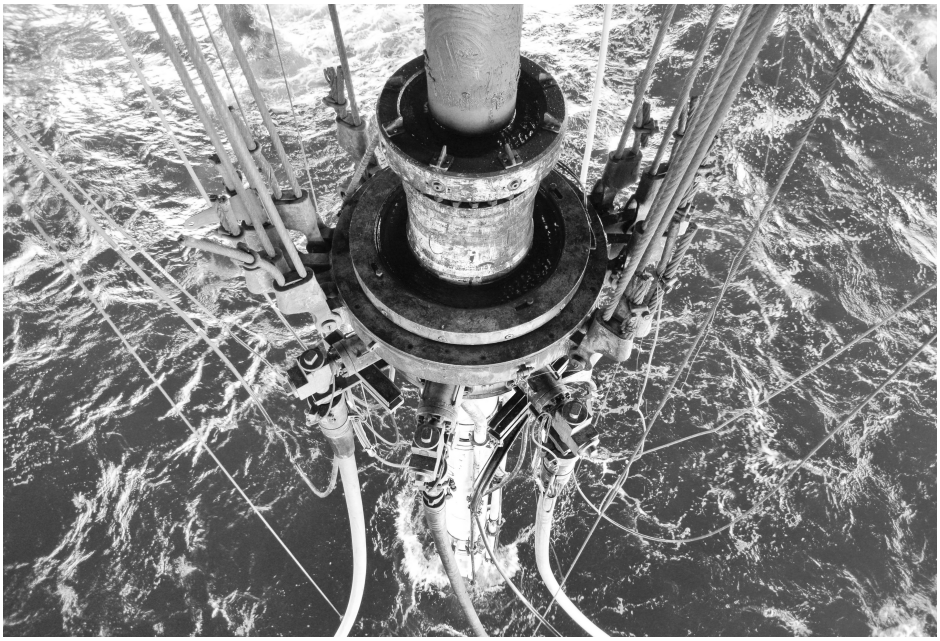

Figure 3.1: Riser, rig connection point and tension ring.

3.2.3 Upper and lower angle magnitudes

The top and bottom angles for each riser could be measured by inclinometers, either electronic riser angle (ERA) or acoustic riser angle (ARA) measurements [35]. In the industry additional bending stiffeners are used to limit large rotations in these connections. Depending on the given definition and safety protocol, the top and bottom angles should not exceed an upper limit of $\pm 2^{\circ}$, where deviations larger than $5^{\circ} - 8^{\circ}$ may be fatal [47].

3.2.4 Local environmental parameters for the Gulf of Mexico

The conceptual riser location used in this thesis is a typical deep water location in the GoM. The GoM is a mediterranean sea with a maximum depth reaching approximately 3700 m deep. The U.S. Energy Information Administration consider that 23 % of the United States total offshore petroleum production comes from the GoM (2012).

Geology

The Gulf of Mexico is classified as a backarc basin (BAB), meaning that the seafloor formed over an active subduction zone (a tectonic plate moves under another, at a tectonic boundary), in the late Jurassic time, about 150 million year ago [42]. It contains several large shelves: West Florida Shelf, Texas-Louisiana Shelf and the Campeche Platform. The deep central part of the Gulf is called the Sigsbee Deep or Sigsbee Abyssal Plain. Widespread salt deposits are present through much of the area, and the salt structures act to create subsurface traps (oil trapping geological mechanism) and topographic features on the seafloor [41].

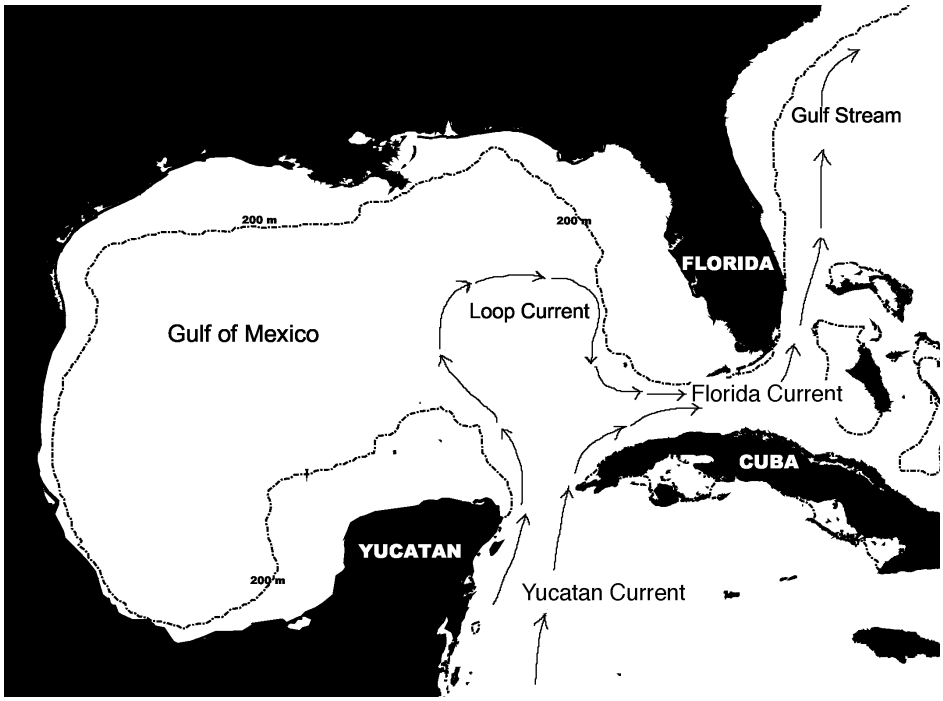

Figure 3.2: Map over the Gulf of Mexico and the local currents.

Local currents

The Gulf of Mexico has two oceanic connections, the Atlantic Ocean (through the narrow Florida Strait) and to the Caribbean by the Yucatan Channel, illustrated in Figure 3.2. Large currents are present in the Gulf of Mexico, the Loop Current is the the clockwise flow that extends northward into the Gulf of Mexico and joins the Yucatan Current and the Florida Current generating large current velocities and an asymmetric current profile [19]. These currents can reach current velocities as high as $2.5\frac{m}{s}$ [17]. Nevertheless, the environmental conditions in the Gulf are considered relative mild, compared to the harsh conditions experienced in the North Sea. In the North Sea, storms are frequent and result in more stringent design requirements. The Gulf of Mexico might, however, experience periodic hurricanes during the summer months posing a potential treat to offshore facilities. Still these hurricanes are infrequent and several years can go by without a single major hurricane. Hurricanes can induce inertial high-current regions which can reach speeds as high as $1.1\frac{m}{s}$, they are fortunately short lived and decay once the storm has passed.

3.3 Mathematical model concepts

The partial differential equation (Equation (6.1)) which governs the static and dynamic response of a riser can not be solved analytically, therefore a numerical model is developed based on the finite element method (FEM), later to be reformulated in a state space model. The FEM model uses a stiffness matrix and a mass matrix to give a finite element (FE) representation of the problem. The stiffness matrix will have an elastic and geometric component. The elastic component accounts for the axial and bending stiffness. The geometric stiffness will depend on the changes in global geometry and the corresponding stiffness generated by the effective tension. For large deformations the geometric stiffness can change significantly. However, this effect will be left out in the model. Using a constant geometric stiffness is deemed sufficient for capturing the relevant physics for this thesis. More details on this topic will be covered in Section 6.1 Chapter 6.

The FEM model will be reformulated into a state space model for facilitating implementation in SIMULINK and be applicable to control purposes. In addition a modal decomposition model is developed, based on decomposition/transformation of the FEM model. Containing vital information of the fundamental modes present in the response, this details can later be used to detect and control resonance vibrations in the riser. Modal decomposition makes it possible to study the load effect on each mode and the resulting behaviour dynamics. The decomposition decouples the partial differential equation using an eigenvector/mode shape based transformation matrix. The true displacement can be found by using the transformation back to the original coordinate system.

3.3.1 Beam element formulation

The model uses beam elements defined in a two dimensional model with four degrees of freedom (DOF). Using two translational DOFs in both ends of the element, one displacement u and one rotation r as seen in Figure 3.3.

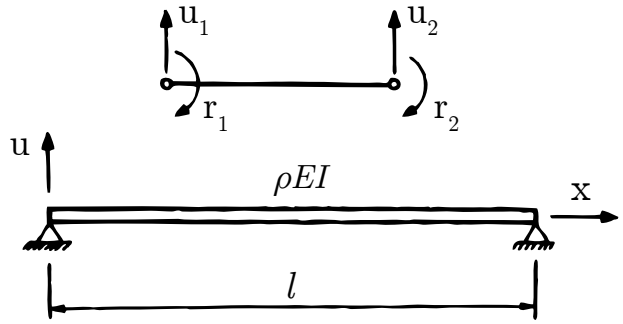

Figure 3.3: Beam element with four degrees of freedom.

The displacement vector w for this beam will consequently be formulated as,

$$w = [u_1, r_1, u_2, r_2]^T, \tag{3.2}$$

where u_1 and u_2 is the transverse displacement for the two node ends on the element, while r_1 and r_2 are the rotations at each node. All the riser elements is modelled as a simply supported beam with uniformly distributed mass/consistent mass. Since the riser is a slender marine structure it has considerable local bending stiffness. Globally however, tension supply stiffness against the lateral forces. At deep water the length is large and hence the riser will behave more flexible, meaning the rise will behave more like a cable and the tension and geometric stiffness will be more important. Since the geometric stiffness is constant, some deviation in the lateral resistance will be expected.

3.3.2 System mass matrix

Each element has a mass matrix ($\mathbf{m}_i$) defined on the local reference frame by

$$\mathbf{m}_i = \frac{\rho l A}{420} \begin{bmatrix} 156 & -22l & 54 & 13l \\ -22l & 4l^2 & -13l & -3l^2 \\ 54 & -13l & 156 & 22l \\ 13l & -3l^2 & 22l & 4l^2 \end{bmatrix}, \tag{3.3}$$

where ρ is the density of the steel used in the riser, A is the cross sectional area of the riser, and l is the length of each element. The mass of the internal fluid ($\mathbf{m}_{fl}$) must also be included in the "dry" mass (not considering submerged weight), so in practice we combine $\rho l A$ to m_{dry}. The influence of added mass ($\mathbf{m}_{am}$) for a circular cylinder in lateral x-direction is equal to the displaced water volume [46]. The total mass matrix for each element is consequently a sum of the riser mass ($\mathbf{m}_{rm}$), internal fluid and the added mass.

$$\mathbf{m}_i = \mathbf{m}_{rm} + \mathbf{m}_{am} + \mathbf{m}_{fl}. \tag{3.4}$$

The full, global mass matrix is then obtained as,

$$M_{global} = \begin{bmatrix} \mathbf{m}_{11}^1 & \mathbf{m}_{12}^1 & & & & \\ \mathbf{m}_{21}^1 & \mathbf{m}_{22}^1 + \mathbf{m}_{11}^2 & \mathbf{m}_{12}^2 & & & \\ & \mathbf{m}_{21}^2 & \mathbf{m}_{22}^2 + \mathbf{m}_{11}^3 & & & \\ & & & \ddots & & \\ & & & & \mathbf{m}_{22}^{n-1} + \mathbf{m}_{11}^n & \mathbf{m}_{12}^n \\ & & & & \mathbf{m}_{21}^n & \mathbf{m}_{22}^n \end{bmatrix}. \tag{3.5}$$

The size of the global mass matrix is $2(n+1) \times 2(n+1)$, where n is the number of elements.

3.3.3 System stiffness matrix

The local stiffness matrix consists of two terms, the elastic stiffness $\mathbf{k}_{elastic}$ and the geometric stiffness $\mathbf{k}_{geometric}$. The geometric stiffness matrix includes the effective axial tension T_t acting on the particular element. The elastic stiffness matrix works in the axial direction, whereas the geometric stiffness in the lateral direction [35].

$$\mathbf{k}_{elastic} = \frac{2EI}{l^3}\begin{bmatrix} 6 & -3l & -6 & -3l \\ -3l & 2l^2 & 3l & 2l^2 \\ -6 & 3l & 6 & 3l \\ -3l & l^2 & 3l & 2l^2 \end{bmatrix}, \tag{3.6}$$

$$\mathbf{k}_{geometric} = \begin{bmatrix} \frac{6T_t}{5l} & -\frac{T_t}{10} & -\frac{6T_t}{5l} & -\frac{T_t}{10} \\ -\frac{T_t}{10} & \frac{2T_t}{15} & \frac{T_t}{10} & -\frac{T_t l}{30} \\ -\frac{6T_t}{5l} & \frac{T_t}{10} & \frac{6T_t}{5l} & \frac{T_t}{10} \\ -\frac{T_t}{10} & -\frac{T_t l}{30} & \frac{T_t}{10} & \frac{2T_t l}{15} \end{bmatrix}, \tag{3.7}$$

where EI is the bending stiffness of the element, l is the length of the element and T_t is the top tension. The resulting stiffness matrix for each element is obtained by adding the elastic and geometric contributions: $\mathbf{k_i} = \mathbf{k_g} + \mathbf{k_e}$. Due to the effective tension the T_t value is different for each element. E.g. the top-tension is larger for the first element than for the second, $T_{t_1} > T_{t_2}$. Therefore the T_t value has to be calculated for each element before being allocated to the global stiffness matrix K_{global}:

$$K_{global} = \begin{bmatrix} \mathbf{k}_{11}^1 & \mathbf{k}_{12}^1 & & & & \\ \mathbf{k}_{21}^1 & \mathbf{k}_{22}^1 + \mathbf{k}_{11}^2 & \mathbf{k}_{12}^2 & & & \\ & \mathbf{k}_{21}^2 & \mathbf{k}_{22}^2 + \mathbf{k}_{11}^3 & & & \\ & & & \ddots & & \\ & & & & \mathbf{k}_{22}^{n-1} + \mathbf{k}_{11}^n & \mathbf{k}_{12}^n \\ & & & & \mathbf{k}_{21}^n & \mathbf{k}_{22}^n \end{bmatrix}. \tag{3.8}$$

3.3.4 System damping matrix

The damping for a submerged riser will consist of contribution from structural damping and hydrodynamic damping, resulting from both radiation and viscous dissipation of energy [35]. In this thesis the damping matrix for a tensioned steel riser is based on proportional *Rayleigh Damping*, assumed proportional to the global stiffness matrix [28].

$$C_{global} = \alpha_2 K_{global}, \tag{3.9}$$

where C_{global} is the damping matrix, α_2 is the Rayleigh damping coefficient and K_{global} is the global stiffness matrix. The Rayleigh coefficient can be found from simple equations if the total damping is known at a specified frequency [35]. Assuming that the structural damping to be 2% of the critical damping at the eigenperiod $T_{load} = 15s$, the damping coefficient can be found using the relation:

$$\xi_s = \frac{c}{c_{cr}} = \frac{1}{2}\alpha_2\omega = \frac{1}{2}\alpha_2\frac{2\pi}{T_{load}}, \tag{3.10}$$

where ξ_s is the relative damping of the riser structure and $\frac{c}{c_{cr}}$ is the critical damping relation. The damping coefficient is fond to be $\alpha_2 = 0.095$. Since Rayleigh damping is linear, the damping will be smaller at lower frequencies, meaning that hydrodynamic damping will be dominating.

3.3.5 State space modelling

The state space procedure used in this section is motivated by the theory and approach used in [18]. The FEM model is reformulated into a state space model for facilitating implementation in SIMULINK and be applicable to control purposes. The model is only valid in two dimensions (x and $z-$plane), neglecting the y-dimension. A state space representation is a mathematical model of a physical system which, depending on the system, has a set of inputs and output state variables related by first-order differential equations [4]. The idea came from state-variable description of differential equations, a re-writing of a high order differential equation into first order form. E.g.

$$\ddot{y} + a_1\dot{y} + a_2 y = bu, \tag{3.11}$$

taking $x_1 = y$ this can be written as

$$\dot{x}_1 = x_2, \tag{3.12}$$
$$\dot{x}_2 = -a_2 x_1 - a_1 x_2 + bu, \tag{3.13}$$

rewriting this into matrix form we get the formulation

$$\begin{aligned} \dot{x} &= Ax + Bu, \\ y &= Hx + Du, \end{aligned} \tag{3.14}$$

where A is the system matrix, B the regressor matrix, C the output matrix, D the feed forward matrix, u is the input vector and x is the system state vector. The second order differential equation written in this form is reformulated into a first order differential equation which can be easily solved using numerical integration. This provides a convenient approach to model and analyze systems with multiple inputs and outputs. The dynamic response of a marine riser can generally be modelled by a second order differential equation of dimension $2(n+1) \times 2(n+1)$, as given in [24]:

$$M\ddot{x} + C\dot{x} + Kx = BF(t), \tag{3.15}$$

where M denotes the system mass matrix ($2(n+1) \times 2(n+1)$), $2(n+1)$ being the number of DOFs, C is the damping matrix ($dofs \times dofs$), K is the stiffness matrix ($dofs \times dofs$), $\ddot{x}$,$\dot{x}$ and x are the node parameters ($dofs \times 1$), B is the regressor vector / input matrix ($dofs \times 1$) which maps the external forces input to the system and finally we have $F(t)$ ($1 \times dofs$) is the dynamic time-varying force acting on the system. Note that since all the elements in the equation are matrices the total system will be a linear multiple degree of freedom system. A typical multi degree system, similar to the one used in this thesis, is presented in Figure 3.4.

Using the matrices from the beam element formulation in Section 3.3.1 and the force definition from Morison's equation in Section 3.2.1, the following relations are made for implementation into the state space representation in Equation (3.15),

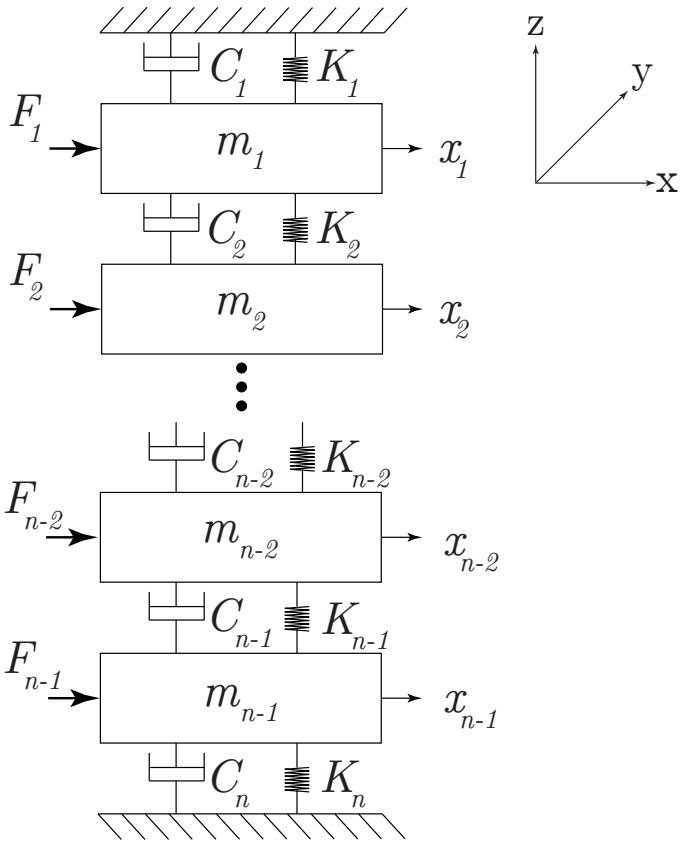

Figure 3.4: Multi degree system example.

$$M = M_{global}, \tag{3.16}$$
$$K = K_{global},$$
$$C = C_{global}, \tag{3.17}$$
$$F = F_{hydro},$$

where F is the $(1 \times dofs)$ force vector and F_{hydro} is the hydrodynamical inertia and drag forces calculated from Morrion's equation.

Using the definitions in Equation (3.16) in the second order model for the riser response, found in Equation (3.15), the first order state space for the riser can be formulated as follows

$$\dot{x} = \begin{bmatrix} 0 & I \\ -\frac{K}{M} & -\frac{C}{M} \end{bmatrix} \begin{bmatrix} x \\ \dot{x} \end{bmatrix} + \begin{bmatrix} 0 \\ \frac{1}{M} \end{bmatrix} F, \tag{3.18}$$

where I is the identity matrix. The state space is reformulated into a more compact from as,

$$\dot{x}(t) = Ax(t) + BF(t). \tag{3.19}$$

Where the definitions above are still valid and $x(t)$ is the state vector, formulated as

$$x(t) = [w_1(t)\ w_2(t)\ ...\ w_{n-1}(t)\ w_n(t)]^T, \tag{3.20}$$

where w_i is the local element displacement vector, defined in Equation (3.2). Equation (3.19) is comparable to the formulation in (3.14). The system matrix size will be given as $(2dofs \times 2dofs)$ and the input matrix size will be given as $(2dofs \times dofs)$. Note that the H matrix in (3.14) is set to the identity matrix, to obtain both the nodal positions and velocities and the D matrix is set to zero.

3.3.6 Modal decomposition

Solving the state space numerically for a large system with many states is computationally time consuming. For a riser system with 50 elements with two translations at both ends, this amounts to 102 distinct states and a 204×204 system matrix. To clarify this an overview over the system matrices and their size provided:

Model parameter	**Size**
Elements (n)	50
DOFs / States used by state space (x)	$2 \cdot (n+1)$
M_{global}, K_{global}, C_{global}	$(dofs \times dofs)$
System matrix (A)	$(2dofs \times 2dofs)$

Table 3.1: Model parameters and size.

The system matrix (A) will have coupling between equations since the global system matrices are included. Coupling means that the solution of one equation will depend on the solution of another equation. Finding a transformation that make the equations uncoupled, so that we obtain diagonal mass, damping and stiffness matrices similar to a single degree of freedom system, this will simplify the problem greatly since the equations can be solved independent of each other. The process of deriving the system response by transforming the equations of motion into an independent set of equations is known as *modal analysis* or modal decomposition.

Modal decomposition, also know as modal superposition is a method for calculating the response of a continuous system using a weighted sum of the fundamental modes shapes [28]. The response can be written as,

$$u(x,t) = \sum_{i=1}^{n} \Phi_i(x) \cdot q_i(t) = \Phi q, \tag{3.21}$$

where $u(x,t)$ is the response at location x at time t, Φ_i is the fundamental mode shape and q_i is the time dependent weighting parameter for each mode. These weighting values are decisive for the contribution for each mode and therefore serves as an distinct interpretation of the total response. These factors will be of importance in Chapter 6 where their usefulness is discussed more in detail. Note that these values are not constant, but change over time.

The fundamental mode shapes of a structure can be found by solving the eigenvalue problem

$$(-\omega^2 M + K)\Phi = 0, \tag{3.22}$$

where K is the global stiffness matrix, M is the global mass matrix and Φ is the fundamental mode shapes. Solving Equation (3.22) is the same as solving the equation of motion with no damping or excitation force. The solution gives the mode shape vector Φ as,

$$\Phi = [\Phi_1 \ \Phi_2 \ \Phi_3 \ .... \ \Phi_n]. \tag{3.23}$$

From Equation 3.21 it flows that

$$q = \Phi^{-1} u. \tag{3.24}$$

By using the orthogonality conditions, a more useful relationship between u and q can be established. Multiplying with $\Phi_i^T M$ to obtain

$$\begin{aligned} \Phi_i^T M u &= \Phi_i^T M \Phi q, \qquad (3.25)\\ &= \Phi_i^T M \Phi_i q_i, \\ &= \bar{m}_i q_i, \\ q_i &= \frac{1}{\bar{m}_i} \Phi_i^T M u. \qquad (3.26) \end{aligned}$$

Using the transformation from Equation 3.26 into the equation of motion and multiplying with Φ_i^T the following expression is obtained

$$\Phi_i^T M \Phi \ddot{q} + \Phi_i^T C \Phi \dot{q} + \Phi_i^T K \Phi q = \Phi_i^T F(t), \tag{3.27}$$

Which is the decoupled system where q is the decoupled coordinate. u and q are connected with the matrix transformation

$$u(x,t) = \Phi q(t), \tag{3.28}$$

to get back to original coordinate system.

The basic concept of modal decomposition is illustrated in Figure 3.5.

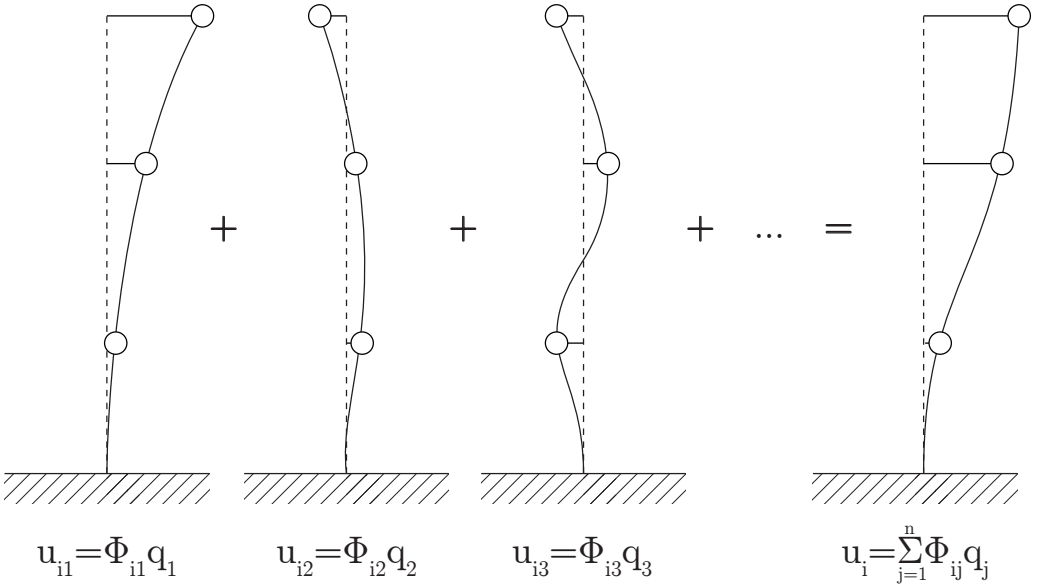

Figure 3.5: Modal composition principles.

Chapter 4

Model verification

Based on the theory in Section 3.3 a simplified FEM based and a modal decomposition model have been built inside Matlab/SIMULINK to study riser behaviour. This section aim to verify and compare the FEM based model and modal model with the commercial riser software SIMA/RIFLEX developed by MARINTEK. The models will be compared to SIMA/RIFLEX simulations in a static and dynamic verification scenario. For clarification, the phrase "Matlab models" will in this thesis include both the FEM model and the modal model. RIFLEX performs static and dynamic analysis of slender marine structures and is built upon the graphical interface SIMA [34]. The principal communication between SIMA and RIFLEX is illustrated in Figure 4.1.

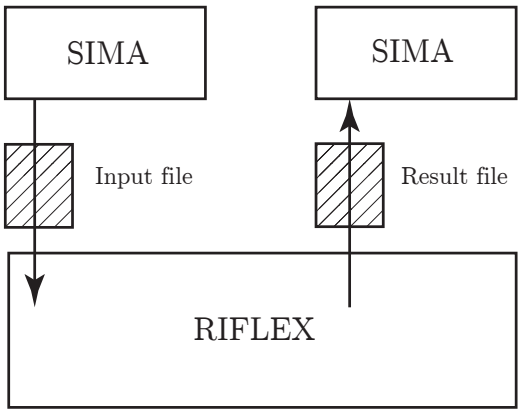

Figure 4.1: SIMA and RIFLEX program flow.

The FEM and the modal model should give reasonable comparability of the global geometry of the riser for both static and dynamic response. The main motivation is to describe and predict the behaviour of the riser and extract information concerning the selected points of interest. In this thesis, mainly the top, bottom and intermediate location around the RCD are of importance. Hence the entire riser should be extensively investigated.

Apart from being physically correct the model must also be convenient and manageable, meaning that:

- It can be implemented in Matlab without the need for more computing power than an ordinary laptop.
- The simulations should be as fast as possible, without sacrificing too much accuracy in the calculations.

- It should be easy to reconfigure and apply to new situations. It should be noted that models first and foremost should describe the fundamental phenomenon they are set up to investigate, but the underlying mathematical model should still be robust and flexible to new applications.

- The model complexity should be kept low when possible, but ensure not to "over simplify" physical factors of great importance.

Keeping this in mind the most crucial simplifications for the FEM model can be found in Table 4.1. The most significant approximation is the number of elements, which directly affect several other model parameters such as curvature. Due to its importance, this effect is discussed in more detail in Section 4.4.

Type	**Description**
Number of elements	The model uses a limited number of elements compared to a typical structural analysis, $n_{FEM} = 50$ and $n_{SIMA} = 1251$.
Hydrodynamic coefficients	The model assumes the riser to behave as a circular cylinder. E.g. drag coefficient is set to $C_d = 1.0$ in both the FEM model and in SIMA.
Vortex Induced Vibrations	VIV effects are neglected, and can potentially exert unmodelled dynamics of the riser.
Effective tension	Updating the effective tension (geometrical stiffness) due to geometrical configuration is performed in SIMA, but not in the Matlab FEM model.
Torsion	The additional effects connected to torsion is not taken into account in the Matlab FEM model.
Internal flow	The fluid inside the riser annulus have been modelled to be static. The mud density is also kept fixed.
Non-linear effects	Non-linear material behaviour is not accounted for, e.g. creep effects in steel.
Damping	The model use Rayleigh damping and neglect viscous damping effects.
3-D effects	The riser is only modelled in 2-D, so the influence of cross flow and other 3-D related hydrodynamics are neglected. As a consequence the loads are unidirectional.
End conditions (top and bottom)	The ends of the riser model are free to rotate, which is conservative in regard to angle magnitudes. Comparing this to the physical termination points where hang up systems and BOP provide additional stiffness to the system, and hence smaller angles.

Table 4.1: FEM model simplifications overview.

The modal model will inherit all these defects, since it is extracted from the FEM model. In addition it will have some additional shortcomings due to the decomposition method necessary for its creation. The most important limitations of the modal model can be found in Table 4.2. The most significant simplification factor to consider is the number of modes used to describe the deflection shape. In [38] and [27] five modes are used to describe riser behavior for riser in deep water, based on data collected from four instrumented risers, carried out as a part of the Norwegian Deepwater Program (NDP). The same number of modes is applied in this thesis. Using five modes results in a very compact system and state space representation using only ten state variables to represent the riser, independent on the number of elements used. This means that the system matrix is of size (10×10), compared to the FEM system matrix (204×204).

Type	**Description**
Number of modes	The modal model uses a limited number of modes to describe the deflection shape. In this thesis the number of modes used is five following the results from [38] and [27].
Curvature	The curvature will increase with the order of the mode, hence a small excitation of the mode will give large contributions to the curvature.

Table 4.2: Modal model simplifications overview.

4.1 Boundary conditions

The boundary conditions are the constraining values consistent throughout time of the differential equation, which in our case refers to Equation (3.15). These conditions provides a set of additional restrains for the riser top and bottom connection. Two different support conditions are used to verify the model, associated with the static and dynamic verification scenarios. They are illustrated in Figure 4.2. Both the static and dynamic riser are hinged at the bottom, while at the top the dynamic condition is movably hinged and the static which is hinged. It should be noted that the boundary conditions are the same in SIMA/RIFLEX and Matlab.

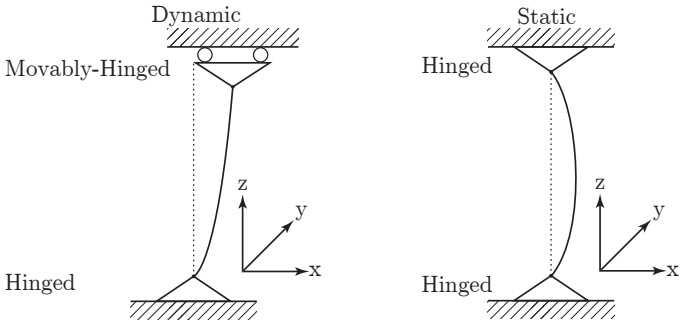

Figure 4.2: Boundary condition for riser support conditions (idealized).

The two idealized cases above follows the definitions given in Table 4.3 and 4.4.

Node location	**Test scenario**	**Condition description**
Top	Static	Restricted to translation in the horizontal plane, but free to rotate around the y-axis. Referred to as Hinged (H).
Bottom	Static	Restricted to translation in the horizontal plane, but free to rotate around the y-axis. Referred to as Hinged (H).
Top	Dynamic	Allowed to move in the horizontal plane and rotate around the y-axis. Referred to as Movably-Hinged (MH).
Bottom	Dynamic	Restricted to translation in the horizontal plane, but free to rotate around the y-axis. Referred to as Hinged (H).

Table 4.3: Description of boundary conditions.

The guidelines from Table 4.3 are presented again with the nodal specific support condition. Notice both conditions have the riser fixed in z-direction at the bottom.

Node location	**Test scenario**	**X**	**Y**	**Z**	**RX**	**RY**	**RZ**
Top	Static	Fixed	Fixed	Free	Fixed	Free	Fixed
Bottom	Static	Fixed	Fixed	Fixed	Fixed	Free	Fixed
Top	Dynamic	Free	Fixed	Free	Fixed	Free	Fixed
Bottom	Dynamic	Fixed	Fixed	Fixed	Fixed	Free	Fixed

Table 4.4: Boundary conditions overview.

4.2 Quasi-static verification with constant current

First a *quasi-static verification* is done using a hinged-hinged (H-H) riser subjected to a uniform current. In deep water, the riser will behave more like a cable due to the weakening flexible rigidity (EI), and hence the geometric stiffness will be of considerable importance. The rigidity will become weaker due to the tension decreasing with depth, towards the bottom section of the riser. This assumption is confirmed by [35] and [38]. Since the Matlab models have a constant geometric stiffness, hence making them less rigid faced with large deformations, it is expected that the Matlab models will have slightly more horizontal displacement than the SIMA/RIFLEX result. This assumption is confirmed in Figure 4.3 which indicates a good correspondence between SIMA/RIFLEX and the Matlab models. The Matlab models differ with 0.2m, compared to SIMA/RIFLEX at the maximum deflection point where the correspondence is worst. The deviation is about 37% of the riser diameter.

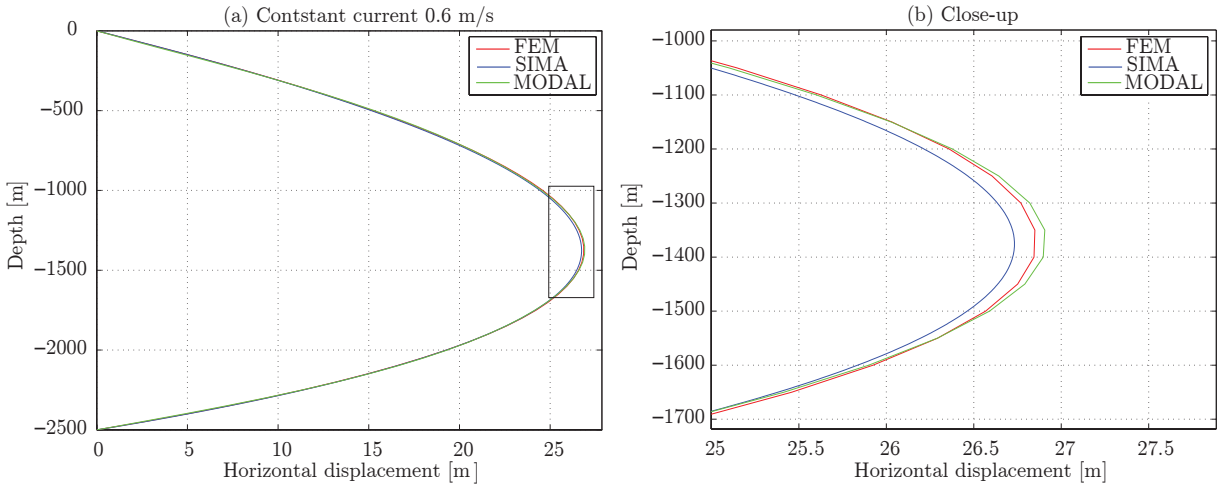

Figure 4.3: Static verification of 0.6m/s uniform current at 2500m water depth.

The point of maximum deflection is around -1370m, which is below the halfway point of the riser. The reason this deflection is asymmetric is due to the effective tension, as mentioned before. Effective tension is the reduction in tension form the top to bottom owing to the relationship between weight, buoyancy and top tension. Plotting the tension distribution for SIMA/RIFLEX and FEM and modal model we obtain the graph in Figure 4.4. Notice that the graph has two "break points" at the top and bottom, due to buoyancy modules. Buoyancy modules are added along the riser length to increase the buoyancy and therefore reduce the need for large top tension in deep waters. Adding buoyancy modules will increase the hydrodynamic diameter, and hence the contribution from waves and current. The contribution from these forces are not welcomed at the top and bottom, and therefore excluded from the first 100m of the riser and the last 50m section. The effective tension for the two models agree very well with an error in the range of 10kN.

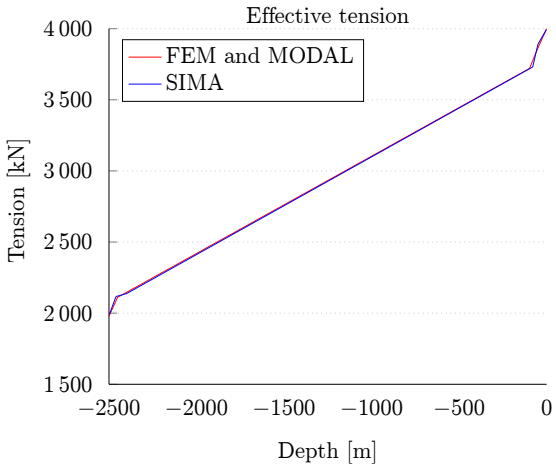

Figure 4.4: Verification of effective tension

4.3 Dynamic verification of response

A dynamic verification scenario is investigated using a movably-hinged, hinged riser, subjected to a harmonic load. The harmonic load is formulated as,

$$F_{harmonic} = 20000 \cdot sin(\frac{2\pi}{T_{period}}t), \tag{4.1}$$

where t is the simulation time and T_{period} is the load period. The load period used in this test scenario was chosen to be at the second resonance period or eigen period, $T_{period} = T_2 = 57.6$s. The load amplitude was set to 2tons or 20kN, which would simulate a slow-drift motion in surge with offsets around 4-6m, which correspond to data used in [11].

Recalling that the boundary conditions set for the dynamic verification scenario now allows for the top end of the riser to move freely in the horizontal plane, a simulation is conducted with the prescribed force at the top node. The most important simulation parameters are presented in Table 4.5.

Parameter	**Value**	**Unit**
Time	500	s
Timestep	0.05	s
Number of modes	5	-
Integration Matlab	ode8 (Dormand-Prince)	-
Integration SIMA/RIFLEX	Newmark	-
Current type	None	-
Current speed	0	m/s
Water depth	2500	m
Elements Matlab	50	-
Element length Matlab	50	m
Elements SIMA/RIFLEX	1251	-
Element length SIMA/RIFLEX	2	m
Top tension	4000	kN

Table 4.5: Dynamic verification simulation parameters.

4.3.1 Global response

The results for all three models are plotted in Figure 4.5. Snapshots of the response are plotted in (a), while (b) is a close-up taken at time $t = 400s$. The dynamic response for the FEM and modal model show good resemblance with the SIMA/RIFLEX model. The error measured in meters can be found as a graph over the riser length in Figure 4.6. As discussed in the static scenario, the constant geometric stiffness used by the Matlab models will give rise to some difference between the models, since SIMA/RIFLEX will use a corrugated stiffness due to displacement. This is reflected

in Figure 4.5 (b) where the horizontal displacement is larger for the Matlab models, indicating reduced stiffness.

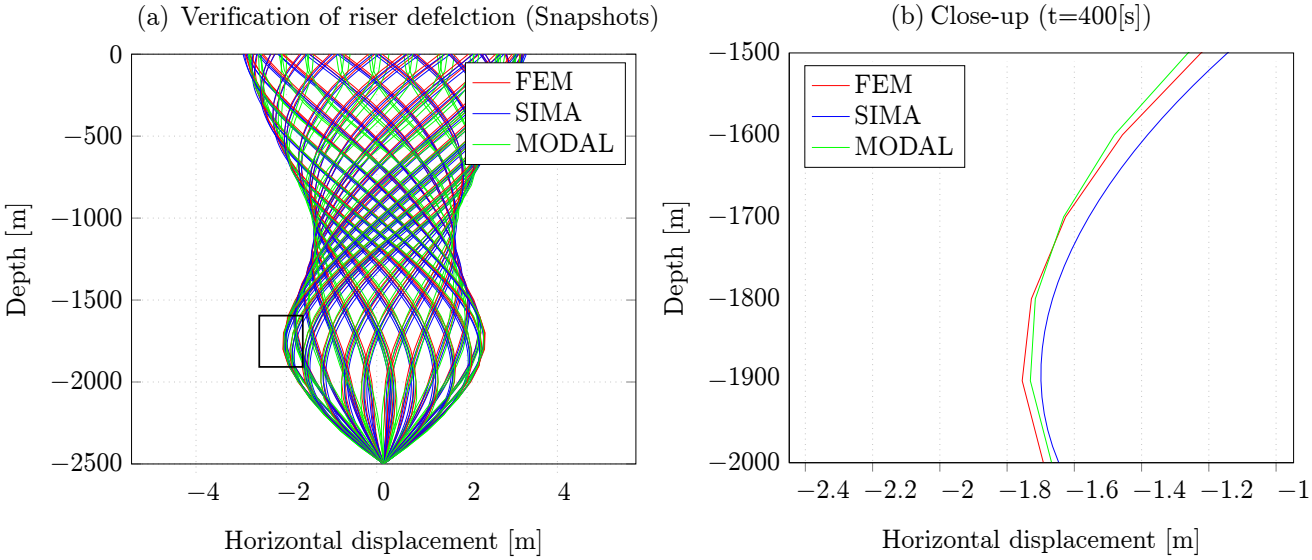

Figure 4.5: Verification of dynamic response, n_{FEM}=50 and n_{SIMA}=1251.

Inspection of the error graphs in Figure 4.6 reveals some interesting facts about the model relations. As might be expected, the best correlation is between the FEM based model and SIMA/RIFLEX. The error seems to be evenly distributed along the riser length, oscillating with an error below 0.25m.

The error between SIMA/RIFLEX and the modal model is larger, with a more dynamic distribution along the length. The mode shape is visible, displaying some form of nodes and anti-nodes. Apart from the top section of the riser, the error between the modal model and SIMARIFLEX is slightly larger than the magnitude of the FEM model (0.3m). The reason for the large deviation in the top section is connected to the mode shapes, shown in Figure 6.4, originating from solving the free vibration in Equation (3.22). Since the origin of force is at the top, all the modes need to have a non-zero component present at this point in order to be excitated. Lack of a component at the origin of force would mean zero modal load, leading to zero deflection. So, in other words, the modal model will experience some error at the top responding to a dynamic force. Solving this problem would require adding synthetic modes similar to adding the zero mode in [27], and combining it to the present solution used here.

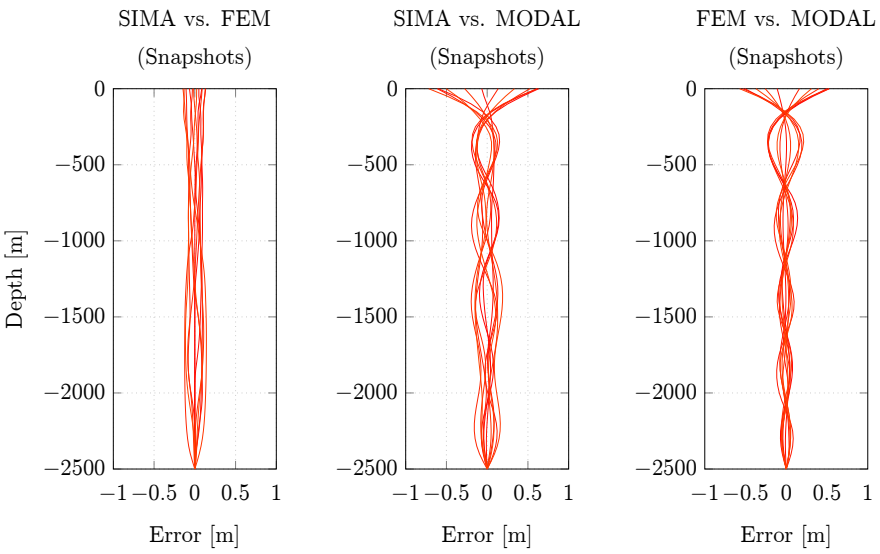

Figure 4.6: Horizontal displacement error for dynamic response.

The last graph in Figure 4.6 is the error between the FEM model and modal model, which indicate a decent match in the sections below 500m with an error below 0.25m. Above this depth the error is larger, displaying around 0.5m at the top. For the use here, this is within the limits of accuracy, considering using the model in a control environment will be supported by measurements. The use of measurements would allow for some correction at the top section.

4.3.2 Local response at top node and RCD

As observed in Figure 4.6 different error dynamics are present in the FEM model and the modal model. To study this closer nodal time series for the RCD at 400m is examined in the graphs found in Figure 4.7. Here the error is calculated as precentage of diameter, which would mean an error of 100% would correspond to a difference of 0.53m.

In (a) the error between FEM and SIMA is oscillating with an amplitude of 20%, with the same period as the harmonic load $T = 57.6s$. The modal model in (b) has the same period, but the error is slightly larger just passing 20%. This is what one would expect for a model which is a simplified version extraction of the FEM model.

The last plot in (c) compares the FEM and modal model at the RCD node. The plot indicate an error of 40%, which might seem strange taken that the two other errors are of magnitude well below this. The explanation can be found in Figure 4.8, which in Figure 4.8 (b) shows that the FEM and modal solutions enclose the SIMA solution. Meaning that the SIMA solution time development is between the curves of the two models.

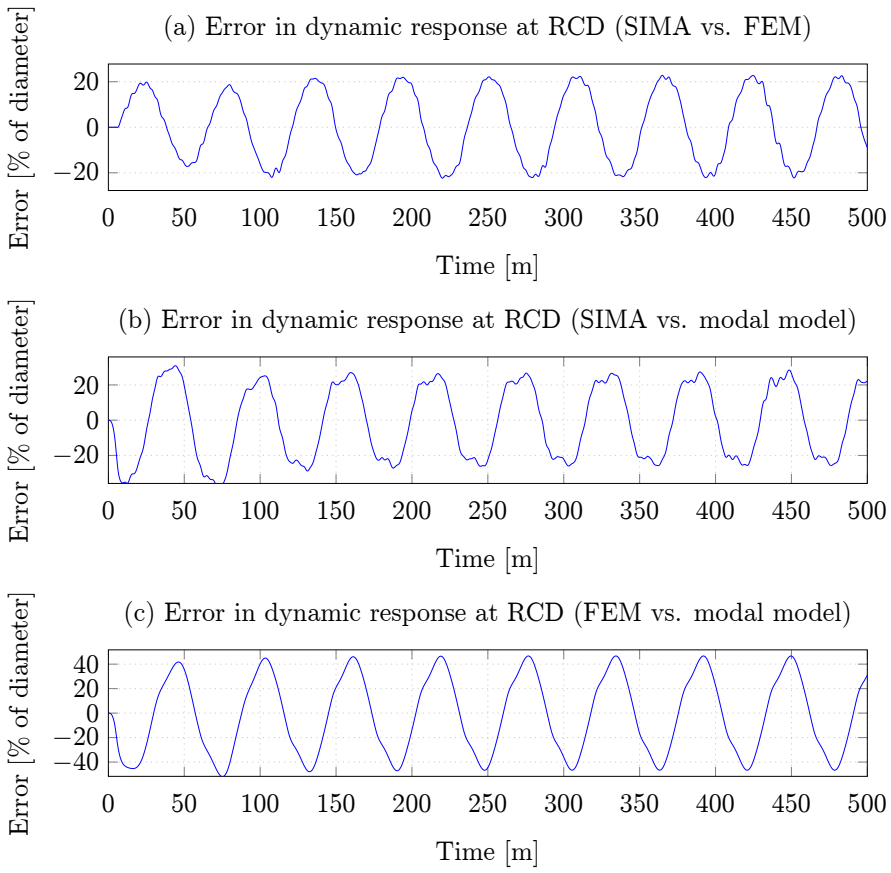

Figure 4.7: Percentage distribution of error for dynamic response at the RCD node.

Another observation of great importance is the two points marked with a circle and a cross in Figure 4.8 (b). They indicate the time required for the force at the top to travel to the RCD node, i.e. the propagation speed of the force response. Since the modal model is inherently stiffer, due to the exclusion if higher modes, it has the shortest reaction time marked with a circle. The FEM model has almost the same reaction time as SIMA, but is a bit faster. This phenomenon is directly connected to the number of elements in the model, fewer elements means that the model is more rigid, allowing for the force to travel faster along the structure and vise versa.

The occurrence of this is "lag" is the stiffness difference in the models. This is important to consider when planing the control strategy. Since the reaction is predicted faster by the model than the physical structure, this must be accounted for in a lead/lag mechanism. Since the number of elements will determine this relation, a trade-off between the number of elements and the acceptable lead/lag must be determined for the control system. Since the modal model is constructed such that a modal load will excite the complete mode shape, and consequentially the whole riser at once, argue for higher order modes to be included. Using only five will mean that large deflections will appear instantly along the length when the designated mode is stimulated.

(a) Nodal time series for RCD

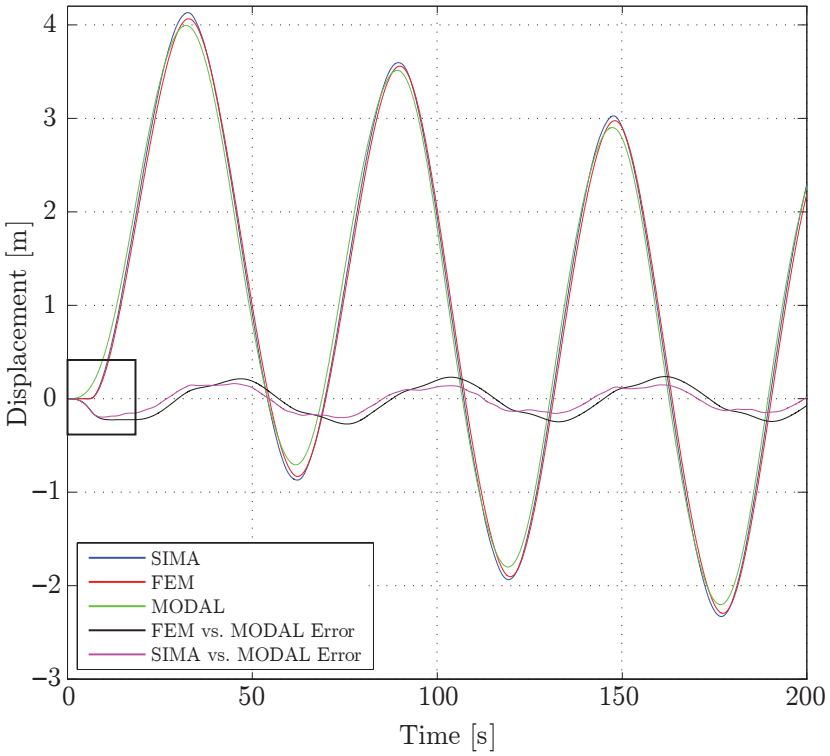

(b) Close–up

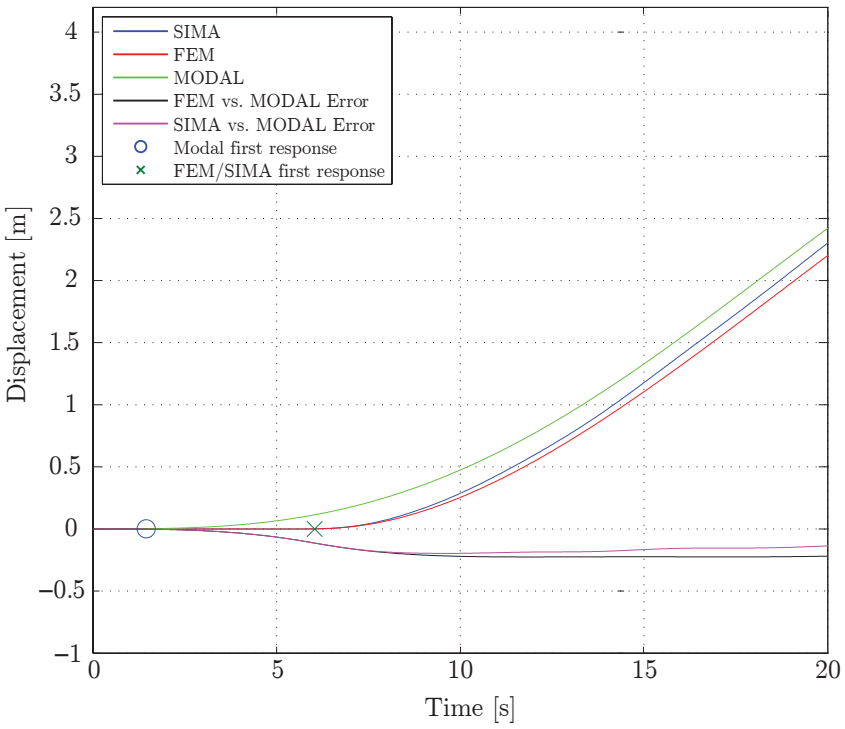

Figure 4.8: Nodal time series for RCD.

4.4 Review of model verification and sensitivity

Changing the element length have impact on the riser behavior and deflection. As previously discussed the apparent stiffness will increase with longer elements, and the solution will be less accurate as a consequence of using the beam theory of small displacements (Euler-Bernoulli beam theory). Bearing in mind that the riser is a slender structure with a large length-to-diameter ratio, the classical beam theory will lack descriptive validity for certain aspects of the riser dynamics. Considering this, the number of elements is increased from 10 to 100 and applied a bi-lateral current load to observe these effects. The results of this analysis in plotted in Figure 4.9 (a) and (b).

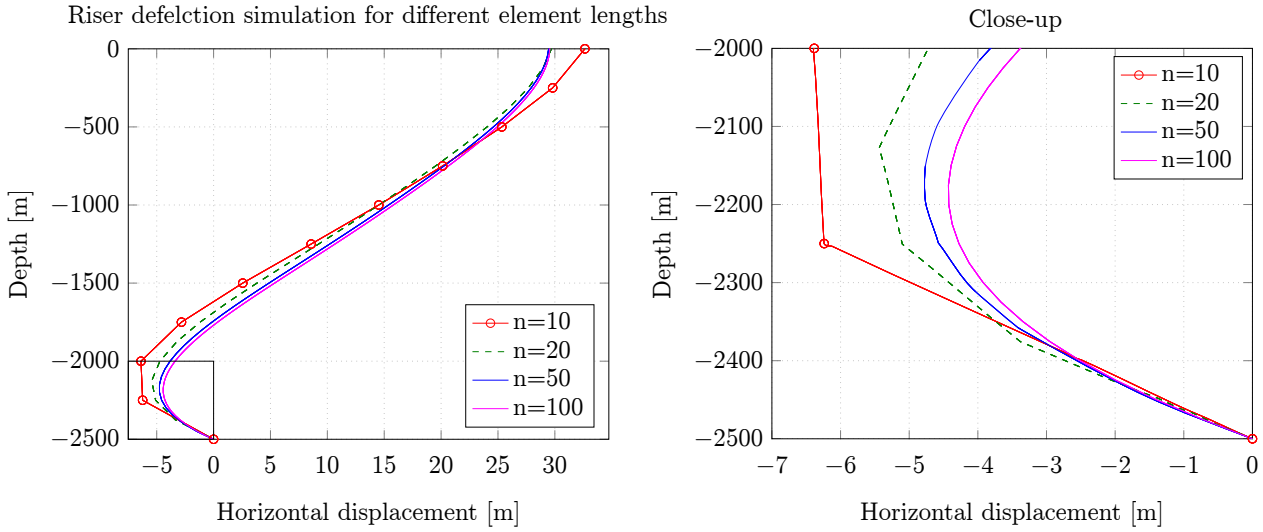

Figure 4.9: Number of elements vs. resulting geometry.

The different deflections demonstrate that increasing number of elements gives a more realistic impressions of the riser curve. The maximal difference separating $n = 50$ and $n = 100$ is at the second deflection (2200m) found to be around 0.5m, which is about the diameter of the riser pipe.

The flowing chapter has verified the accuracy of the FEM and modal decomposition model compared to the commercial riser software SIMA/RIFLEX developed by MARINTEK. The models show good correspondence with the SIMA/RIFLEX simulation both in static and dynamic verification scenarios, despite several notable simplifications. The sensitivity analysis conducted above suggest that the use of n=50 elements will deviate 0.5m from the $n = 100$. This demonstrate that the element length can be reduced, if additional accuracy is of importance. However, the computational aspects suggest that a model using n=100 will have a significant increase in computational time. The results from Section 4.3 demonstrated that the correspondence between the FEM model and SIMA/RIFLEX, using n_{FEM}=50 and n_{SIMA}=1251, retained an response error within 20% of the riser diameter. The use of n=50 is therefore considered sufficient for the use in the conceptual studies carried out in this thesis.

Chapter 5

RIFLEX modelling and simulation

The excessive abrasion of the internal sealing element due to lateral forces, originating from deformation and interaction between the riser and drillpipe is a crucial concern. This chapter will focus on finding these forces acting on a 2500m riser with RCD and seal element, from wave and current forces inherit to the Gulf of Mexico.

The simulation will be conducted using the commercial finite element program RIFLEX. RIFLEX performs static and dynamic analysis of slender marine structures such as drilling risers, using SIMA as a graphical interface. A model is assembled in SIMA containing riser, drillpipe, vessel, top and bottom riser connections, BOP and a simplified RCD representation. Section 5.1 will explain the model components and the loading environment in more detail. The results for the static and dynamic analysis will then be presented in Section 5.3.

5.1 Simulation setup

The RCD unit and seal element are the key components in the simulation scheme, the modelling of these components are therefore of vital importance. The simulation is built inside the SIMA/RIFLEX environment and consists of three main parts.

1. A finite element model of the riser, drillpipe, RCD and its subcomponents.
2. A simulation environment inherit to the Gulf of Mexico, featuring current and waves.
3. A numerical integration method for solving the differential equations.

It is important for the success of the analysis that these three are correctly adapted to each other. E.g. the element length used in the FEM model and time step used by in the integration needs to correspond to the dynamics and load periods set up by the load environment.

5.1.1 Finite element model and boundary conditions

The FEM model is constructed in SIMA/RIFLEX using an intuitive system of so called "super nodes" to define the main start and end points of the pipes. These nodes are located at the ends of the pipe elements and can be assigned boundary conditions, other pipe connections, additional masses and springs depending on the demand [34]. They subsequently make up the framework for connecting the elements together.

Two super nodes are needed to make a pipe, referred to as a *line* in SIMA. The line can then be split up into smaller *segments* where the local element and node division is done based on choice of the user and the desired grid precision. The grid/element size can be chosen individually for each

segment as illustrated in Figure 5.1.

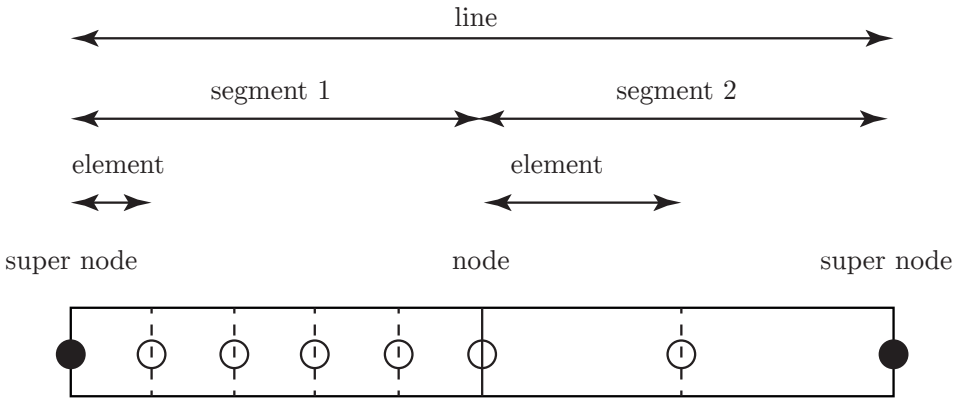

Figure 5.1: SIMA element structure.

Boundary conditions can be specified for the super nodes in all DOFs. Additionally it is possible to assign prescribed displacements and create master-slave pairs. These master-slave connections can either be between super nodes or support vessels. In Figure 5.2 all the super nodes in the model are displayed with the corresponding name. This includes the nodes for the riser, drillpipe and tensioners. The nodes are assigned to the boundary conditions found in Table 5.1.

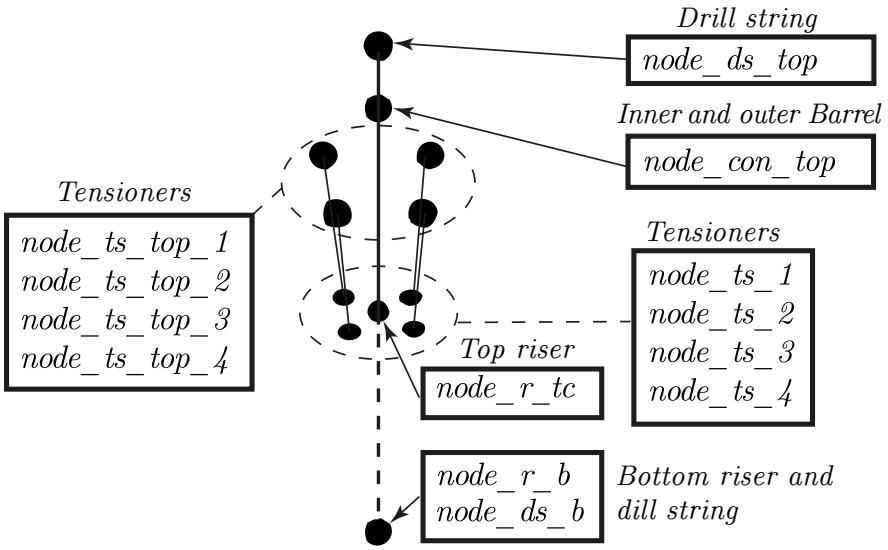

Figure 5.2: Super node overview.

Notice that there are six nodes that are slaved to the vessel. This includes the top of the tensioners, drillpipe and inner barrel (slip joint), represented in Figure 5.3. The base of the tensioners

Node name	Z-axis	X	Y	Z	RX	RY	RZ	Slaved to
node_r_tc	6m	Free	Free	Free	Free	Free	Free	-
node_r_b	-2500m	Fixed	Fixed	Fixed	Fixed	F. Joint	Fixed	-
node_ds_top	34m	Fixed	Fixed	Free	Fixed	Fixed	Fixed	Vessel
node_ds_b	-2500m	Fixed	Fixed	Fixed	Fixed	Free	Fixed	-
node_con_top	28m	Fixed	Fixed	Free	Fixed	Fixed	Fixed	Vessel
node_ts_1	6m	Slaved	Slaved	Slaved	Slaved	Slaved	Slaved	*node_r_tc*
node_ts_2	6m	Slaved	Slaved	Slaved	Slaved	Slaved	Slaved	*node_r_tc*
node_ts_3	6m	Slaved	Slaved	Slaved	Slaved	Slaved	Slaved	*node_r_tc*
node_ts_4	6m	Slaved	Slaved	Slaved	Slaved	Slaved	Slaved	*node_r_tc*
node_ts_top_1	30m	Fixed	Fixed	Fixed	Fixed	Fixed	Fixed	Vessel
node_ts_top_2	30m	Fixed	Fixed	Fixed	Fixed	Fixed	Fixed	Vessel
node_ts_top_3	30m	Fixed	Fixed	Fixed	Fixed	Fixed	Fixed	Vessel
node_ts_top_4	30m	Fixed	Fixed	Fixed	Fixed	Fixed	Fixed	Vessel

Table 5.1: Super node location and boundary condition.

are slaved to a single node located at the top termination point of the riser, named "*node_r_tc*". This node is totally free in all DOF, so when the tensioners are activated creating a force pulling upward, this will create the top tension force on the riser. It should also be noted that this table is compiled for the water depth of 2500m.

5.1.2 Vessel connection modelling

The vessel connection model is intended to simulate the connection between the vessel, tensioners, drillpipe and riser. The components are shown in Figure 5.3 (a). To simulate the motion of the vessel a designated response amplitude operator (RAO) is applied, based on a typical semi-sub in DP. The tensioners and drillpipe are linked to the vessel using a master-slave relationship. The master-slave rig/vessel connection transmits the response originating from the rig/vessel to the riser. This includes the motion response and top tension forces. The top tension is applied through four tensioned beams, intended to simulate a wire-line hang up system in Figure 3.1. The magnitude of the force is set according to the industrial notion of having around 600kN or 60ton tension at the BOP. The tensioners attach to a massive ring, known as a tension ring or a "spider", which acts as the actual hang up point for the riser. The ring is modelled as a point mass in SIMA/RIFLEX located at the riser termination point. In addition to the tensioners and tension

ring, the riser accommodates the drillpipe in a pipe-in-pipe (PIP) model. The riser structure is heave compensated using special elements above the riser, namely the outer and inner barrel. The heave damping is done creating a slip joint segment with very low axial stiffness. The heave motion will be reduced as the slip segment absorbs the vertical forces by acting as a damper. Compared to a real life heave compensation system, the simplified system is less effective and give more heave motion. This means more axial forces will propagate along the riser and drillpipe. Also a flex joint is added to the top of the inner barrel to simulate the hang up point for the drillpipe and inner barrel termination point.

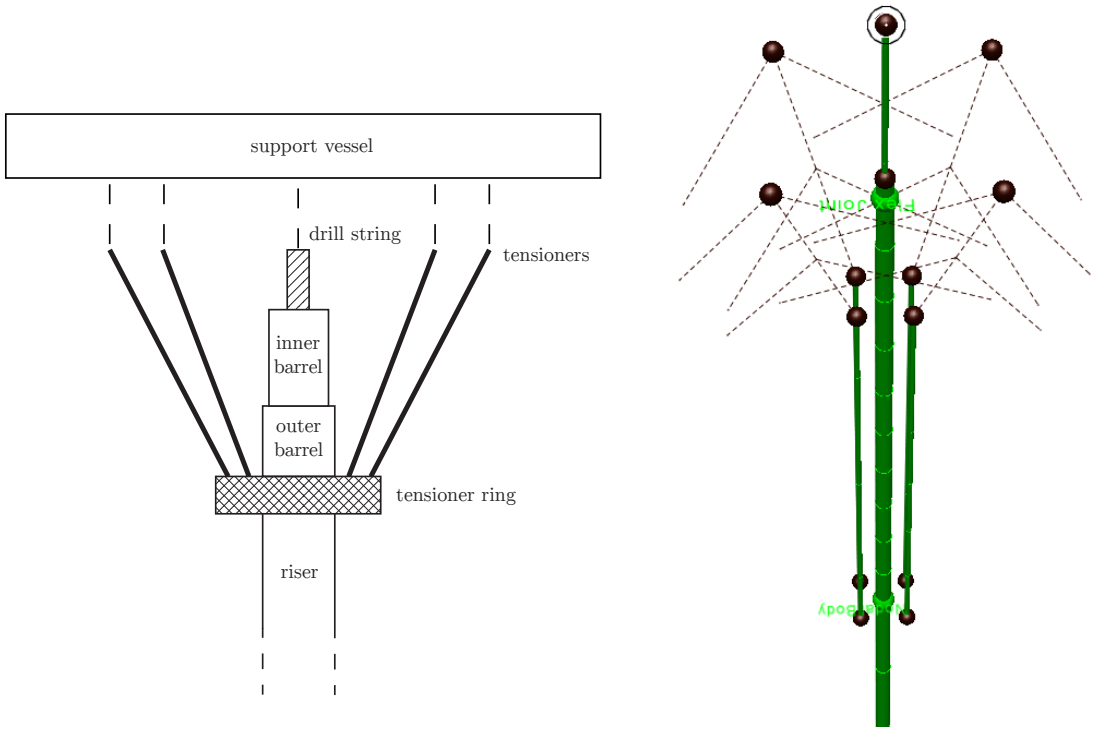

(a) Principle model

(b) SIMA/RIFLEX model

Figure 5.3: The conceptual and modelled vessel connection.

5.1.3 Riser modelling

The riser is a standard marine drilling riser with specifications given in Table 5.2. The riser is equipped with buoyancy modules to support the weight of the 2500m long pipe, as can be seen in Figure 5.4. The riser is then split into ten segments to attain more flexibility regarding modelling of the RCD and PIP relations. Notice that the number of elements per meter is increased towards areas of interest; top, bottom and RCD. This is to achieve the necessary precision and better capture the dynamics at these points. Usually, the riser has a number of peripheral lines running along the side used to control the BOP. However, these lines are not considered in this model. The riser cross section around the RCD has special properties for calculating the lateral contact forces

created by the PIP definition. Also note that the density of the drilling mud changes during the drilling operation and depth, but is kept fixed in the model.

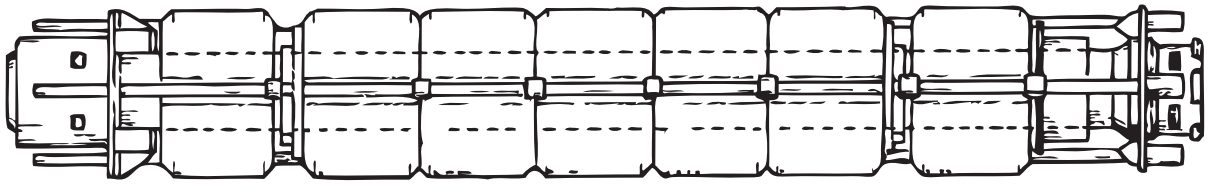

Figure 5.4: Typical marine drilling riser with buoyancy modules.

Riser parameter	**Value**	**Unit**
Riser length	2500	m
Outer diameter	0.5334	m
Wall thickness	0.016	m
Density steel	7850	$\frac{kg}{m^3}$
Density seawater	1025	$\frac{kg}{m^3}$
Density mud	1500	$\frac{kg}{m^3}$
Drag coefficient	1.0	-
Elasticity module	206×10^9	$\frac{N}{m^2}$
Tension at BOP	6000	kN
Buoyancy module (BM) density	400	$\frac{kg}{m^3}$
Buoyancy module (BM) thickness	0.15	m

Table 5.2: Riser characteristics.

Riser segment	Depth	Length	Elements	Cross section	Component
1	2500m	20m	20	Cs no BM	-
2	2480m	1949m	20	Cs BM	Flex joint
3	531	60m	12	Cs BM	-
4	471	50m	25	Cs BM	-
5	421	10m	10	Cs BM	-
6	411	10.5m	20	Cs RCD	-
7	400.5	0.5m	10	Cs RCD	RCD
8	400	96m	10	Cs BM	-
9	300	250m	25	Cs BM	-
10	50	50m	10	Cs no BM	-

Table 5.3: Riser segments used by SIMA/RIFLEX.

To clarify the notation used in Table 5.3, "Cs BM" refers to a cross section with buoyancy module, "Cs no BM" refers to no buoyancy module and "Cs RCD" is the cross section type for the RCD. Note that Segment 7 contains the RCD component and Segment 2 contains the flex joint associated with the BOP, located 20m above the seafloor.

5.1.4 Drillpipe modelling

The drillpipe is modelled in a PIP configuration with the drilling riser as the master pipe. It is made up by eight segments and house the internal part of the RCD (located in Segment 5) as shown in Table 5.5. It is a standard drillpipe, with specifications given in Table 5.4. The top tension is applied at the top node with a magnitude of 4000kN.

Drillpipe parameter	Value	Unit
Length	2530	m
Outer diameter	0.168	m
Wall thickness	0.027	m
Top tension	4000	kN

Table 5.4: Drillpipe characteristics.

DP segment	Depth	Length	Elements	Cross section
1	2500	80m	8	Cs ds
2	2420	1959m	20	Cs ds
3	461	50m	25	Cs ds
4	410	10m	10	Cs ds
5	400	0.5m	2	Cs ds RCD
6	399.5	134m	13	Cs ds
7	265	250m	25	Cs ds
8	15	50m	50	Cs ds

Table 5.5: Drillpipe segments used by SIMA/RIFLEX.

5.1.5 RCD modelling

The key component of the analysis is the RCD unit, in which the seal element separate the riser and the drillpipe. The abrasion process is dependent on the friction force between the drillpipe and seal. The lateral force, set up by the relative offset between the drillpipe and riser, is directly connected to this friction force. The relative offset will force the drillpipe out of the center, while the seal will force the drillpipe to stay centred in the riser. This creates lateral forces which causes a disproportional amount of abrasion over the seal surface. Acquiring these forces are the main priority.

Illustrated below is the principal model concept implemented in SIMA/RILFEX for the lateral seal contact force. In order to simulate the forces originating from the interaction between riser and seal element a additional special PIP contact force model is applied. By letting the cross section diameter of the drillpipe in the RCD segment slightly smaller than the riser diameter, this will approximate the internal seal conditions. The RCD and seal topography can be seen in Figures 2.4 and 2.5. Since the drillpipe and riser is in a PIP configuration there will, in the case of riser deformation, be contact forces created between the seal contact surface and the riser contact surface. This is the lateral force dynamics of interest. To obtain the lateral force acting over the seal length the upper and lower shear forces is summarized. This sum will be the resulting lateral force component, following from force equilibrium relations.

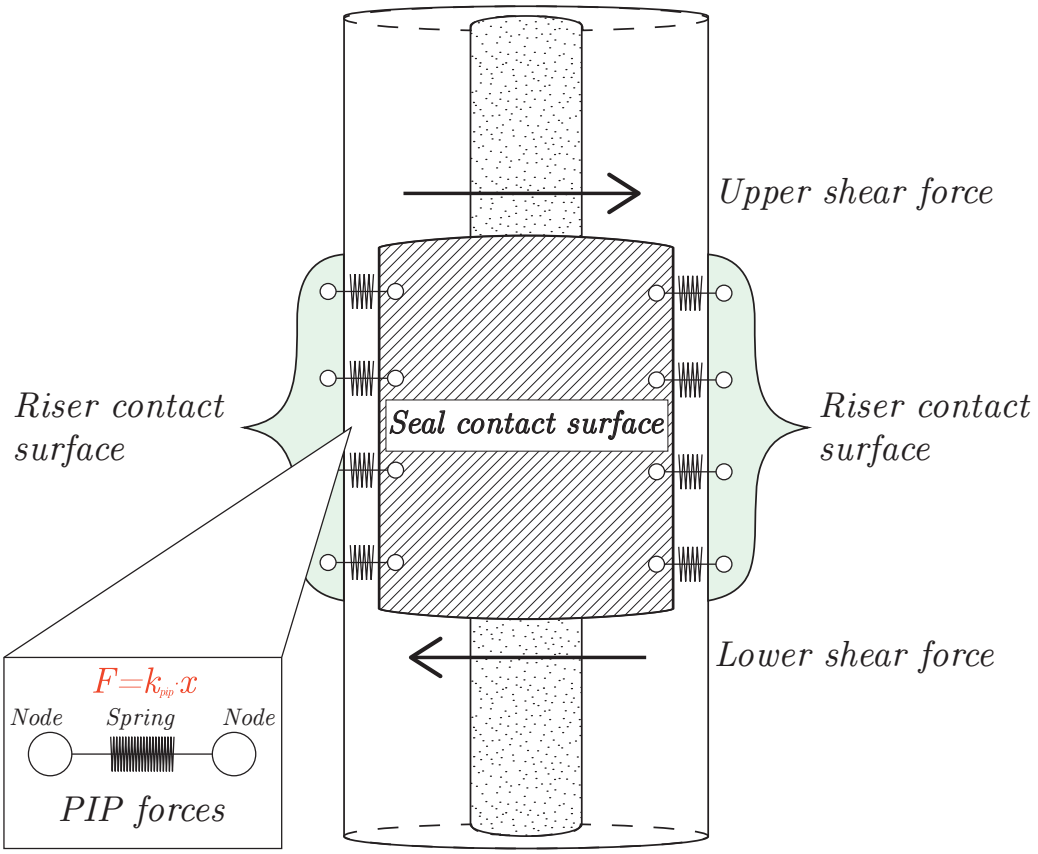

Figure 5.5: RCD model with PIP contact forces.

5.1.6 PIP modeling

The PIP contact force is defined as a spring stiffness where the force is proportional to the displacement formulated as

$$F = k_{pip} \cdot x, \tag{5.1}$$

where k_{pip} is the linear stiffness constant and x is the displacement in the spring direction. Such that a compression of will give a positive force in opposite direction. The relation in Equation (5.1) is created between the nodal system in the riser and the nodal system in the drillpipe. It is the relative movement between the nodes in these two local systems that create forces. Setting a high spring constant will simulate a "hard" wall, while a lower value will allow some surface penetration and a "soft" wall. The model uses two PIP definitions: *PIP upper* and *PIP lower*. They are defined in Figure 5.6.

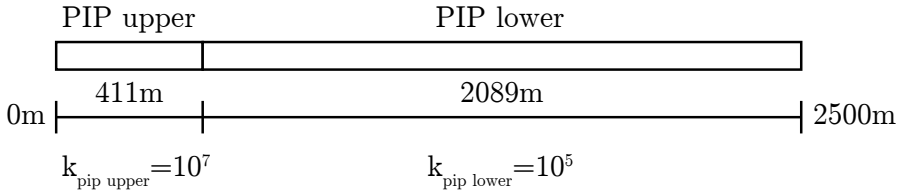

Figure 5.6: PIP definitions for the model.

5.1.7 BOP modelling

The BOP is approximately 20m tall and stand on the seafloor above the wellhead. The BOP weight is set to 150 tons, which would constitute to a heavy type. The SIMA/RIFLEX model includes the BOP as a heavy 20m segment terminated with a flex joint. This additional stiffness ensures a more realistic angle magnitude for the lower riser point. The top and bottom angles should not exceed an upper limit of $\pm 2°$, where deviations larger than $5° - 8°$ may be fatal [47].

5.1.8 Simulation environment

The different design environments are based on cases from ISO standard 19901-1, found in [17], containing metocean design and operating conditions for offshore structures in the Gulf of Mexico. Data is selected from the combined extreme (100 year return period) for loop currents and bottom currents, containing a combination of wind, waves and currents. The data provides indicative values for metocean parameters which can be suitable for conceptual studies, without considering local structural details. In the riser analysis, the governing parameter is the current velocity profile. For this thesis, five distinctive profiles are considered: *Uniform, Bilateral, Skewed, GoM* 1 and *GoM* 2. *GoM* 1 and *GoM* 2 are two local loop current profiles from the Gulf of Mexico. *GoM*2 is a cold current, meaning the maximum current velocity is below the surface. The profiles are illustrated in Figure 5.7.

A total of four separate scenarios are simulated in SIMA/RIFLEX. Each scenario have five distinctive sub scenarios, with different environmental parameters. All scenarios focus on the lateral forces between the riser, drillpipe and sealing element in the RCD. The environmental parameters for the scenarios can be found in Table 5.6. Only unidirectional loads are considered, meaning that the waves and currents forces are applied in one direction only. The scenarios are presented below.

Scenario 1.1 - 1.5

Scenario 1 investigates the effect on the lateral force from increasing current speed. The speed is ramped up from 0.2m/s to 1.0m/s. Surface waves are also present.

Scenario 2.1 - 2.5 Extreme

Scenario 2E focuses on the location of the RCD. The RCD is moved from 300m to 500m deep, with 50m increment. The environment features both large waves and strong currents.

Scenario 2.1 - 2.5 Normal

Scenario 2N focuses on the location of the RCD. The RCD is moved from 300m to 500m depth, with 50m increment. Compared to the extreme environment this will be much less severe featuring smaller waves and modest currents.

Scenario 3.1 - 3.5

Scenario 3 will exclusively investigate the lateral force subjected to the five different current profiles in Figure 5.7. Surface waves are also present.

Scenario 4.1 - 4.5

Scenario 5 will feature the five current profiles and an extreme wave condition with a significant wave height of 6m.

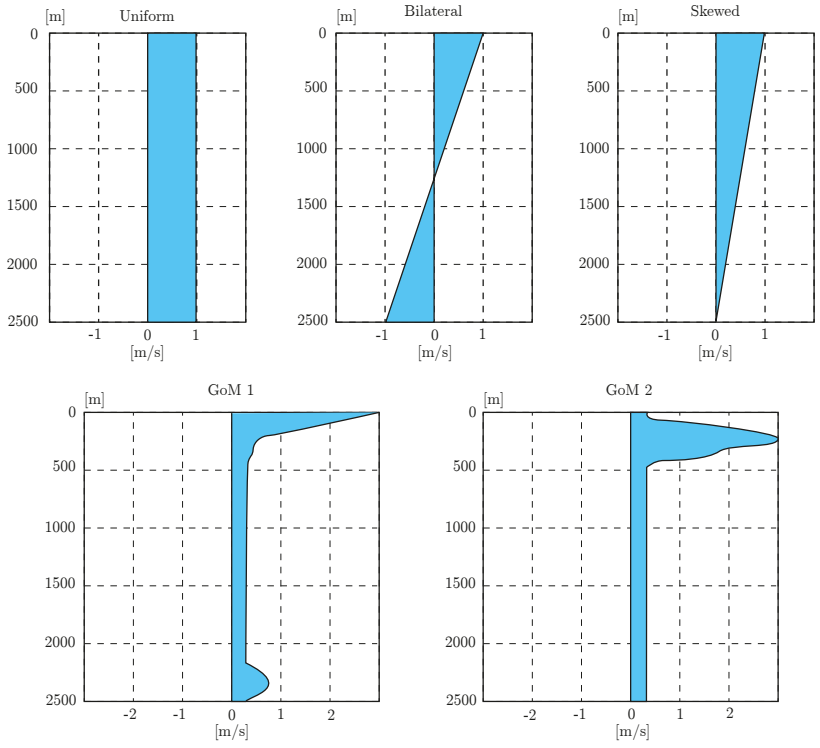

Figure 5.7: Current profiles used in the simulations.

Scenario	RCD location	Profile	Waves	Tp	Hs	Max. curr.vel
1.1	400	uniform	Normal	5	1.5	▶ 0.2m/s
1.2	400	uniform	Normal	5	1.5	▶ 0.4m/s
1.3	400	uniform	Normal	5	1.5	▶ 0.6m/s
1.4	400	uniform	Normal	5	1.5	▶ 0.8m/s
1.5	400	uniform	Normal	5	1.5	▶ 1.0m/s
2.1.E	▶ 300	Exteme GoM1	Large	11	6	2.25m/s
2.2.E	▶ 350	Exteme GoM1	Large	11	6	2.25m/s
2.3.E	▶ 400	Exteme GoM1	Large	11	6	2.25m/s
2.4.E	▶ 450	Exteme GoM1	Large	11	6	2.25m/s
2.5.E	▶ 500	Exteme GoM1	Large	11	6	2.25m/s
2.1.N	▶ 300	Normal GoM1	Normal	5	1.5	0.5m/s
2.2.N	▶ 350	Normal GoM1	Normal	5	1.5	0.5m/s
2.3.N	▶ 400	Normal GoM1	Normal	5	1.5	0.5m/s
2.4.N	▶ 450	Normal GoM1	Normal	5	1.5	0.5m/s
2.5.N	▶ 500	Normal GoM1	Normal	5	1.5	0.5m/s
3.1	400	▶ uniform	Normal	5	1.5	▶ 1.0m/s
3.2	400	▶ bi-directional	Normal	5	1.5	▶ 1.0m/s
3.3	400	▶ skewed	Normal	5	1.5	▶ 1.0m/s
3.4	400	▶ GOM 1	Normal	5	1.5	▶ 2.5m/s
3.5	400	▶ GOM 2	Normal	5	1.5	▶ 2.5m/s
4.1	400	▶ uniform	Large	11	6	▶ 1.0m/s
4.2	400	▶ bi-directional	Large	11	6	▶ 1.0m/s
4.3	400	▶ skewed	Large	11	6	▶ 1.0m/s
4.4	400	▶ GOM 1	Large	11	6	▶ 2.5m/s
4.5	400	▶ GOM 2	Large	11	6	▶ 2.5m/s

Table 5.6: Test cases analyzed in SIMA/RIFLEX.

▶ markes the changes in the conditions.

5.1.9 Computational aspects

The most demanding aspect of the analysis is the PIP model. The model simulate the loads related to contact forces between two pipes. The force is activated when the two contact surfaces come into contact with each other, resulting in forces being turned on fast, with no or little transient. As explained in Section 5.1.6, the PIP model uses two segments (upper and lower) to cover the whole riser, resulting in hundreds of nodal relations needing continuable updating. All these nodes and their local neighbours lead to a computationally demanding system. The magnitude of the PIP forces and the short load period have significant impact on the numerical integration procedure,

requiring smaller time steps. In Figure 5.8, the effect of increasing the time step is shown to affect the behaviour of the solution. Comparing the red signal and green signal, it is evident that large time steps introduce noise/chattering behaviour. The force transient is faster than the numeric algorithms, causing some lag in the calculation. However, the integration converges, but has ripples due to the large time steps compared to the force dynamics. This is confirmed by examining the filtered signals. The signals are filtered with a simple 4th order butterworth lowpass filter to obtain more smooth signals. All the signals show consistent results for larger times steps and are therefore considered valid.

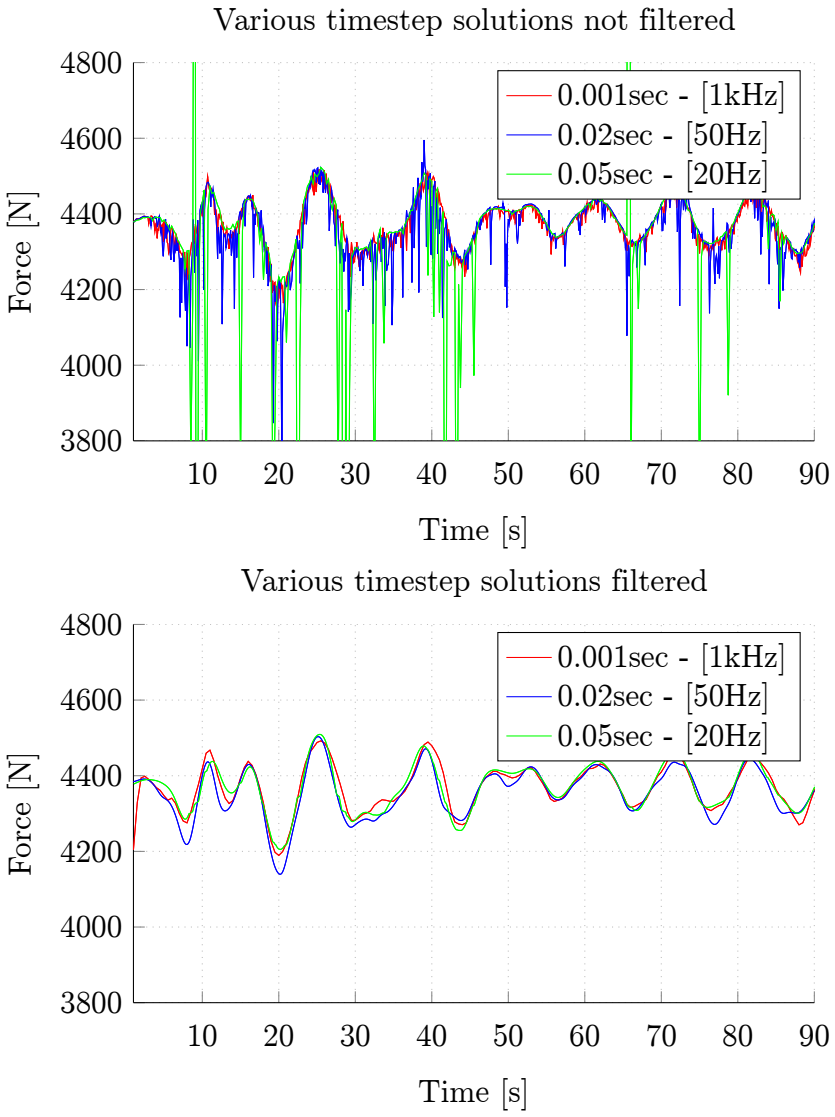

Figure 5.8: Effect of different time steps.

5.2 Governing equation

A brief introduction is given here into the governing equation used to describe the drilling riser, to support the familiarisation of the basic concepts before reading Section 5.3. This will be covered in more detail in Chapter 6 Section 6.1.

A drilling riser can be modelled as a slender tensioned beam with transverse loads [31]. Using this the equation for a beam with constant tension and small deflection angles, can be found in [37] formulated as,

$$EI\frac{d^4u}{dx^4} - T\frac{d^2u}{dx^2} = q(x), \tag{5.2}$$

where EI is the bending stiffness, T is the effective tension and $q(x)$ is the load function. The x-axis is defined positive along the length of the beam, the y-axis is transverse, as shown in Figure 3.3. Equation (5.2) relates the force equilibrium set-up by curvature, tension and the bending stiffness of the beam to the load distribution $q(x)$. The lateral contact forces between the riser and the drillpipe are essentially shear forces set up by a variation in deflection between the riser and the drillpipe. This variation is manifested in the riser curvature, dictating the change in deflection for the drillpipe. Large curvature means that the riser orientation is changing fast and over a short distance, which again forces the drillpipe to follow the same curvature profile. Based on basic beam theory in [37] and [23] the shear force is defined as

$$\frac{dQ}{dx} = -q(x), \tag{5.3}$$

where Q is the shear force and $q(x)$ is the load distribution from Equation (5.2). Thus the shear force is not only governed by the tension and curvature, but also the bending moment contributes to the balance.

This introduces an important relationship between bending stiffness and curvature forces impact on the lateral force. Since the lateral force not solely rely on the curvature and tension to counterweight the loads, but also the bending moment, both terms in Equation (5.2) must be considered when searching for an optimal operational location for the RCD unit and the internal sealing element. Since the riser is a slender structure with limited influence from the bending stiffness, the curvature term will in most instances be the governing factor for the lateral force. Nevertheless, large deflections can induce significant bending, leading to unanticipated results.

5.3 Simulation results

In this section, the SIMA/RIFLEX results of the riser model proposed in Section 5.1.3 are presented. The first part will be a sequential summary of all four environments and their main results. This is followed by a comparative part which look at the entirety of the simulations and the main observations discovered.

Since the vessel connection point is situated 35m above the mean sea surface, the displacement curves are shifted towards the left by a small amount. This is due to the angle in the hang up system, created by the current or waves forcing the riser towards the right (x-axis). Additionally, the curves start 20m above the seafloor at the top of the BOP, hence the offset from the seafloor. This applies to all plots in this section.

5.3.1 Scenario 1 - Increasing the current velocity

The aim of Scenario 1 is to study the magnitude of the lateral force subjected to increasing current velocity. The velocity is ramped up from 0.2m/s to 1.0m/s. The current is uniform over the entire riser, accumulating significant load. Such a scenario would be considered an extreme case. The current will normally be more moderate and not act uniformly in one direction. Small surface waves are also present to provoke the vessel dynamics. The significant wave heigh H_s is selected based on what would constitute as a normal day at a deep water location in GoM.

Scenario 1 static

In Figure 5.9, the static displacements for each velocity increment is displayed. As might be expected a larger velocity produce larger loads, and hence greater deformation. The point of maximum deflection for the curves is located just above 1500m water depth. Note that the circle represent the RCD location.

Scenario 1 dynamic

Increasing current velocity will give larger riser deflection and hence more force is required to keep the drillpipe centred, yielding larger lateral forces between the riser and the drillpipe. Larger deflection will give an elongation of the riser, which in turn will increase the geometric stiffness. This means that the tension in the riser will increase and the riser structure will be less sensitive to waves or other small magnitude dynamics. Figure 5.10 displays such a phenomenon clearly. As the current velocity increases from 0.4m/s, the wave and vessel motion is dominated by the horizontal deflection tension, almost eliminating the visible wave contribution. The wave oscillations present in the lateral force signal associated with velocity 0.2m/s are strong enough not to be governed by the deflection tension, producing a signal which is significantly different.

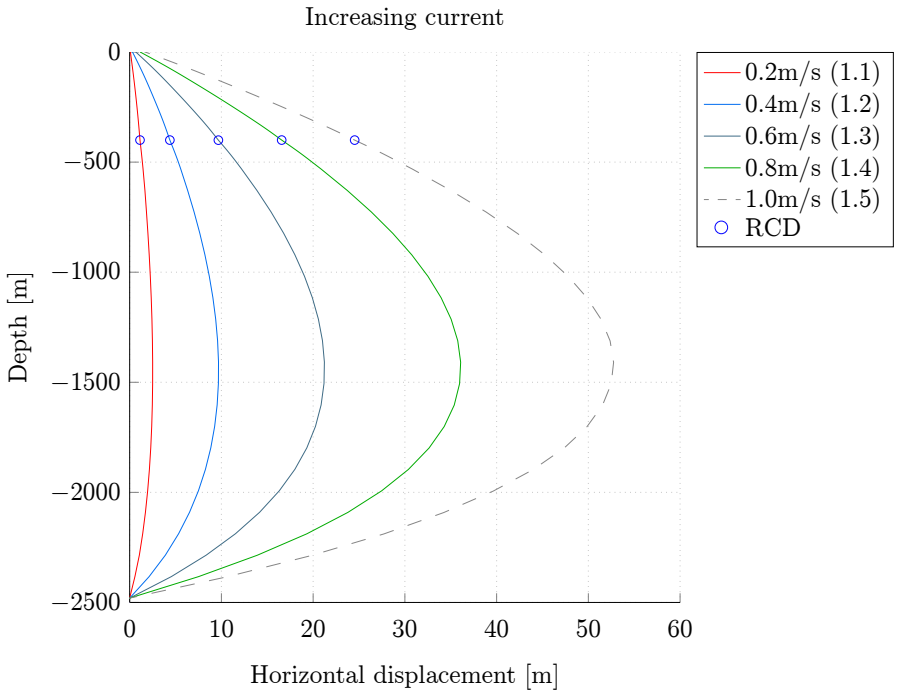

Figure 5.9: Horizontal displacement due to increasing current.

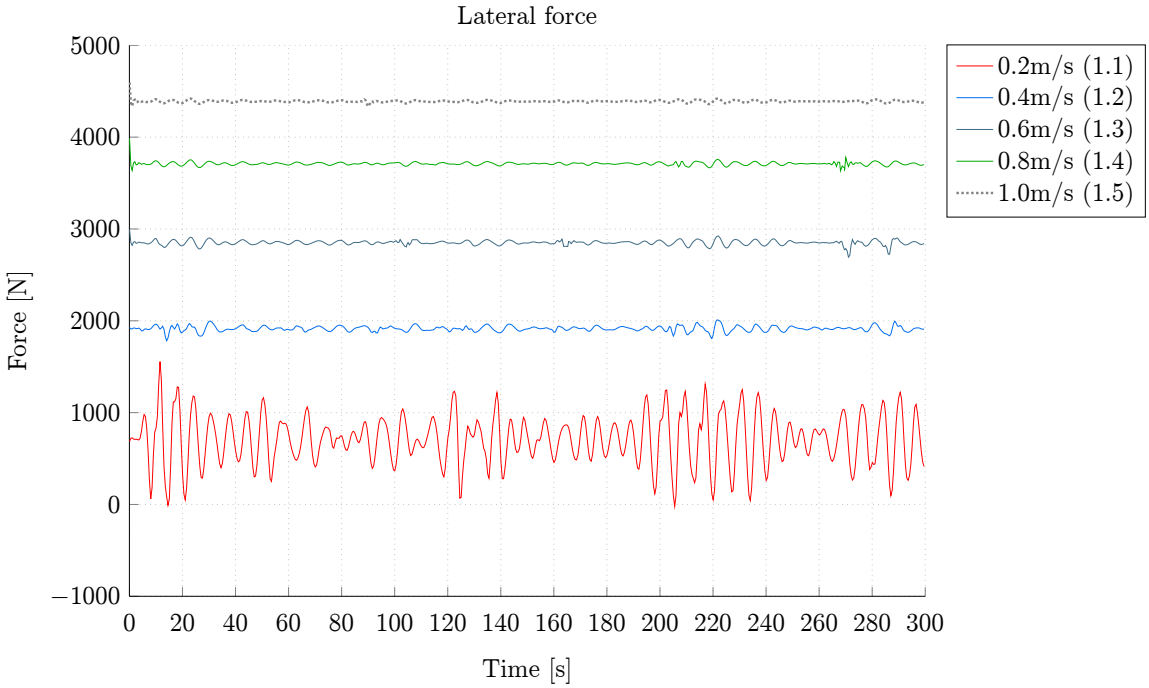

Figure 5.10: Lateral force due to increasing currents.

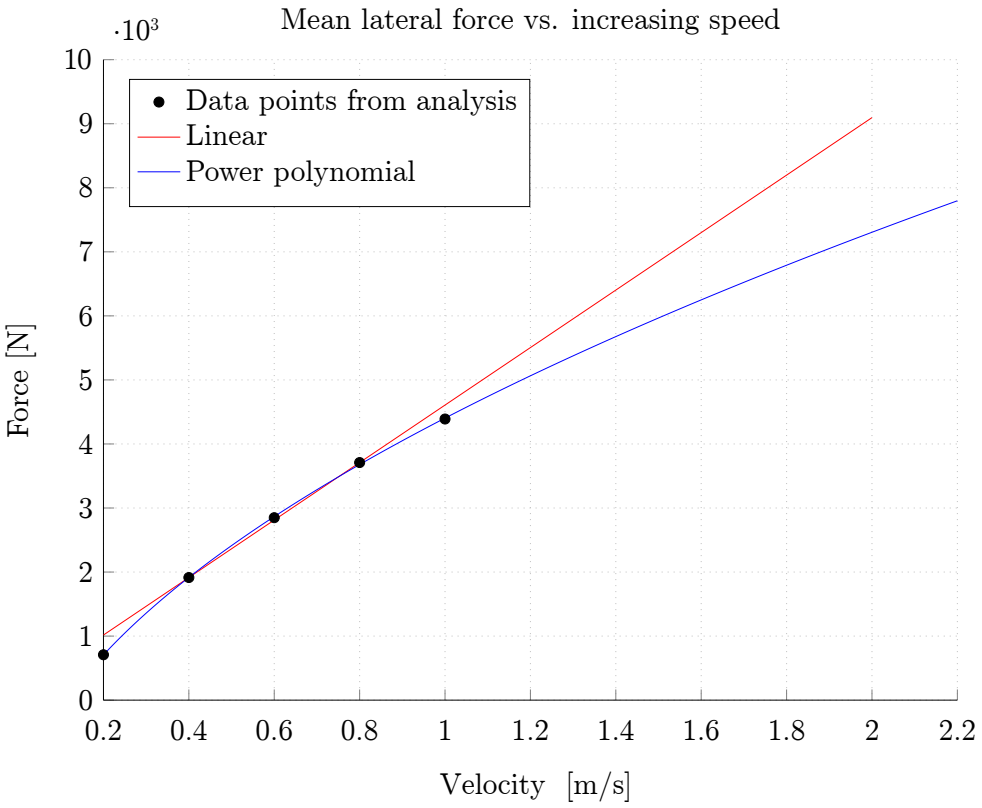

Figure 5.11: Lateral force due to increasing velocities.

Taking the mean value for the signals in Figure 5.10, the mean lateral force between the riser and the drillpipe is obtained. Using the mean force, interpolation of the mean lateral force versus the increasing current velocity, is calculated and displayed in Figure 5.11. Linear and power polynomial interpolation of the data gives a sense of the force magnitude expected at a given current velocity. It is unlikely that a uniform current extending over the entire riser length would have an average value larger than 1.0m/s, based on the metocean parameters given in [17]. Larger current velocities occur, but will not act over larger portions of the water column with the same intensity. The values extracted from Figure 5.11 should therefore be regarded a suggestion for what can be called a "worst case scenario" for the lateral force.

5.3.2 Scenario 2 Extreme - Various RCD locations

In Scenario 2E five different RCD locations are explored, exposed to both severe waves and strong currents. Scenario 2E and 2N consists of two similar cases, one "extreme" case and one "normal case", found in Table 5.6. Finding the optimal location for the RCD, where the lateral forces are small, is the objective of Scenario 2E and 2N.

Scenario 2 Extreme static

The asymmetric current profile *GoM1* is a strong hurricane generated surface current, in contrast to *GoM2* which has maximum current velocity below the surface. The resulting static displacement for the riser is illustrated in Figure 5.12. Due to the strong surface current, the vessel offset at the top is almost 2m, which would constitute a top angle magnitude of 3°. This is confirmed by simulating the equivalent case using the FEM model in Matlab. The maximum deflection point is found at 800m water depth.

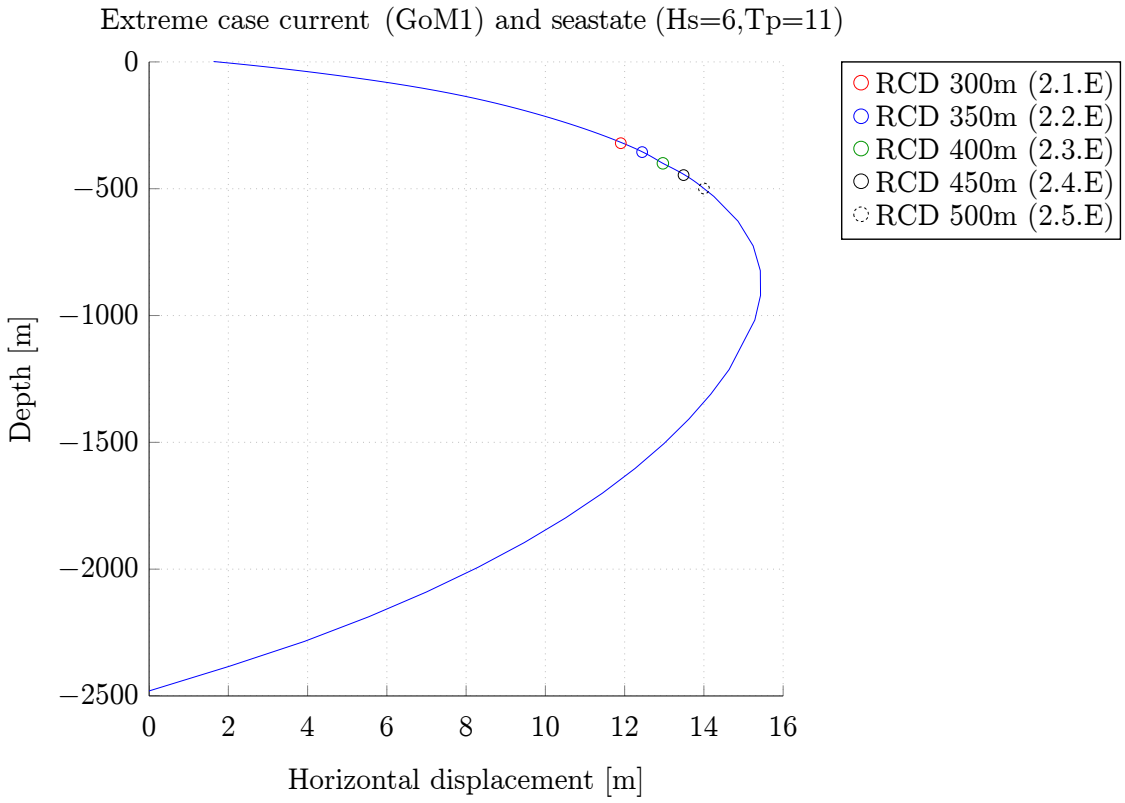

Figure 5.12: Horizontal displacement associated with current profile *GoM 1*.

Scenario 2 Extreme dynamic

Before presenting the dynamic results, a short discussion about the curvature and its impact on the lateral force is examined with connection to the theory presented in Section 5.2.

The curvature for Scenario 2E is plotted in Figure 5.13. The curvature change from 100m to 2000m is small and barely increasing before approaching the end, where the curvature increase rapidly, for eventually dropping to zero again at 2500m. Due to weight of the riser, the effective tension close to the end is substantially less compared to the top of the riser. Since the stiffness

is smaller, the curvature here can increase in magnitude, explaining the difference in curvature between top and bottom in Figure 5.13. What is important to extract from Figure 5.13 is the distance along the riser where the curvature is nearly constant. This imply that the deflection variation between the pipes is small, or that the pipes are traveling in the same direction for a long time with small change in orientation. Allowing more flexibility for the drillpipe to move around, hence making it easier to pass trough the center of the riser and ultimately the sealing element.

In other words, the longer the distance along the riser with small curvature, the better conditions for the drillpipe to move within the riser confinement and consequently pass through the center of the riser seal element where the lateral contact forces are minimal.

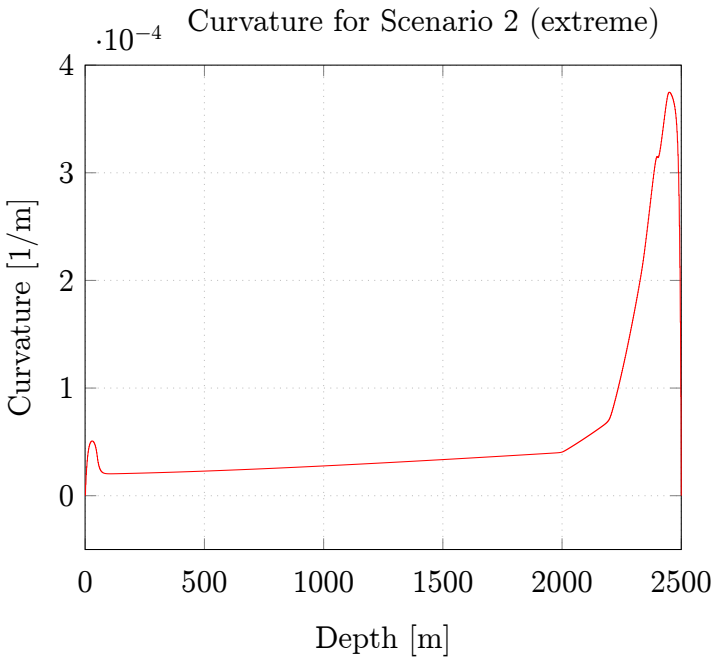

Figure 5.13: Curvature for the static displacement in Scenario 2E, with current $GoM1$.

The lateral forces for Scenario 2E in Figure 5.14, indicate higher lateral loads higher at shallower locations. At 300m the force is around 5500N, while at 500m the force have dropped to around 3500N. As mentioned above, small curvature over a long distance enforce less restrictions on the pipe leading to smaller forces at deeper locations.

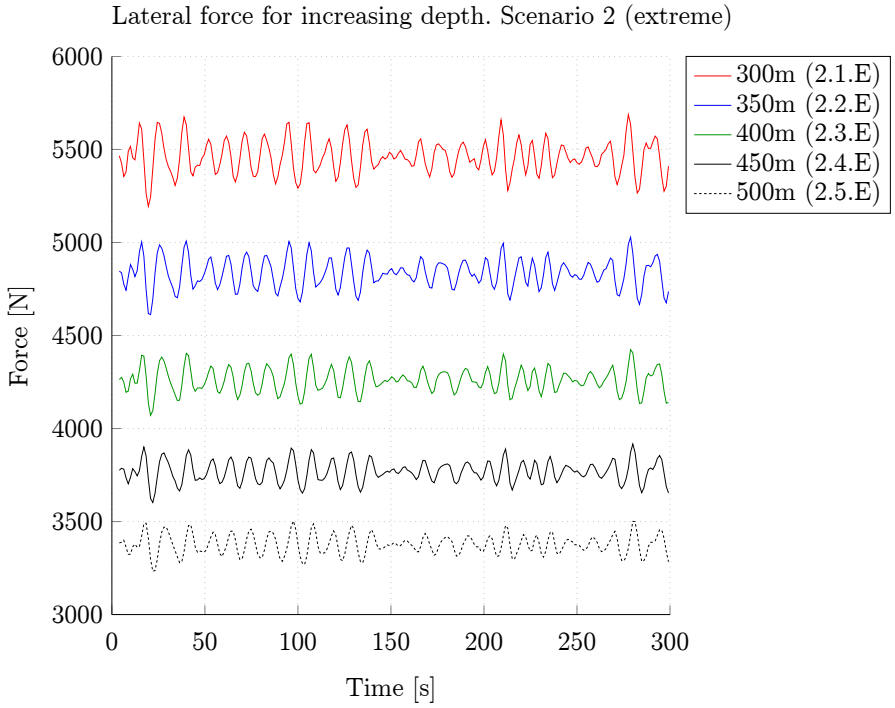

Figure 5.14: Lateral forces for RCD seal element depending on depth, exposed to strong current.

Subjected to strong current with curvature profile similar to $GoM1$, the lateral force will decrease with depth. To illustrate this further, the mean force for both sub scenarios in Scenario 2 is plotted in Figure 5.17. In both instances the decrease is almost linear from 300m to 500m. The maximum force at the different locations are shown in Figure 5.21 and Table B.1.

5.3.3 Scenario 2 Normal - Various RCD locations

Scenario 2N is a more moderate variation of the extreme case, and is intended to simulate a common summer environment for the GoM. Based on a standard case from [17], with wave heights around 1.5m, and wave periods below 8s. Similar to Scenario 2E, five different locations for the RCD are explored.

Scenario 2 Normal static

The deflection shape is more symmetric in Figure 5.15 compared to Figure 5.12 and the maximum horizontal displacement is also smaller. Since the overall displacement is smaller, the lateral forces are also expected to be smaller than in Scenario 2E.

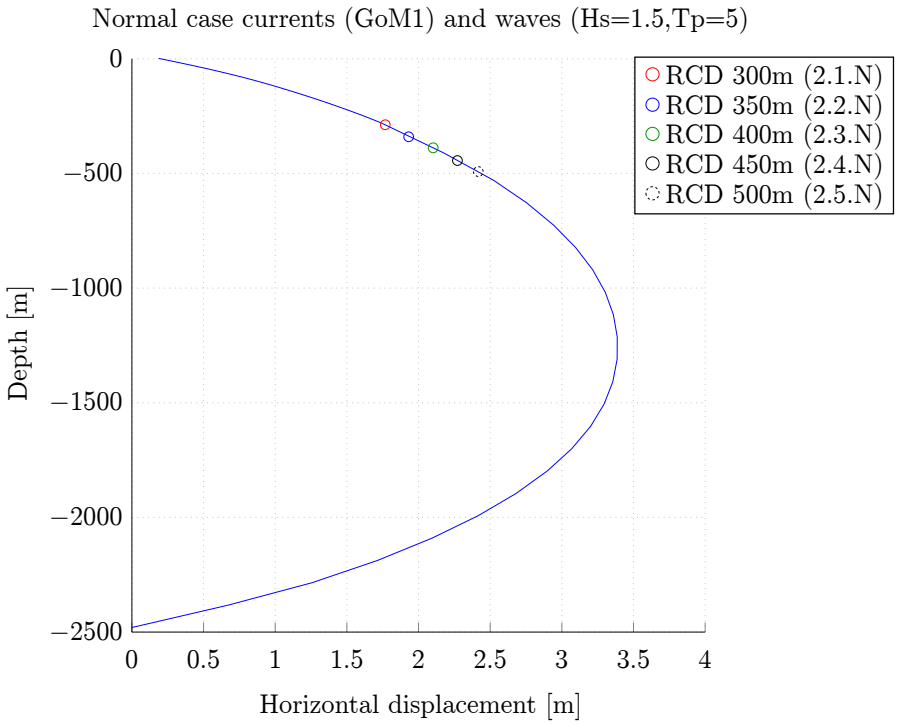

Figure 5.15: Horizontal displacement caused by normal currents ascribed to current profile $GoM1$.

Scenario 2 Normal dynamic

So far, results indicate that reduced horizontal displacement, decrease the curvature and the tension contribution from geometric stiffness. Consequently the lateral forces decrease as well, this is in agreement with the results in Figure 5.16. The wave dynamics will be more visible, due to the smaller tension. The plot also shows that the influence from the waves decrease with depth. Assuming deep water, the velocity potential for the waves at 300m is close to zero. One would therefore expect the wave influence to be smaller than observed. Reasons for this can be contribution from vessel motion, deficiency in structural damping or the simplified heave condensation model. The have compensation model, which basically is just a pipe segment with low axial stiffness, will have significantly lower efficiency compared to a more comprehensive slip-joit model.

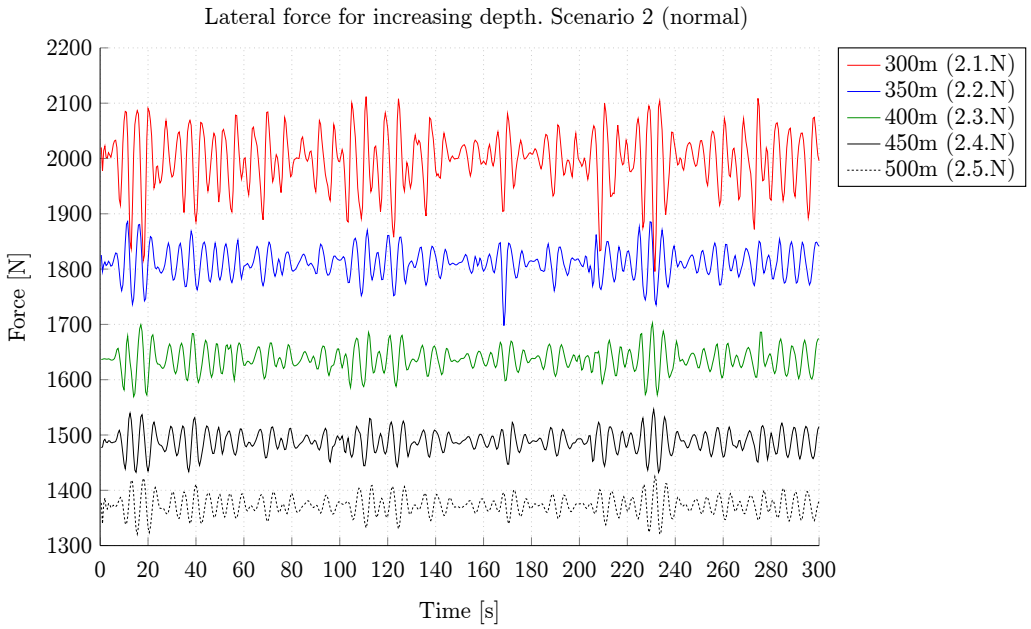

Figure 5.16: Lateral forces for RCD seal element depending on depth under normal conditions.

Comparing the results from Scenario 2E and 2N, Figure 5.17 indicates that the lateral force decrease almost linearly with depth. The maximum force for the different locations can be found in Figure 5.21. The force magnitude is, as might be expected, lower for the normal normal scenario compared to the extreme scenario.

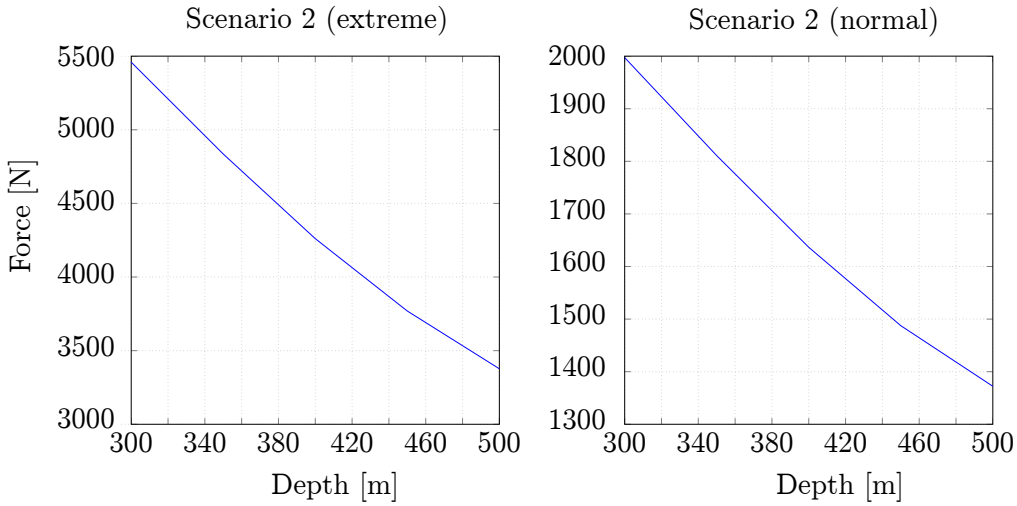

Figure 5.17: Mean lateral force for RCD seal element vs. depth.

5.3.4 Scenario 3 - Different current profiles

The purpose of Scenario 3 is to investigate influence from different current profiles. Five distinct current profiles are tested, namely the *Uniform, Bi-lateral and Skewed profile*. They are typical profiles chosen in conceptual studies and illustrated in Figure 5.7. They are simple and the results can tell much about the physics of the system. $GoM1$ and $GoM2$ are based on the 100 year return period for current originating from the well known loop currents, present in the GoM.

Scenario 3 static

The static displacements ascribed to the five current profiles, can be found in Figure 5.18. The Uniform current has the largest horizontal displacement for the RCD, followed by GoM2, GoM1, Skewed and Bilateral. The RCD vertical position is approximately 400m for the various static displacements. Indications suggest that large displacement give considerable curvature and consequently large lateral forces, the analysis carried out here will investigate this further.

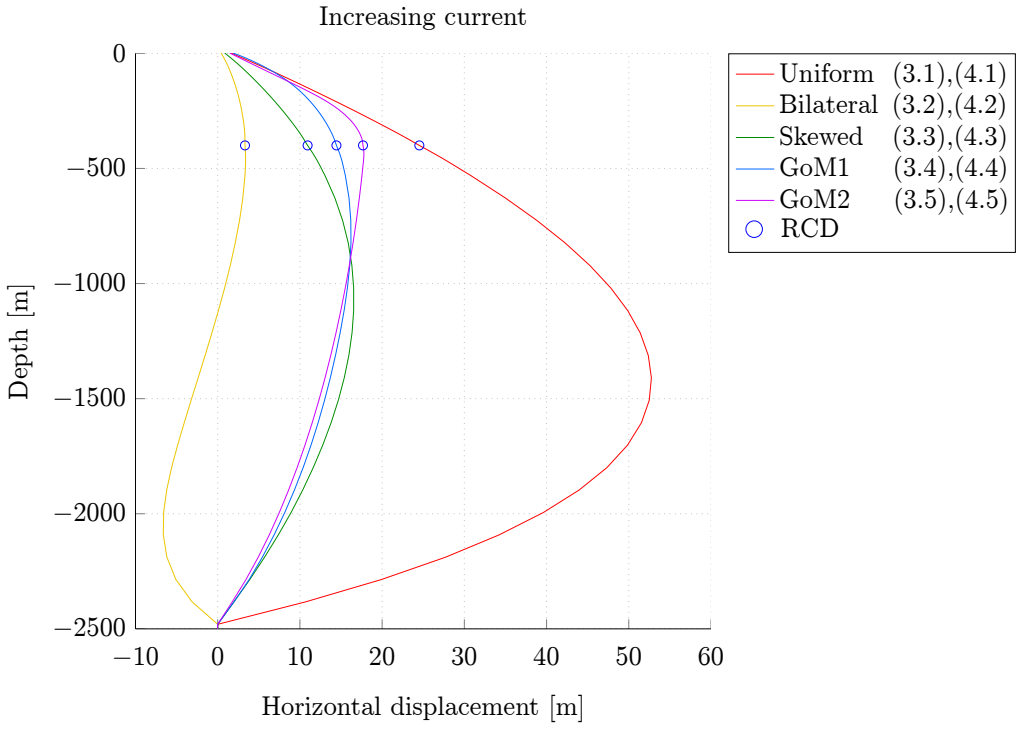

Figure 5.18: Horizontal displacement due five simulated current profiles.

Scenario 3 dynamic

The large deflections in Scenario 3 introduce more tension and reduced sensitivity to wave dynamics, which obviously is greatly suppressed in Figure 5.18. The force magnitude associated with GoM2 is clearly much higher than the other responses. The horizontal displacement is large, but still smaller than the uniform current. The key factor, leading to such high magnitudes, is the combination of horizontal displacement and curvature. The static deflection shape from Figure 5.18 indicate a substantial bending point just around 400m, creating an increase in curvature, forcing the riser and drillpipe against each other. The Uniform current has a more continuous configuration, yielding smaller curvature and hence smaller forces.

The Bi-lateral displacement curve has the smallest horizontal displacement and as a consequence the lateral force also become small. So, for Scenario 3 the maximum force envelope is in the region of 9000N and the minimum is close to 3000N.

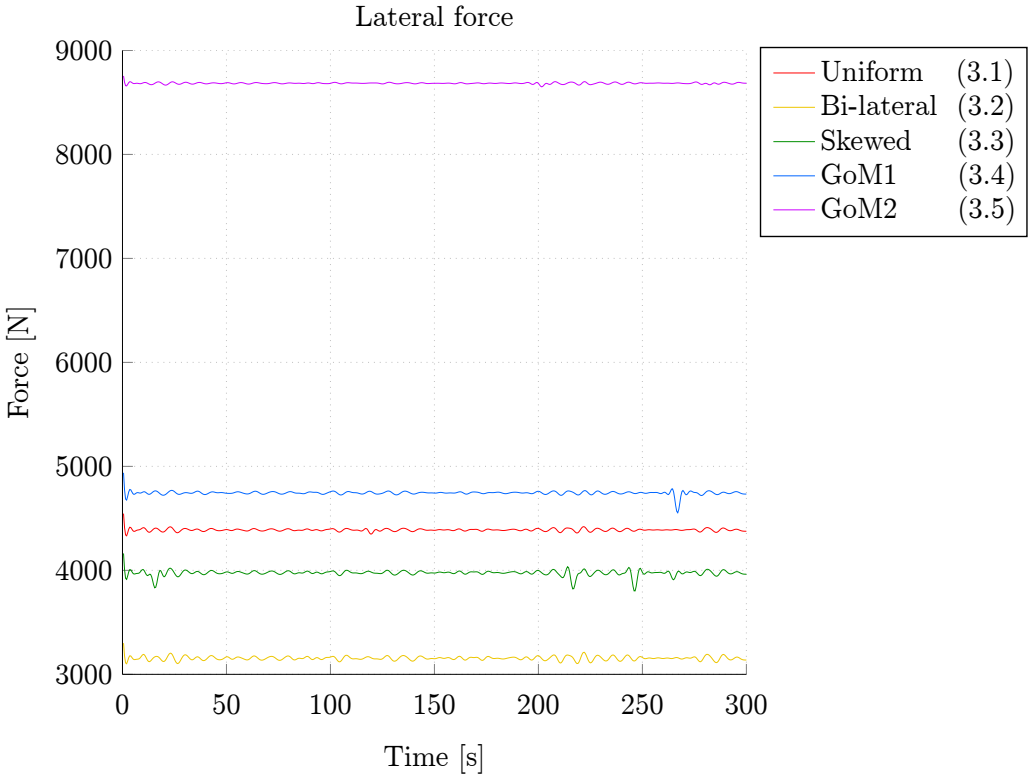

Figure 5.19: Horizontal displacement due five simulated current profiles.

5.3.5 Scenario 4 - Investigation of waves and current

Scenario 4 is, together with Scenario 2E, the most severe load environment, featuring both 100 year wave and current. The currents in Scenario 4 are the same used in Scenario 3, found in Figure 5.7. One might expect the mean lateral force to be approximately the same as in Scenario 3, but with more wave dynamics. The static displacement for Scenario 4 is the same as Scenario 3, due to the same current loading. The static riser displacement is therefore visible in Figure 5.18.

Scenario 4 dynamic

The results in Figure 5.20 are very similar to the ones obtained in Figure 5.19, but the force oscillate more due to the wave influense from the intense sea state. The effect of tension on wave suppression is visible examining the amplitude in the Bi-lateral and GoM2 signals. As emphasized earlier, the wave dynamics are not suppressed as much as a more comprehensive heave compensation system, due to the model approximation of the slip joint.

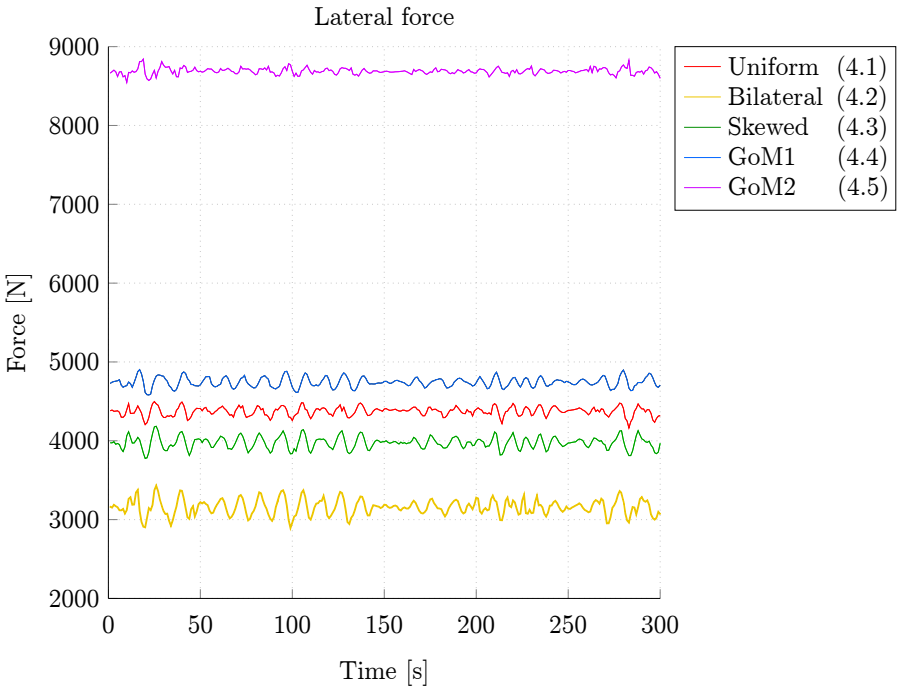

Figure 5.20: Lateral forces in extreme conditions subjected to large waves and strong currents.

5.4 Simulation review and discussion

This section will look at the entirety of the preceding simulation results and their implications for the sealing element. The simulation time used is limited to 300s. Taking into account that this is a conceptual study, the duration is considered sufficient. Also the practical aspect of computation time must be considered. Due to the extensive PIP model, a simulation time of 300s had 1week calculation time in SIMA/RIFLEX, using a time step of 0.001s. Longer time steps was later implemented, but preprocessing was necessary afterwards (refer to Section 5.1.6 for more details). The water depth was fixed at 2500m. As discussed in Section 3.3.1 the riser dynamics will vary greatly with depth and tension, and the results obtained here must be evaluated based on the specific riser properties, meaning that the results are only valid for a specific riser with given structural properties and water depth.

In total 25 separate sub scenarios where simulated in SIMA/RIFLEX, the key results are displayed in Figure 5.21, based on data from Table B.1 in Appendix B.1.

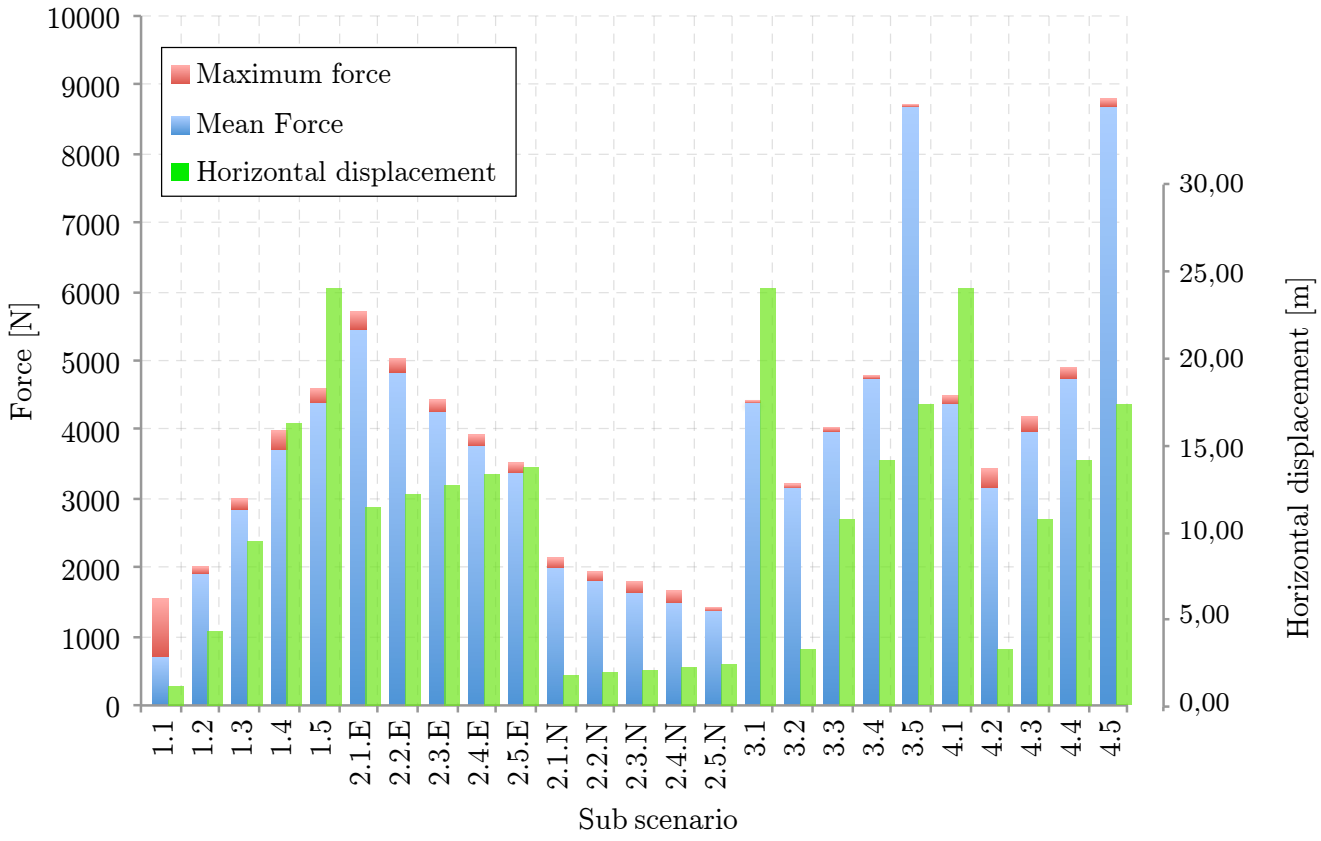

Figure 5.21: Test results for all sub scenarios.

To relate the force magnitudes obtained in the analysis, the forces are compared to the seal clamp force. The clamp force is applied to keep a tight seal around the drillpipe to ensure that there is no communication between the two DGD fluid volumes separated by the RCD. The force is acting over an area of $17300mm^2$ with 15Mpa, resulting in a total force of 259kN. The lateral contact forces are approximately in the range from 2000N to 9000N. Accepting 9000N as the maximum force, will lead to the conclusion that **the maximum force will be below** 4% **of the seal clamping force**. This will cause additional abrasion wear on the seal, but will most likely be operationally insignificant. Comparing the results obtained here to the 3400N force obtained from the hand calculations in Appendix A.1, indicate that the force magnitudes are reasonable.

5.4.1 Parametric discussion

Changing important parameters such as water depth and tension will have considerable implications for the overall riser behaviour. On the basis of the SIMA/RIFLEX analysis, this discussion will try to relate the observations to tensioned beam behaviour discussed in [35] and [37], and explore implications for lateral loads.

The concept study for this particular riser is confined to deep water around the GoM. The water depth is expected to vary from 2000-3000m. There is no doubt that shallow water is easier to operate in, compared to deep water. Deeper waters will make the riser behave more like a cable, with less influence from bending stiffness (EI), resulting in more behavior dictated by tension and curvature. In deeper water the drilling riser would become more sensitive to current profile due to length of the riser and the limitations of top tension available would result in riser deflections and angle magnitudes becoming larger, possibly causing more fatigue [16]. Due to end effects (forces generated by the support conditions at the top and bottom of the riser) the curvature will be larger close to the riser supports, this can be seen in in Figure 5.13. Since the riser tension is smaller towards the lower section, the end effects can dominate and cause larger deformations. This results in higher curvature magnitude at the bottom of the riser. A more flexible riser would also be more prone to VIV problems [27]. In terms of the modal model developed in Chapter 3, a longer riser will urge the need for incorporating higher modes [7].

The drag coefficient used in the simulations is set to $C_d = 1$ which is conservative, compared to what is used in [37]. This means that the drag force likely is larger than what would be true in a more physically correct context. Resulting in larger deformations and horizontal displacement.

5.4.2 Key observations

Several key observations can be made based on the preceding sections and the comprehensive plot of the lateral forces in Figure 5.21. The most essential are collected in Table 5.7.

Observation	Description
Lateral force and horizontal displacement.	Increased horizontal displacement gives larger curvature and consequently larger lateral force.
Curvature change over distance	Pipes traveling in the same direction (over a long distance) with small change in orientation, allow more flexibility for the drillpipe to move around, making it easier to pass trough the center of the riser and ultimately the sealing element. Leading to smaller lateral forces. The results from Scenario 2 indicate that the lateral force decrease almost linearly with depth.
Tension, displacement and wave influence	Large deflections force the riser to stretch. Resulting in increased geometric stiffness and tension. This rigidity suppress the wave influence on the riser, because the the magnitude of the tension dominate the system.
Optimal locations for RCD based on lateral force simulations	Deeper is better regarding wave influence, since the wave potential decrease with depth. Also in cases where change in the curvature conditions are not changing fast over short distances, the best location (where the forces are small) will be at the centre of this zone. Keeping in mind that also the curvature below the location influence the force. Dictating that a suited location is far away from curvature end effects. So, one may also conclude that, in cases where the curvature is increasing fast along the riser, shallower can be better.
Curvature at top and bottom	The curvature is always large at the top and bottom of the riser due to end effects [37], and is therefore not a suitable location for internal seals, such as the one accommodated by the RCD.
Worst case	The combination of large a curvature change region supplemented by large horizontal displacement will give the highest loads. This occur to some degree in Scenario (3.5) and (4.5).

Table 5.7: Key observations from SIMA/RIFLEX analysis.

Chapter 6

Control of local and global riser response

Most research in the field riser control focus on the upper and lower flex joint, stress concentrations and tension measurements as control objectives. Submerged drilling equipment such as the RCD adds additional requirements to the riser integrity for handling control of intermediate locations along the riser length, i.e. local control of the riser. Before local control can be considered the global integrity of the system must be guaranteed, calling for a combination of local and global control. Additional equipment attached to the riser, at submerged locations, will be sensitive to a range of resonance phenomena originating from the rig/vessel motion, waves, current and VIV giving rise to large motions along the riser. The resonance characteristics of the riser system is reflected in the modal frequencies, which then can be exploited by riser control system to avoid unwanted excitations. A closer study of the resonance sensitivity is therefore needed and is addressed in Section 6.3.4. Extending the riser control to attenuate dynamic behaviour can help reduce damage and fatigue, and additionally increase the safety and operational margins. Exploiting the modal properties of the riser, this chapter aim to explore and develop control guidelines and objectives for control of local and global riser response. Achieving this can be done through rig/vessel motion, manipulation of top tension and static offset. Controlling the modes using dynamic rig/vessel motion will have physical limitations for the higher modes, due to the accelerations required to achieve the corresponding modal frequencies. However, the restraints between the achievable and non-achievable modal response exist and will be investigated. The simulations and analysis will be based on the two-dimensional riser models (FEM and Modal) in Matlab/SIMULINK. Given the dual gradient configuration presented in this thesis, an optimal location (inline on riser) for the RCD unit must be selected. Using the experiences from Chapter 5, an evaluation of the optimal location is carried out based on curvature and operational aspects connected with drilling.

The first part will consider the most important factors for riser dynamics relevant for localizing the RCD. Topics applicable for riser control is also covered. Next, a sensitivity study of the resonance dynamics using low frequent rig/vessel motion is carried out. The riser specifics is similar to the one used in SIMA/RIFLEX, applied to the Matlab framework. Finally, control strategies and guidelines are presented for global and local control of riser behaviour using the modal components as a basis.

6.1 Riser dynamics relevant for RCD installation and control objectives

In order to evaluate application of riser control and find an optimal RCD location, some fundamental principles in riser dynamics are presented. Building on the theory presented in Chapter 3 and the results obtained in Chapter 5, this section will focus on the structural aspects relevant for controlling riser shape/geometry and the influence on the RCD location.

A drilling riser can be modelled as a slender tensioned beam with transverse loads, acting due to the effects of hydrostatic and hydrodynamic pressure [31]. For the case with constant bending stiffness, the *tensioned beam equation* can be written as follows,

$$EI\frac{d^4u}{dx^4} - T\frac{d^2u}{dx^2} - w\frac{du}{dx} - q(x) = 0, \tag{6.1}$$

where EI is the bending stiffness, T is the tension, w is the apparent weight per unit length, $q(x)$ is the applied load distribution, x is the longitudinal coordinate (along the beam) and u is the transverse displacement. For the special case of constant tension (i.e. for $w = 0$), the weight term w can be neglected, and Equation (5.2) in Chapter 5 is obtained. Chen, in [5], presents a more elaborate and accurate description of the riser is given, taking into account varying flexural rigidity, axial force and mass density (i.e. $E(x), I(x)$), resulting in a more accurate description of a deep water drilling riser. However, the dynamics studied in this thesis will use the definition formulated in Equation (6.1) discretized over the riser length, to account for these variations. This results in the development of a FEM model in Matlab/SIMULINK, where the approximations in Equation (6.1) can be justified when the element length is sufficiently short. However, the fact that the terms in reality are non-constant will in part account for the complex dynamic response that can be observed in more physically correct models.

From this point, the fourth order differential equation for tensioned-beam deflection and curvature in Equation (6.1), set in FEM perspective, discretized using elements, is assumed to describe the dynamics of the drilling riser.

6.1.1 Natural periods

The natural periods are the fundamental frequencies associated to the undamped harmonic transverse vibrations of the riser structure. The mode shapes represent the waveform connected to a given natural period. Natural periods for drilling risers are generally dictated by two important factors; top-tension and length. Using the tensioned beam formulation to describe the riser, the natural periods can be approximated. Considering the riser to be a vertical beam with constant tension, the natural periods T_{p_n} (for mode "n") are defined in [38] as,

$$T_{p_n} = \frac{2\pi}{\omega_n} = \frac{2L/n}{\sqrt{\frac{T_t}{m} + [(\frac{n\pi}{L})^2\frac{EI}{m}]}}, \tag{6.2}$$

where ω_n is the angular frequency, L is the length, n is the mode number, T_t is the top tension, m is the mass and EI is the bending stiffness. A lot of information can be obtained from Equation (6.2), which already has been observed in Chapter 5. Increasing length will tend to reduce the influence form the bending stiffness, increasing the natural periods. Top tension will be the governing factor deep water, increasing top tension will greatly decease the natural period. Bending stiffness will have small impact at low modes, for higher modes the bending is larger and consequently the influence of the term. Adding mass to the system will increase the natural period, e.g. increasing

mud density, adds mass, but no stiffness.

For deep water risers, the situation is a bit more complicated. Rather than having constant tension, an effective tension is acting over the riser length, which accounts for buoyancy and weight. Due to this asymmetrical distribution of tension, the periods and mode shapes deviate from the results obtained in Equation (6.2). Yielding non-trigometric mode shapes, with greater amplitudes toward the end of the riser where the tension is smallest [36]. Additionally, the damping will vary along the riser, due to the current speed and the local amplitude and frequency. However, since no reliable estimate of the damping can be obtained a priori, the damping could just as well be set to a precalculated constant value [27]. The mode shapes, obtained numerically from the Matlab/SIMULINK model, cannot be expected to be exactly identical to the true physical mode shapes, but constitute the "best" a priori approximation available. Considering the dynamical aspects, a natural mode will dominate the overall behaviour of the system. When the frequency of the imposed force, is tuned to one of the natural frequencies of the elastic system, large responses are generated producing resonance [7]. It is therefore important that the drilling riser should be designed and the top tension selected, based on the anticipated environmental frequencies as well as the functional requirements. As emphasised earlier, submerged equipment will be sensitive to a range of resonance phenomena originating from the rig/vessel motion, waves, current and VIV giving rise to large motions along the riser. To get a sense of the frequency range the riser operate in Figure 6.1 display the most important periods associated with common marine systems.

As illustrated in Figure 6.1, the period range from swell, semi submersible and the bandwidth of the DP system are overlapping. Indicating that resonance effects can emerge from interaction between these systems. E.g. a moored structure can display large amplitude low frequent motion, medium amplitude wave frequency motion and small amplitude, very high frequency vortex induced vibrations [48]. A moored system supplied by DP capabilities can reduce the motion characteristics and "tighten" up the system, but will not remove the influence completely. Low frequent motion like this will be transported to the riser and can in some instances lead to resonance. Knowing the modal characteristics of the riser, the marine unit and DP system can be controlled to alter the riser behaviour, moving the riser out of the sensitive frequency range. Leading to the notion that, proactive control of the DP system can be used to handle undesired dynamic riser response. Moreover, if it is desired to control riser geometry, one possible approach would be triggering a relevant mode, or modes, which constitute to the appropriate geometry. This will be investigated more in Section 6.5.1. However, deliberate resonant control is not structurally healthy considering factors such as fatigue.

Low frequent motions can come from several sources, moored structures are already mentioned to have resonance oscillations in the horizontal plane, but all six DOFs can be effected. For instance a freely floating structure with low water plane area will be sensitive to slow drift motions in heave, pitch and roll. Slow drift motions are resonance oscillations excited by non-linear interaction effects between the waves and body motion [11]. Current, wind, mooring and risers also contribute to the resonance dynamics. Having a small water plane area will result in low damping properties, consequently large motions can occur. Typical natural periods for this phenomena can reach as high as 2min, which in typically in domain of mode 1 for deep water risers.

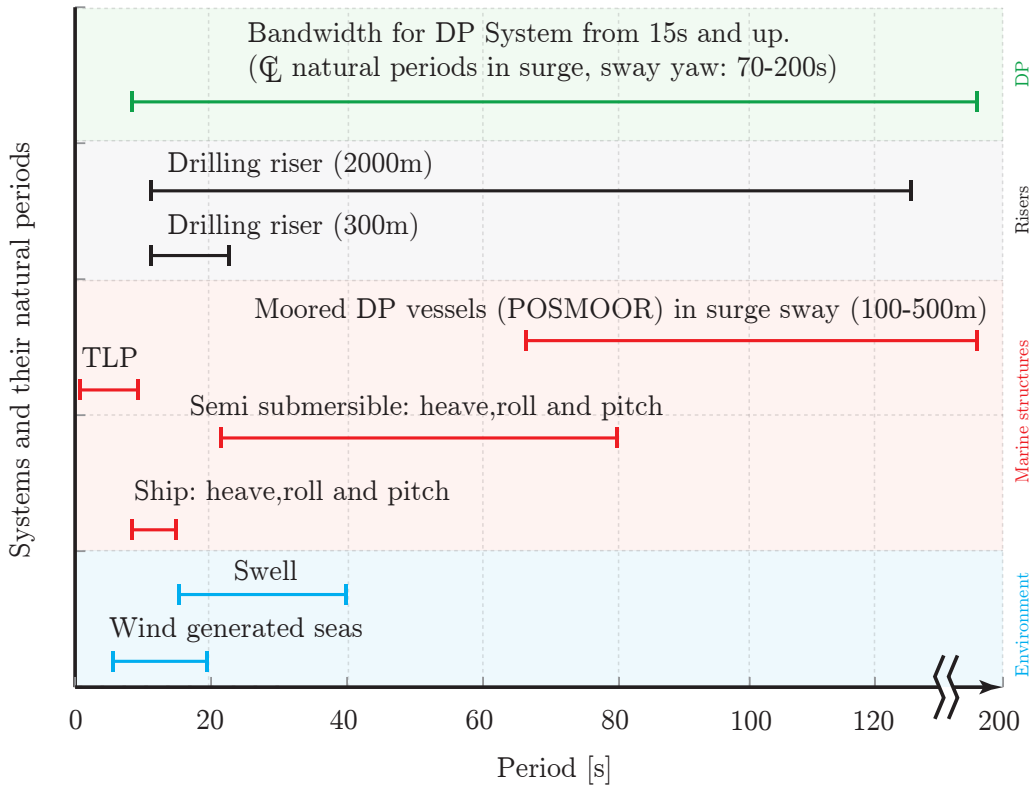

Figure 6.1: Different periods of interest for marine vessels and structures.

6.1.2 Vortex induced vibrations (VIV)

A short introduction to VIV is provided to support the interpretation of the forthcoming material. The VIV theory presented her is based on material covered by Larsen, Zhao and Lie in [29] and [30].

The drilling riser is a slender marine structure with eigen frequency f_0, given in still water. Subjected to ocean currents, flow conditions around the riser will create an alternating pressure field. This pressure originates from vortices that are shed on both sides of the pipe structure. The vortex shedding subsequently cause the riser structure to vibrate, hence the expression "vortex induced vibrations". The vortex shedding period T_{sh} is the full periodic cycle between the shedding of two vortices, one on each side of the cylinder. This is exemplified in Figure 6.2.

The riser trajectory for the centre point is seen marked red in Figure 6.2. Bearing geometrical resemblance to the shape of the number eight (lemniscate) the riser oscillate both inline and transversal direction, due to the interaction between the lift and drag force. These forces arise from the dynamic pressure distribution created by the flow conditions. The cross flow vibration amplitudes, created by lift forces, are larger compared to the inline amplitudes, created by drag forces. Due to this, cross flow is therefore usually the most relevant. Additionally, the frequencies

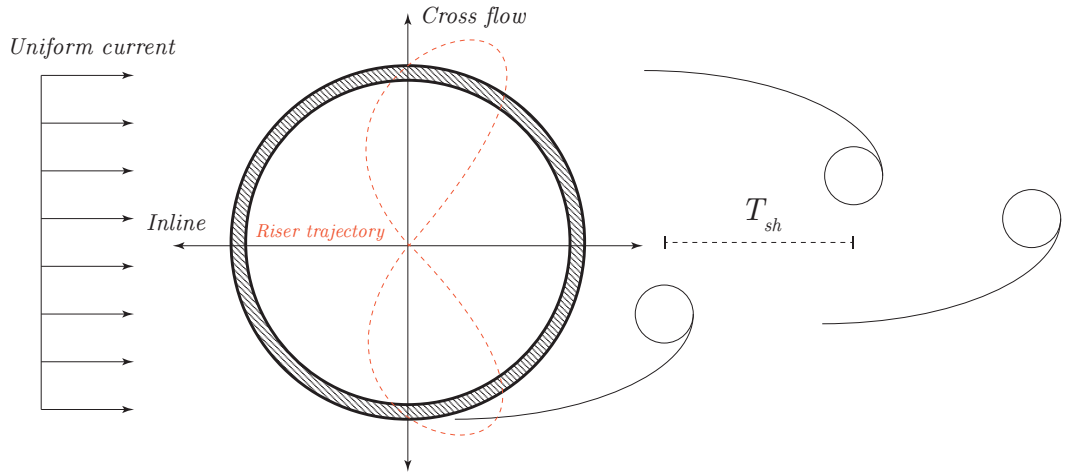

Figure 6.2: Vortex shedding and resulting motion.

for inline drag vibrations are twice that of the cross flow lift vibrations, $2f_{cf} = f_{il}$, causing the structure to oscillate in inline direction at lower current speeds. One condition necessary for cross flow vibrations to occur, is that the vortex shedding frequency f_{sh} is close to an eigen frequency of the structure, $f_{sh} \approx f_0$. From [29] the vortex shedding frequency is given as,

$$f_v = \frac{St \cdot U}{D}, \tag{6.3}$$

where St is the Strouhal number, U is the current velocity and D is the outer diameter. The Strouhal number changes with Reynolds number defined as

$$Re = \frac{UD}{\nu}, \tag{6.4}$$

where ν is the kinematic viscosity. The Reynolds number is a dimensionless measure that is used to characterise different flow regimes. Laminar flows (fluid flows in parallel) occur at low Reynolds numbers, while turbulent flow (chaotic flow) occur at high Reynolds numbers. The Strouhal number has a constant value of around 0.2 in a large region of the Reynolds number, and is therefore often approximated to be this value.

To conduct a diagnosis of the potential risk for VIV occurrence a general requirement is often used as a guideline. Assuming that Strouhal number is 0.2 and that cross flow vibrations occur when the vortex shedding frequency f_{sh} is close to an eigen frequency of the structure, $f_{sh} \approx f_0$, Equation (6.3) is rewritten to obtain

$$U \geq 5Df_0. \tag{6.5}$$

This gives an approximate value for the fully developed cross flow vibrations [29]. Based on this, the potential occurrence of cross flow VIV can be evaluated for given current velocities. For clarification the the term "VIV" will be related to cross flow VIV for the rest of the thesis.

6.1.3 Curvature

Pointed out in Chapter 5, the curvature is related to the "sharpness" of bending, e.g. a small circle will have larger curvature than a big circle. Large riser curvature will impose restrictions on the internal drillpipe which translates into horizontal forces. Finding an optimal location for the RCD, and indirectly the seal element, is thus closely connected with curvature. The beam curvature (denoted as κ) is defined according to the *Bernoulli deformation theorem* in [23] as,

$$\kappa = \frac{M_m}{EI} = \frac{d^2u}{dx^2}, \tag{6.6}$$

where M_m is the bending moment and $u(x)$ is the deformation at location x along the beam. In [38] the riser moment is defined as always continuous, hence the curvature must also inherit that property. From Equation(6.6) it is evident that large moment will give large curvature magnitude. Again from Chapter 5 there was a strong connection between the deformation and the curvature size, giving substance to the statement. Also stressed was the curvature change over distance, or the curvature rate. The curvature rate will also affect the lateral force between the riser and drillpipe, and thus influencing the determination of the RCD location and the control guidelines. Obtaining the correct curvature can be a challenge due to differentiation and element length, of already approximate models, leading to imprecise results and discontinuities. The curvature for the mode shapes is calculated using the `diff`-function in Matlab, yielding an approximate curvature solution based on differentiating the displacement twice. While, the Matlab/SIMULINK model is based on the *Hermite interpolation polynomials*, rendering a more accurate result in terms of geometric accuracy. However, due to the long element length and the validity of Euler-Bernoulli beam theory, corrections must be implemented, which again leads to approximate curvature results. The level of curvature accuracy obtained from these approaches is considered acceptable for conceptual studies.

One approach for finding an optimal location for the RCD, only considering lateral forces, would be to seek for the sector on the riser with the lowest curvature magnitude and neighbouring curvature rate. The principles from modal decomposition formulates that the resulting displacement as a sum of the fundamental riser mode shapes. Assuming, that mode 1 to 5 are equally likely to be excited, an approach to find the ideal location would be to use the modes as basis. Since the contribution to the modal response is not unimodal, but rather shifted towards some distinct modes dependent on the environmental load frequency, some modes are more prone to contribute more than others. E.g. in [14], the full-scale measurements indicated that mode 2 was the "leading frequency", given the particular load conditions and riser parameters. Local load frequency conditions must therefore be considered and the governing modes be used as the basis, for the approach to be successful. Regardless of this, an approximation for conceptual purposes can be made, to give a suggestive estimate before conducting laboratory experiments. A more comprehensive discussion about mode selection can be found in [27] and [18]. The results indicated that modes up to the fifth could occur, the fifth only on rare occasions. Also the notion that higher modes will have a tendency to dissipate more energy and therefore have a higher damping capacity, will point to more expected influence from the lower modes. Assuming that the lower modes are more likely to contribute, a study of the curvature and curvature rate from mode 1-5 is conducted. To enquire into the possible implications for the lateral force and consequently the RCD location.

6.2 RCD location assessment

The overlapping periods in Figure 6.1 suggest that modes, with periods higher than 15s can be excited by low-frequent motion originating from slow drift motion, low frequent DP oscillations, swell seas and in some cases wind driven seas. Motivated by this, the mode shapes is used as a basis for exploring the suitable locations for the RCD unit, when subjected to the characteristic system periods in Figure 6.1. A study of the 2500m riser used in the SIMA/RIFLEX analysis in Chapter 5 is carried out, considering the mode 1-5 as basis for isolating the best suited locations for the RCD, focusing on lateral forces. Other elements relevant for the location of the RCD equipment, such as drilling operational factors and economy will only be handled in brief, where relevant. From a DGD standpoint, approximately 300m is required for achieving the appropriate hydrostatic pressure, RCD locations above this limit is therefore not relevant.

Since both location and control aspects are important, different boundary conditions need to be considered for each separate case. The riser will therefore use two set of mode shapes, illustrated in Figure 6.3. E.g. the introduction of a prescribed force, when considering the control using a moving rig/vessel, requires new support conditions necessary to represent the problem.

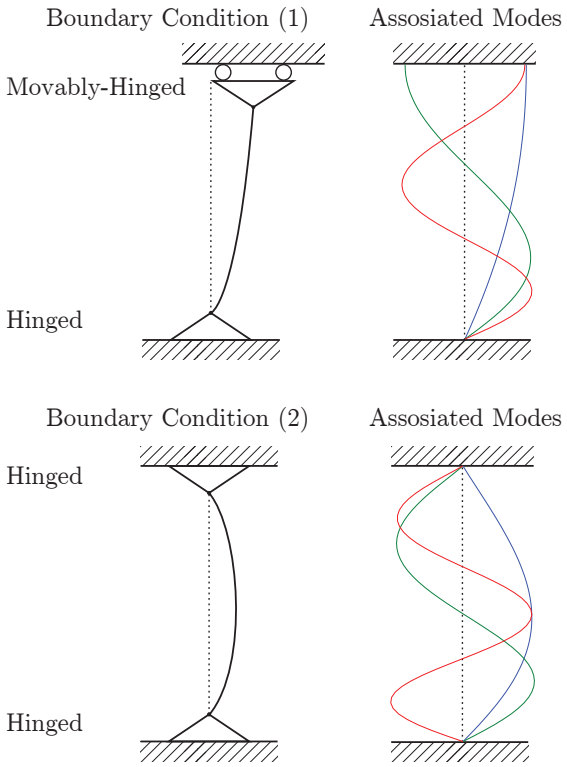

Figure 6.3: Different boundary conditions and their associated modes.

The first, Boundary conditions (1) in Figure 6.3, assumes free translation at the top, comparable with a riser connected to a moving rig, applicable in control. The other , Boundary conditions (2)

in Figure 6.3, is hinged in both ends, comparable with a riser connected to a rig conducting DP drilling operations, applicable for RCD location. Since the purpose in this chapter is to investigate possible locations for the RCD, the mode shapes associated with boundary conditions (2) in Figure 6.3 will be applicable.

6.2.1 Curvature considerations

Mode 1 to 5 and their respective curvature are displayed in Figure 6.4. For illustrative purposes the curvatures are scaled, so that they can be displayed next to the mode shape. Note that they are scaled separately. All modes are non-trigometric, and have maximal modal deflection towards the lower end. Consequently the loads acting towards the lower end will have greater modal contribution potential. This is expected, since the effective tension is smaller towards the lower end of the riser. Each mode constitute a realization of a distinct load pattern. E.g. load distributions such as uniform current will match the displacement form of mode 1. While bi-lateral current will be be compatible with mode 2. Keeping this in mind, complicated load distributions resulting in displacements shapes such as connected to mode 5, is very uncommon. Again emphasizing the occurrence of lower modes as supposed to higher modes and the need for knowledge concerning the local metocean parameters for current. For example the static displacements obtained in 5 Section 5.3, owing to the current profiles $GoM1$ and $GoM2$ from [17], showed contribution from mode 1 and 2. However, VIV effects can initialize higher modes and have several frequency components active over the riser, this is assumption is based on material presented by *Larsen et al.* in [30]. In this thesis, VIV is considered a fatigue problem with modest amplitudes, deemed unavoidable and of less importance to static lateral forces and seal element. However, fatigue can influence the location if the dynamic aspects are considered, but since a priori estimates are hard to assess, a static approach is the "best" approximation.

To give a more accurate picture of the modal curvature and their magnitude the plots in Figure 6.5 is provided. The curvatures, which now are not scaled, are superimposed and color coded to each mode. The sections where the overall curvature magnitude is small is labeled with *zone 1-7*. These zones coincide closely with the modal curvature nodes for each mode. To find the location with the expected lowest curvature, will again depend on the assumption of which modes are most likely to contribute to the modal response at the designated location, in addition to the neighbouring curvature rate. Based on the overlying assumption of only considering mode 1 to 5, this thesis evaluate the modal contribution in three different ways:

Option 1: **All modes are considered equally likely to contribute** (Figure 6.5 (a)). If this is the case, *zone 2* is the most sensible location. Due to the many unpractical consequences of installing the RCD in *zone 1* at 2050m.

Option 2: **Considering mode 5 to appear only on rare occasions** (Figure 6.5 (b)). This choice is based on the conclusions made by Kaasen and Lie in [27]. Under this assumption, *Zone 5* would be most sensible choice. Again, due to the depth of *zone 3* and *zone 4*. *zone 5* stretches 300m from about 550m to 850m below the surface.

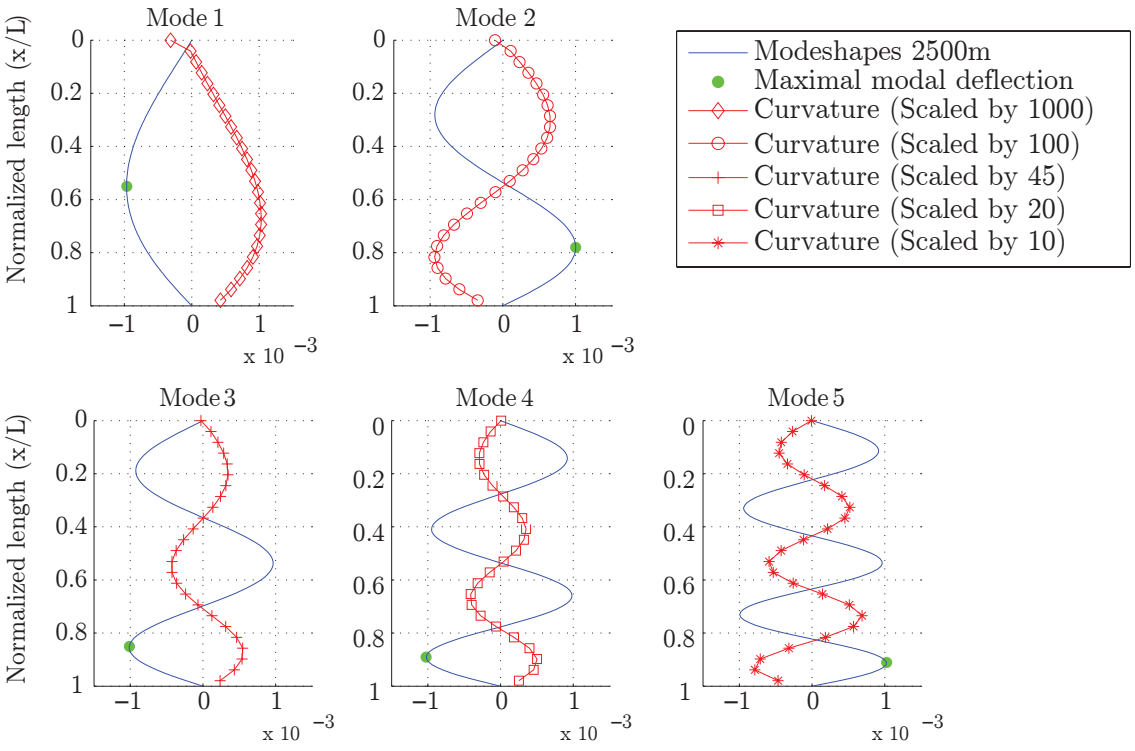

Figure 6.4: All five modes and their corresponding curvatures.

Option 3: **Assuming mode 1 - 3 to be the governing modes** (Figure 6.5 (c)). Based on this, *zone 7* will be the most evident choice, again due to impracticalities of installation and cost of more depth robust equipment.

All in all, *zone 1,5 and 7* are the main sectors of interest, due to other zones being located in far greater depths necessary for the DGD operating scope. In addition such depths would require expensive, robust and depth resistant equipment. Based on the analysis conducted here, the section spanned by *zone 1,5 and 7* from 400m to about 1000m, are the most suitable. Considering curvature magnitude and depth limitations.

6.2.2 Curvature rate considerations

The curvature rate is the change in curvature over distance. Evaluating this for each section can help to narrow down this first location estimate. The curvature rate for each mode is presented in Figure 6.6. The curvatures are scaled up, to be more presentable. The term "zero crossings" is used to describe the locations where the curvature rate is small and close to zero. The sudden discontinuity at the top originates from artefacts from differentiation of the simplified mode shape,

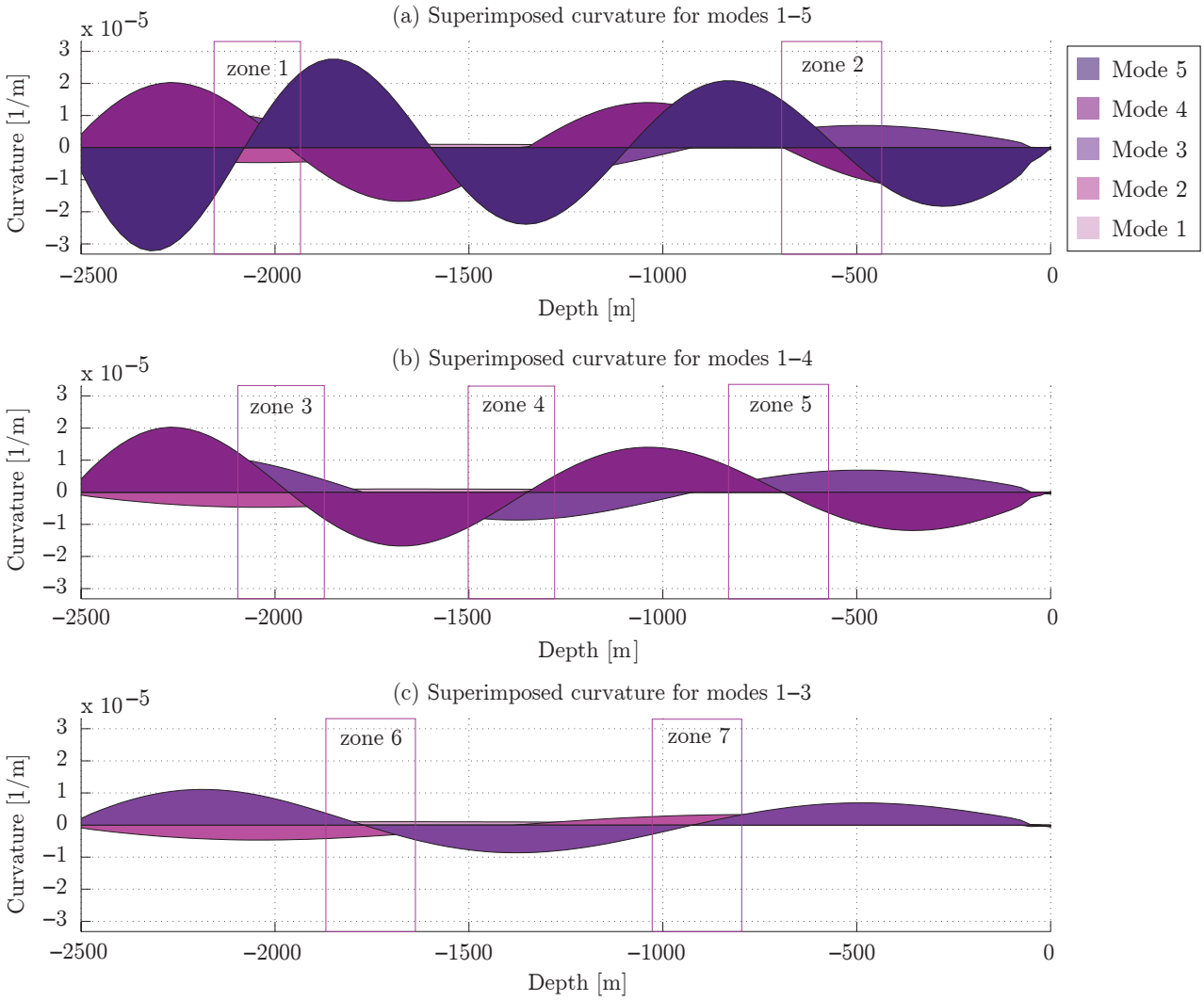

Figure 6.5: Modal curvature zones.

these point are outside the region of interest. Considering that the curvature rate of mode 1 is practically constant, concern will be on the four remaining modes. The region deemed suitable for the DGD configuration is from 300 to 600m, based on equipment durability and robustness. Operating outside this region would be considered impractical, due to the hydrostatic column needed for the DGD system and the increase in robustness going into deeper water, e.g. mud diverting pumps would need to be revamped.

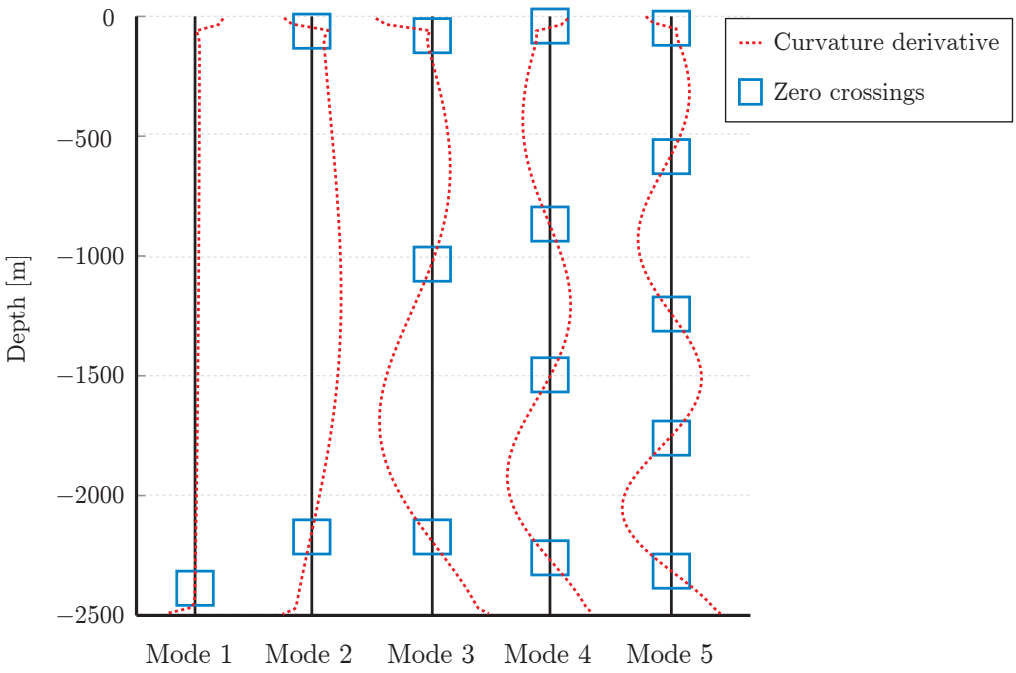

Figure 6.6: Curvature rate for modes 1 to 5.

Assuming the mode distribution in ***Option 1***, mode 3,4 and 5 have minimum points at 1000m, 875m and 625m. Mode 2 will have slowly increasing curvature rate, favouring shallower locations. Leading to the notion of a suitable location in proximity of 625m. This location assessment is labeled ***Region 1.***

Assuming the mode distribution in ***Option 2***, more emphasis will be directed towards the lower modes. Leading to a more complex assessment. The curvature rate of mode 2 is nearly constant, suggesting mode 3 and 4 are governing. Now that mode 5 is trivial, the minimum points for mode 3 and 4 at 1000m and 875m are at the limits of the applicable section, deemed suitable considering curvature magnitude. This would be outside the DGD restraint, leading to a preference for shallower locations. The curvature rate of mode 3 between 400 and 1000m, is at a maximum at about 600m, favouring sections above this depth. The same tendency can be seen in the curvature rate for mode 4, which is slightly more evenly distributed. The totality of this leads to a region in proximity of 400m. This location assessment is labeled ***Region 2.***

Finally the mode distribution in ***Option 3***, will be considered. As stressed in the above paragraph, mode 2 will have nearly constant rate, leading to mode 3 and 4 as dominating elements. Since mode 4 is neglected, mode 3 is again the governing factor. Leading to the same conclusion as above, namely ***Region 2***.

6.2.3 RCD location review

Taking curvature and curvature rate considerations into account, the only region within the assumed operating region for the DGD system is ***Region 2***. It will be stressed here that this is a region, which means that locations about ***400m*** $\pm$**50*m*** are suited to accommodate the RCD. A deviation of about $\pm$50m can be considered reasonable, which is approximately two times the length of the elements used by the Matlab/SIMULINK model.

The analysis carried out here is mainly based on static assumptions. Dynamic aspects are, as pointed out in [27], harder to asses when no solid a priori information can be obtained about the expected load distribution. This can also be forwarded to damping which depends on the current speed. For the local considerations in the GoM affecting locations close to 400m, the cold currents such as current profile $GoM2$ will become the "worst case". With a maximum current speed at 250m the local curvature in the whole top section of the riser, will be severely affected. In this case, deeper locations could be considered safer, but again the unaffected regions would be deeper than the practical scope for the DGD setup. For the the wave dynamics affiliated with deep locations in GoM, the influence is deemed small at this depth.

6.3 Dynamic analysis of riser resonance sensitivity to low frequent rig/vessel motion

Now that a suitable region for the RCD equipment is identified, a dynamic analysis of the riser resonance sensitivity is carried out using the FEM and modal model in Matlab/SIMULINK. The aim of the analysis is to confirm that low frequent motion, similar to that originating from slow drift motion of a rig/vessel can excite distinct modes. Additionally, the modal information is evaluated in light of application in potential control systems. Since the rig now is free to move in the horizontal plane the boundary conditions needs to be changed to replicate the physics. Therefore boundary condition (1) from Figure 6.3 is used. The simulation model is the 2500m SIMA/RIFLEX riser used in the previous sections. The results obtained from these simulations are important for the evaluation of the possible control strategies developed in the succeeding section.

6.3.1 Eigenperiods

In the dynamic analysis the rig/vessel is allowed to move freely in the horizontal plane, and hence the support conditions correspond to boundary condition (1) in Figure 6.3. As mentioned in the introduction to this chapter, the probability of exciting higher order modes such as mode 4 and 5 is limited, due to the acceleration associated with the modal frequency. Mode 1,2 and 3 have lower modal frequency and are within the boundary of what is plausible to excite with rig/vessel motion. The eigenperiods for the drilling riser used in this thesis (found in Table 5.2), is displayed

in Figure 6.7. Note that eigenperiod correspond to both the natural period and the modal period.

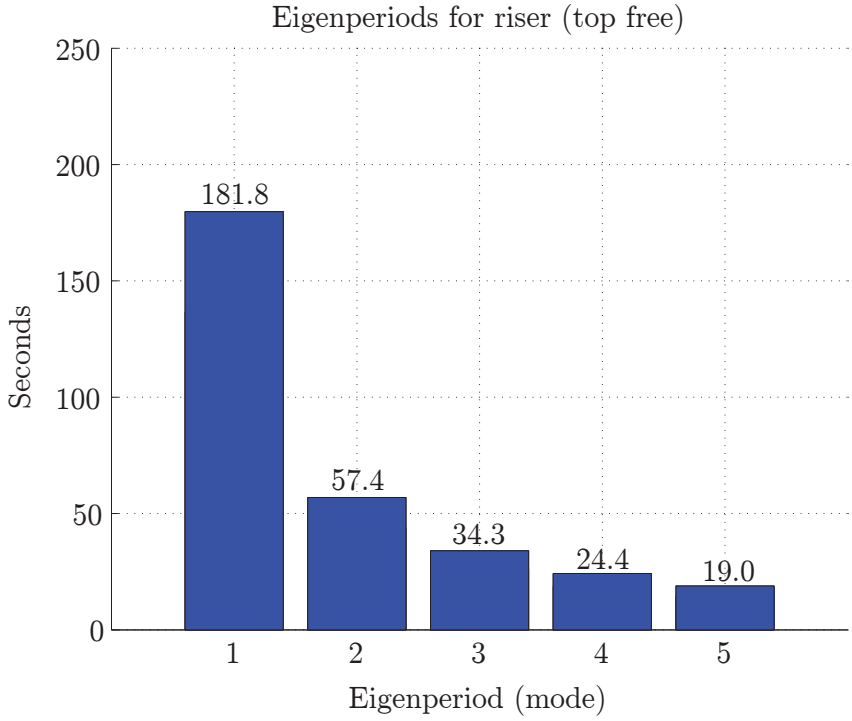

Figure 6.7: Eigenperiods for riser (2500m and top free).

6.3.2 Rig/vessel motion

Based on the material in [11] and [48], the low frequent motion is synthetically replicated using white noise processed through a 2nd-order filter. In the same manner the synthetic wave frequency model presented in [48], the low frequent motion is formulated as

$$\frac{LF\ motion}{N_{n_i}}(s) = \frac{K_{n_i}}{s^2 + 2\xi_{n_i}\omega_{n_i}s + \omega_{n_i}^2}, \tag{6.7}$$

where N_{n_i} is the white noise input, $\omega_{n_i} = \frac{2\pi}{T_{LF}}$ is the circular frequency corresponding to the slow drift period T_{LF} and ξ_{n_i} is the relative damping (typically in the range 0.05-0.10). Using this synthetic form of motion will give a better physical representation of the rig/vessel motion, yielding more credible results. By choosing T_{LF} close to the modal resonance periods in Figure 6.7, the low frequent motion would be in resonance with the selected mode shape(s). For purposes of studying the physics properties, harmonic motion will also be examined. The harmonic motion will be a simple harmonic sine wave with periods T_{LF}. Both motions will be applied at the top node, through a force vector representing the horizontal component from the riser hang up point set in motion by the low frequent motion. This is a simplified representation of the actual riser rig/vessel interaction force. Usually the top joint motion is represented using prescribed motion on basis of the rig RAO, which is assumed to be the same for the riser top point.

6.3.3 Matlab/SIMULINK model

The simulation parameters will be calculated in Matlab and subsequently simulated using the SIMULINK environment. The SIMULINK model is illustrated in Figure 6.8. The hydrodynamic forces such as drag and added mass inertia force are calculated in the large blue blocks to the left in Figure 6.8. This force is added to the low frequent motion force from the rig/vessel, which is generated in the orange block in the middle of the figure. The force vector is then handled differently by the modal and FEM model, due to the decomposition property used to reduce the size of the system. The force vectors then advance to the modal and FEM state space blocks (in red) which calculate the resulting response. All the output from the response is stored for the current time step and velocity is sent back to the hydrodynamic block for correction of the relative velocity, used in relation to Morison's equation. The curvature is calculated using interpolation polynomials in the bright green block.

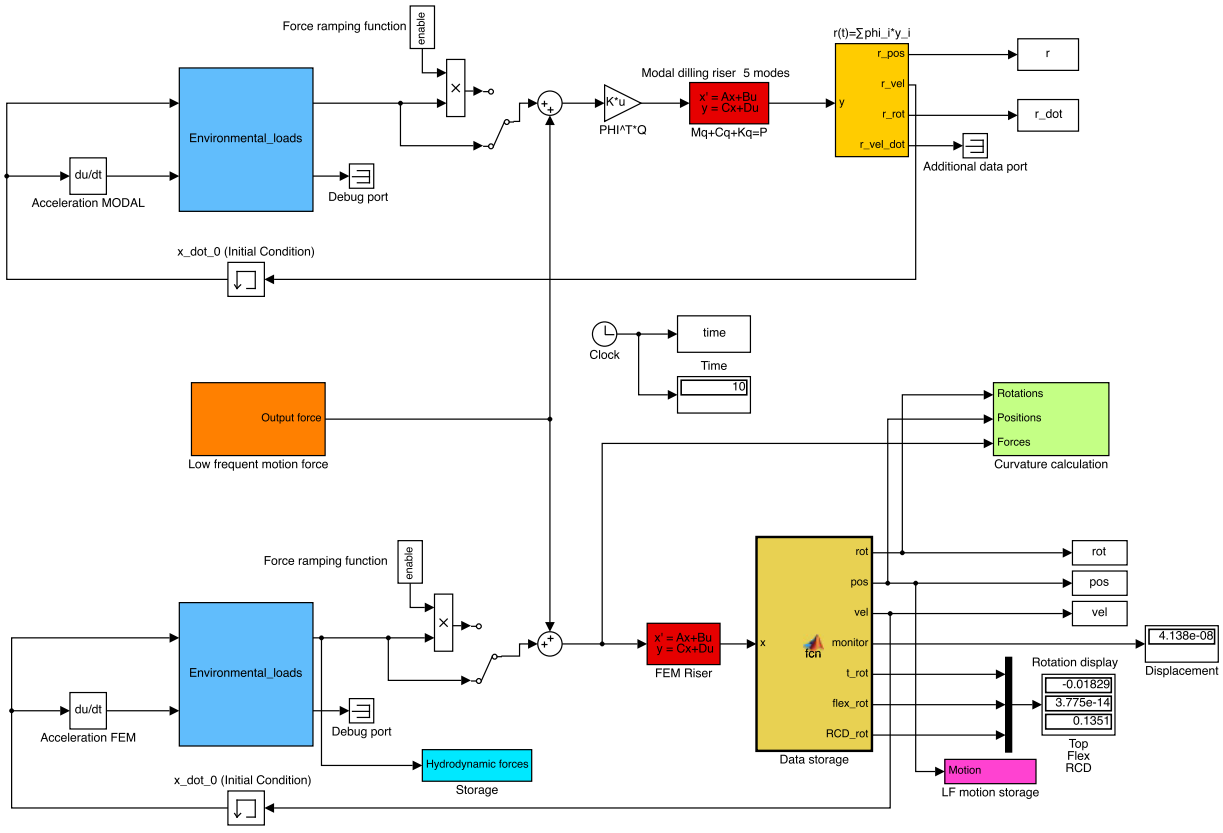

Figure 6.8: The SIMULINK environment and riser model

6.3.4 Low frequency resonance simulation

The simulation of the riser responses will be computed in SIMULINK using the model parameters defined in Matlab. The focus will be on the correspondence of the displayed response to modal resonance, i.e. the resonance sensitivity of the behaviour. The modal distribution is found using the weighting parameters, q_i in Equation (3.21), generated by the modal model, providing an estimate of the modal influence form each mode. These results can ultimately be used qualitatively in context of riser control, based on the modal composition of the response. The most important simulation parameters used in the analysis is presented in Table 6.1. Ten simulations is carried out, five synthetic motions and five harmonic motions. For each of the five modal resonance periods T_{LF_i} .

Parameter	**Value**	**Unit**
Start time	0	s
Stop time	500	s
Step type	fixed	-
Fixed step size	0.1	s
ODE solver	ode8 (Dormand-Prince)	-

Table 6.1: Simulation parameters for dynamic analysis in SIMULINK

Synthetic motion results

Results are displayed in subfigures, the periods and corresponding figure name can found in the caption under the figures. The synthetic simulation overview can be found in Table 6.2.

Simualtion	T_{LF}	**Mode**
1	181.8	1
2	57.4	2
3	34.3	3
4	24.4	4
5	19.0	5

Table 6.2: Synthetic simulations overview.

Snapshots of the riser responses is found in Figure 6.9. The responses is noticeably affected by the non-harmonic motion and display slightly chaotic behaviour. The modal resonance is hard to spot in the first subfigures (a) to (c), but becomes more evident in (d) and (e) which clearly illustrate resemblance with mode 4 and 5. Due to the model rigidity of the modal model, the modal response is shifted relative to the FEM model at the top. Figure 6.15 shows the nodal response in more detail, indicating that the models correspond fairly well despite some deviation at the top. The riser shape will be influenced by the non-constant tension leading to both variance in amplitude and wavelength as the top motion progress along the riser. This effect is also present in the harmonic simulations.

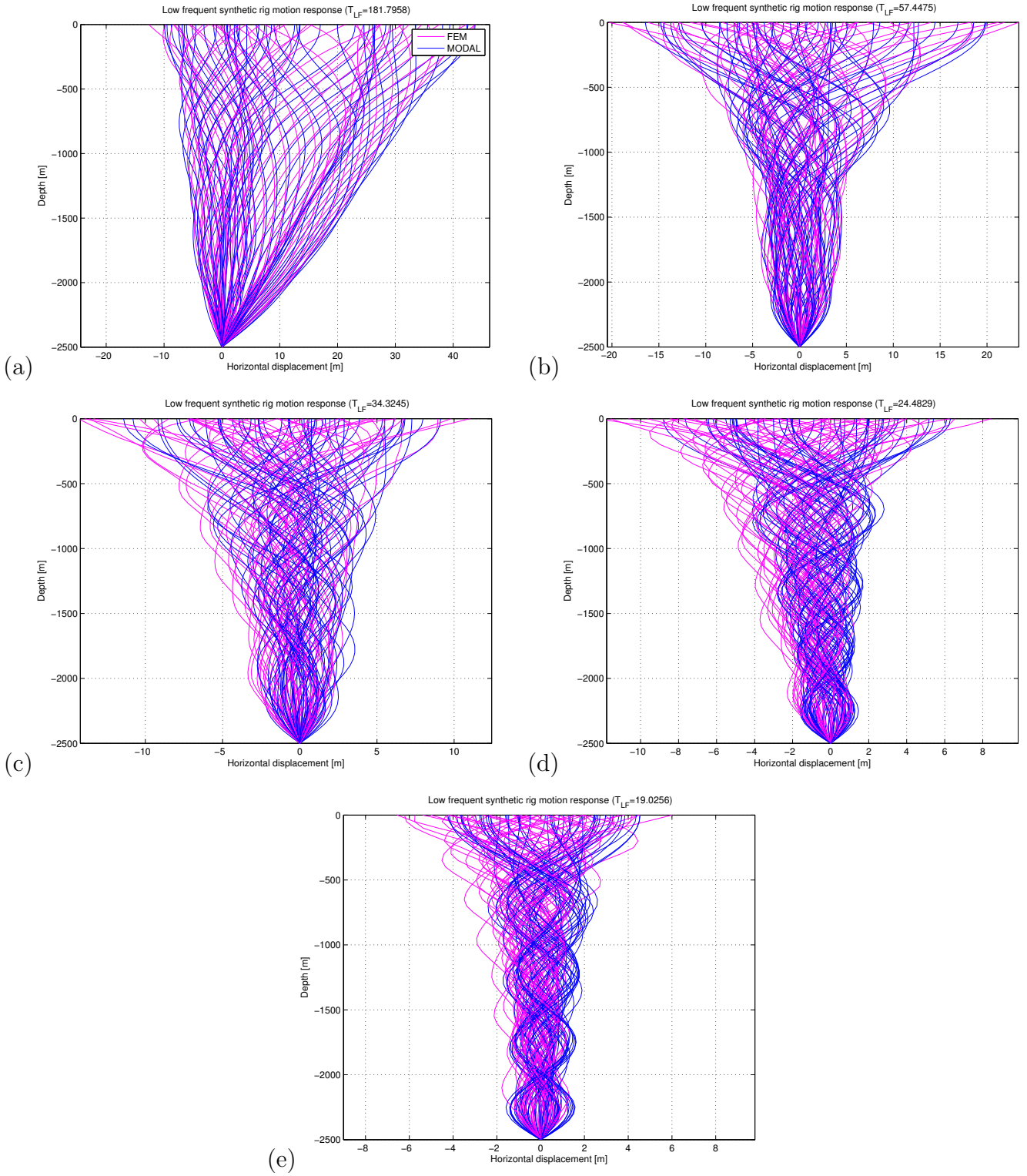

Figure 6.9: Snapshots of response for low frequent motion for (a) $T_{LF} = 181s$, (b) $T_{LF} = 57s$, (c) $T_{LF} = 34s$, (d) $T_{LF} = 24s$ and (e) $T_{LF} = 19s$.

The visualisation of the motion in Figure 6.9 can be decomposed into a sum of mode shapes using information in the modal model. Making use of the weighting factors, the influence from each modal component can be obtained for each time step. This is represented in Figures 6.10 and 6.11 as time developing area graphs, where a large value equals large modal contribution factor. Figure 6.10 shows simulated motion with period corresponding to the resonance period of mode 1, which results in large contributions from mode 1. The influence from mode 2 and 3 is noticeable, while mode 4 and 5 have limited impact on the response. Control systems can use modal composition data to decompose the underlying dynamics present in the riser behaviour and use the information to detect resonance and initiate control action. The use and implementation of this information can be studied further in [18], where this information is used to detect current profiles.

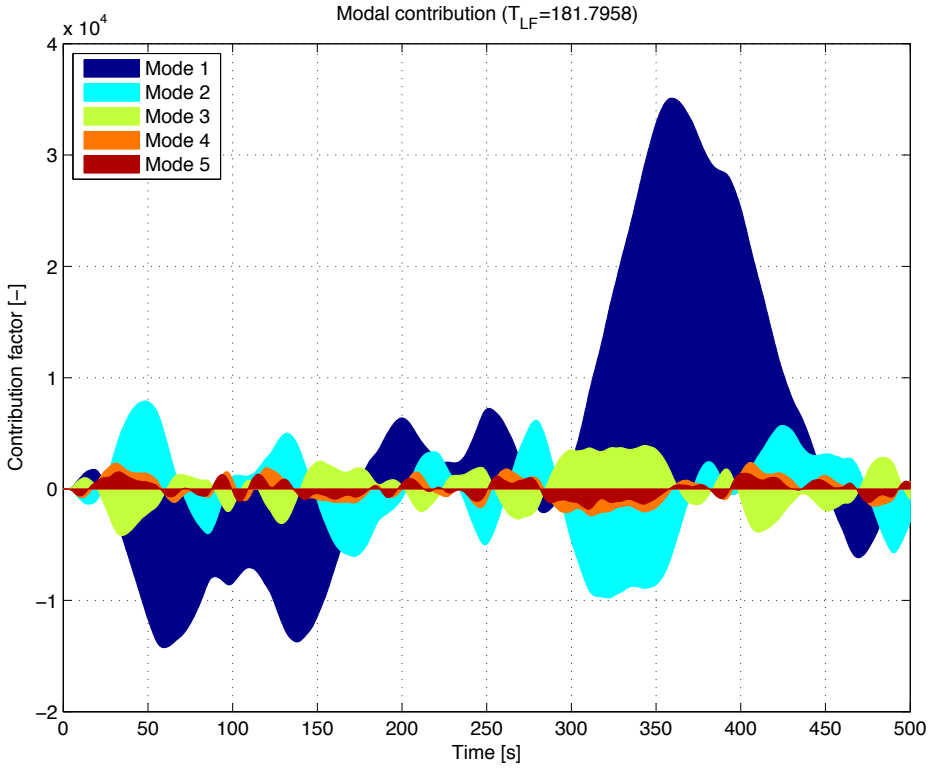

Figure 6.10: Modal contribution factor for $T_{LF} = 181s$.

In Figure 6.11 (a) more oscillatory behaviour is seen. Since the motion is periodic and oscillating around zero the contribution will change sign, meaning the mirrored mode shape is excited when the area graph is below zero. Comparing Figure 6.10 and (d) in Figure 6.11 the mode shape is repeatedly reflected between the mirrored and non mirrored version of the mode at a higher frequency, when the response period becomes smaller. Even though the motion is tuned to a certain mode, the motion dynamics is non unimodal, consisting of a group of modes. The non-harmonic properties in the synthetic motion is responsible for this modal mixing. The frequency spread in the motion spectrums in Figures 6.13 and 6.14 clearly indicate the same.

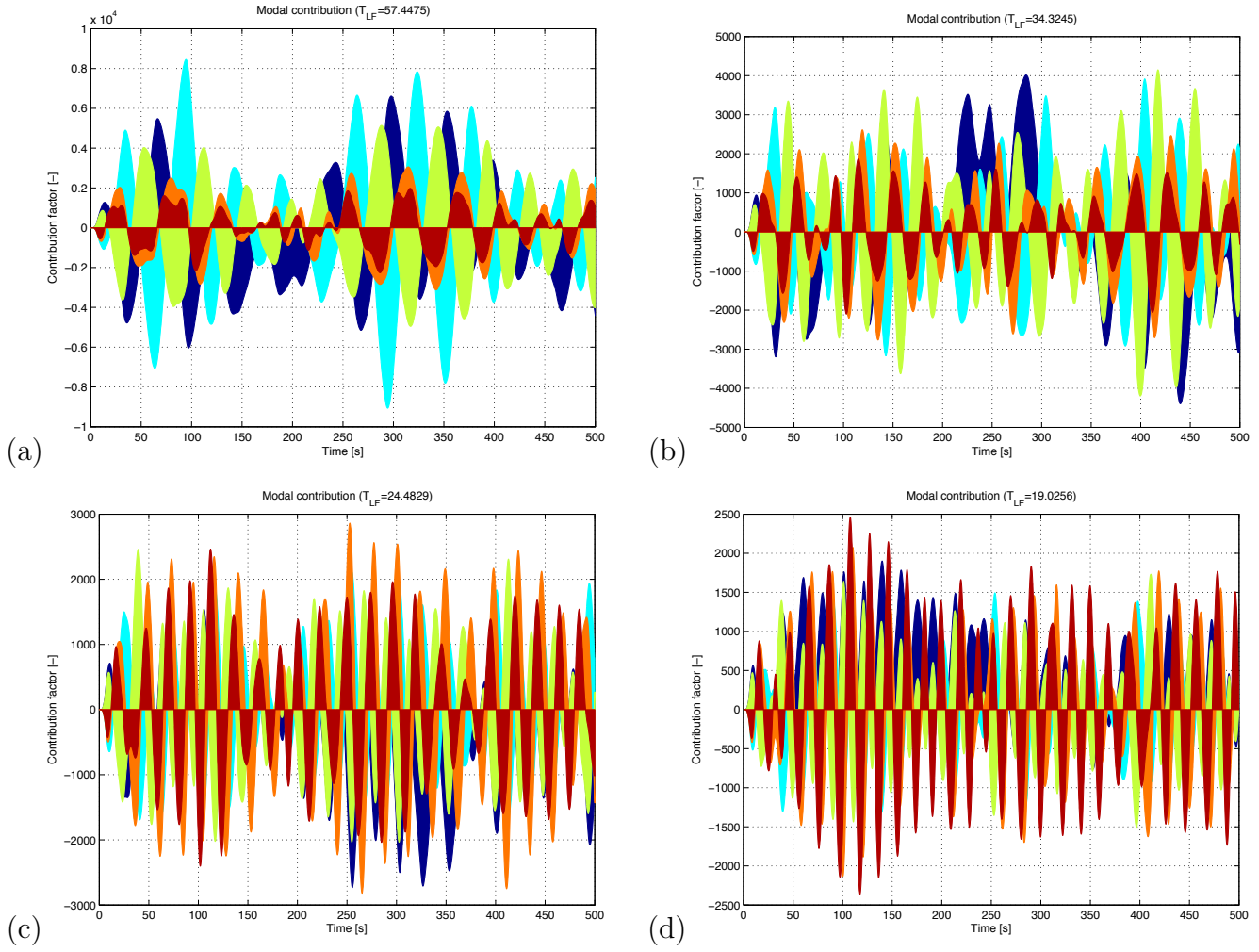

Figure 6.11: Modal contribution factors for (a) $T_{LF} = 57s$, (b) $T_{LF} = 34s$, (a) $T_{LF} = 24s$ and (d) $T_{LF} = 19s$.

The total percentual response contribution form each mode is calculated and displayed in Figure 6.12. The modal contribution from mode 1 is roughly 60% in Figure 6.12 (a), indicating that resonance effects are occurring. Studying Figure 6.12 (b) indicates that mode 2 is the governing mode constituting for 31% of the motion, but that the resonance effects are smaller. The same can be said for (c), (d) and (e) where the governing mode is constituting for about 27% of the motion. The load is only applied at the top node resulting in a load distribution witch favours deformation shapes more comparable with lower order modes, which have larger modal contribution for such load distributions. This results in larger damping for higher order modes, since their modal load pattern favour a more spread distribution. This again leads to greater difficulty achieving resonance, explaining why the resonance effects are smaller for smaller periods.

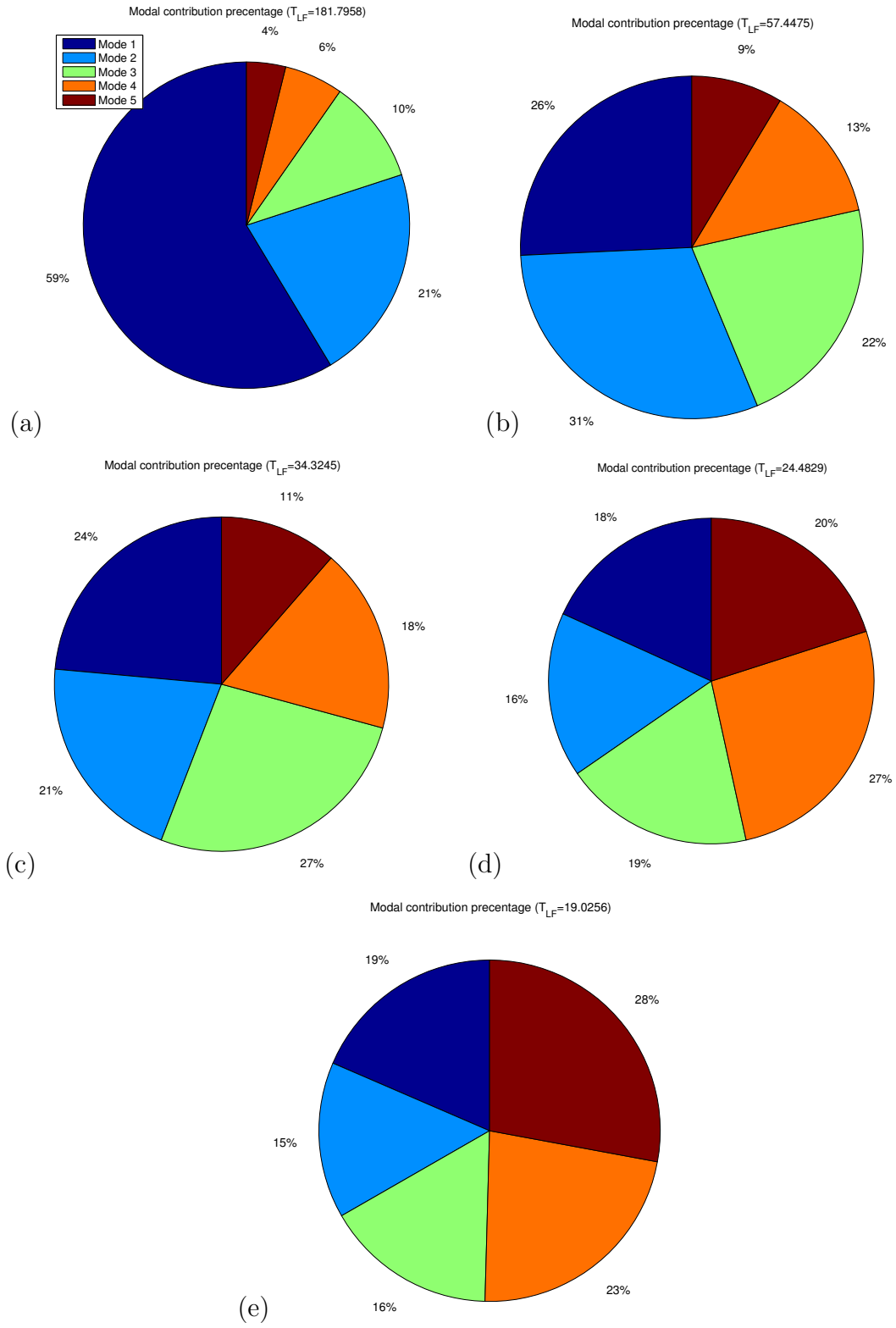

Figure 6.12: Distribution percentage of modal factors for (a) $T_{LF} = 181s$, (b) $T_{LF} = 57s$, (c) $T_{LF} = 34s$, (d) $T_{LF} = 24s$ and (e) $T_{LF} = 19s$.

The motion and curvature details can be found in Figures 6.13 and 6.14. The top graph shows the time development of horizontal displacement for the top point of the riser. The middle graph displays the frequency spectrum for the motion, while the last graph presents the curvature development using snapshots at given time intervals. Evaluating the motion Figure 6.13 it is visible that the rig/vessel motion is non-harmonic and slowly varying, having several frequency components. The riser curvature graph shows the declining curvature response traveling downward along the riser like waves, clearly indicating larger curvature magnitude closer to the surface. The curvature is gradually damped out and reach modest values about 1500m water depth.

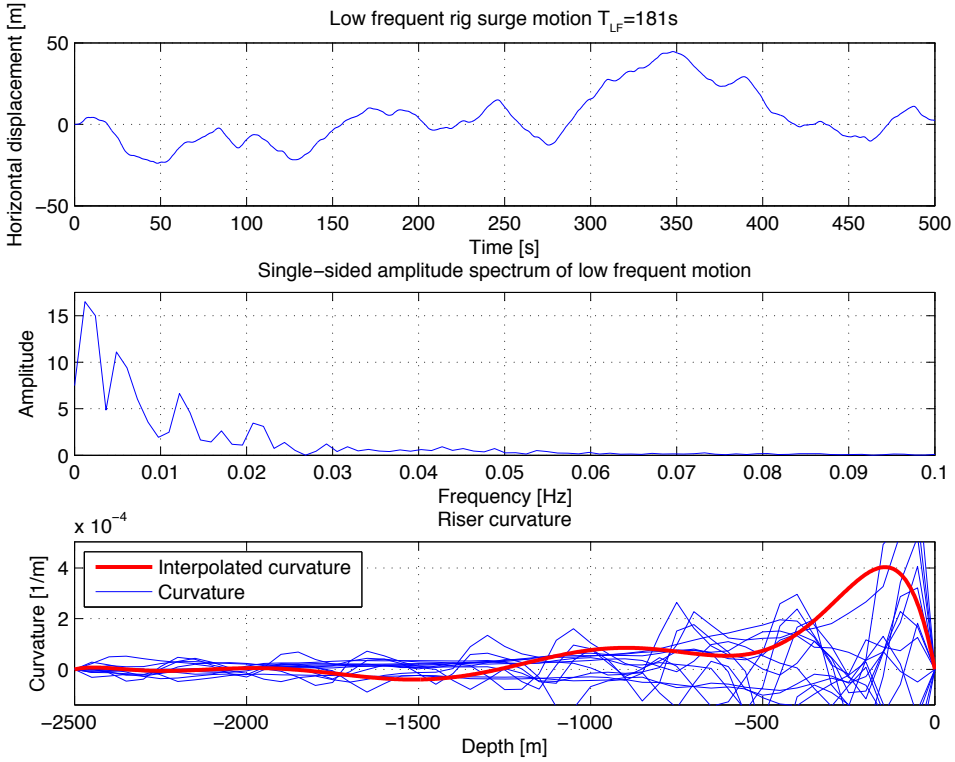

Figure 6.13: Low frequent motion, frequency spectrum and curvature development for (a) $T_{LF} = 181s$.

Investigating the motion details for the subfigures in Figure 6.14 the motion frequency is increasing and shifting the spectrum left. Due to initialisation of the motion the spectrum always have a low frequency component located to the right corner. This "start-up" phenomena can also be found in the nodal time series in Figure 6.15 where a low frequency trend can be found. The effect is more visible in the harmonic time series found in Figures 6.17 and C.1. The curvature is gradually decreasing with depth for all the subfigures, but the curvature extent is deeper for increasing period. Figure 6.14 (d), which correspond to the modal resonance periods of mode 5, display distinctive curvature envelopes identical with mode 5. Tendencies can also be seen in subfigure (c), associated with mode 4. Curvatures in these figures are more visible due to the curvature properties of higher order modes, possessing more change in the mode shape deflection, yielding larger curvature magnitudes.

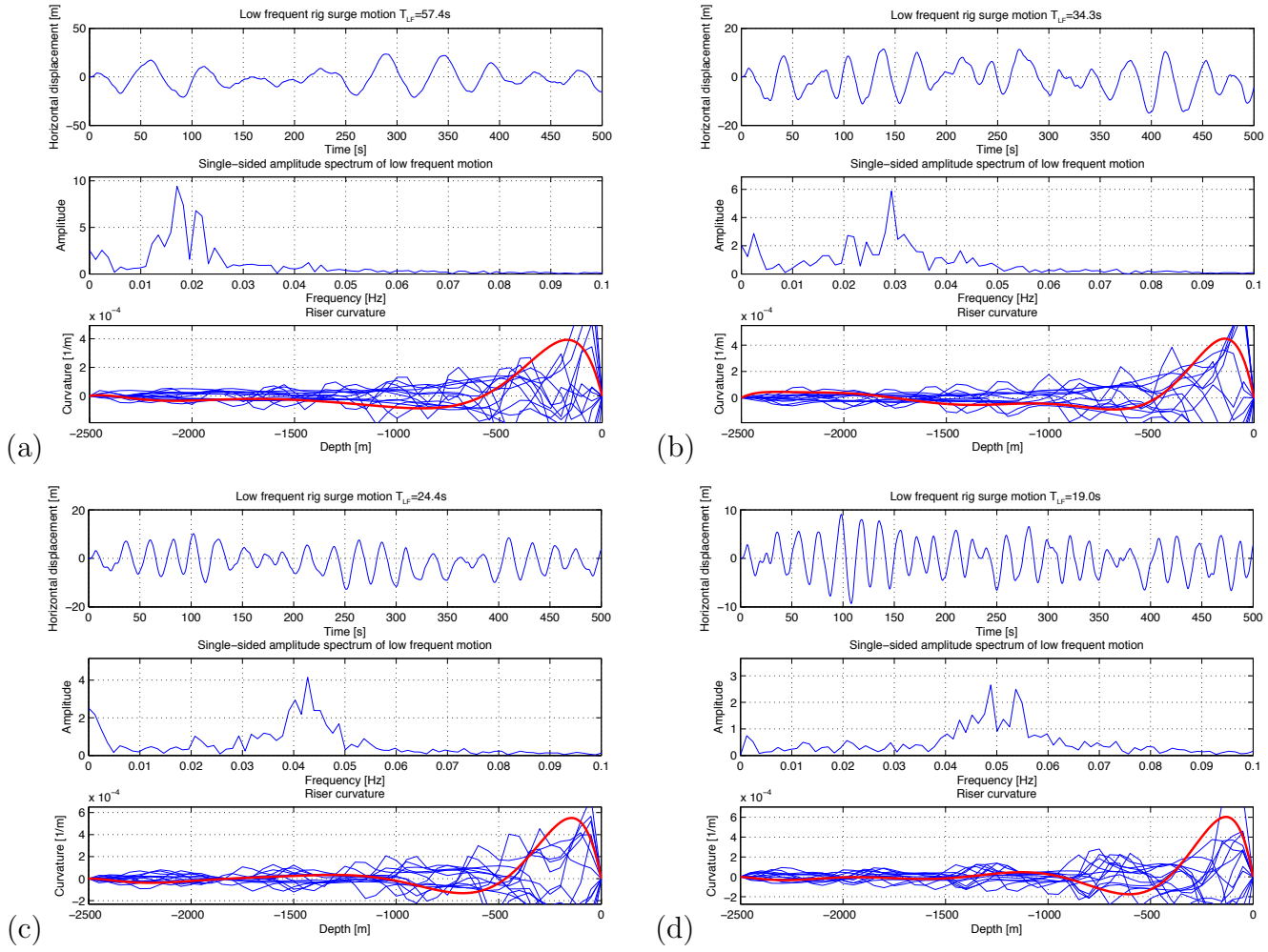

Figure 6.14: Low frequent motion, frequency spectrum and curvature development for (a) $T_{LF} = 57s$, (b) $T_{LF} = 34s$, (c) $T_{LF} = 24s$ and (d) $T_{LF} = 19s$.

The correspondence between the modal and FEM model is vital for the use of the modal decomposition data. If the goal is to use the modal information in a control system the accuracy of the decomposition data is essential for the success of the strategy. The nodal time series in Figure 6.15 show the agreement between the two models at two important locations on the riser, the top node (top joint of the riser) and the RCD node (RCD location at 400m). As emphasised in Chapter 4, the rigidity of the modal model arising from the inclusion of a limited number of modes will lead to some divergence. However, the graphs in Figure 6.15 show fairly good correspondence between the models. A slight inaccuracy can be noted, most visible at the top node plot in the bottom graph of the subfigures. The response is larger at the top node compared to the RCD node located further down on the riser. This effect is best observed in Figure 6.15 (e), where the difference in response is clearly visible.

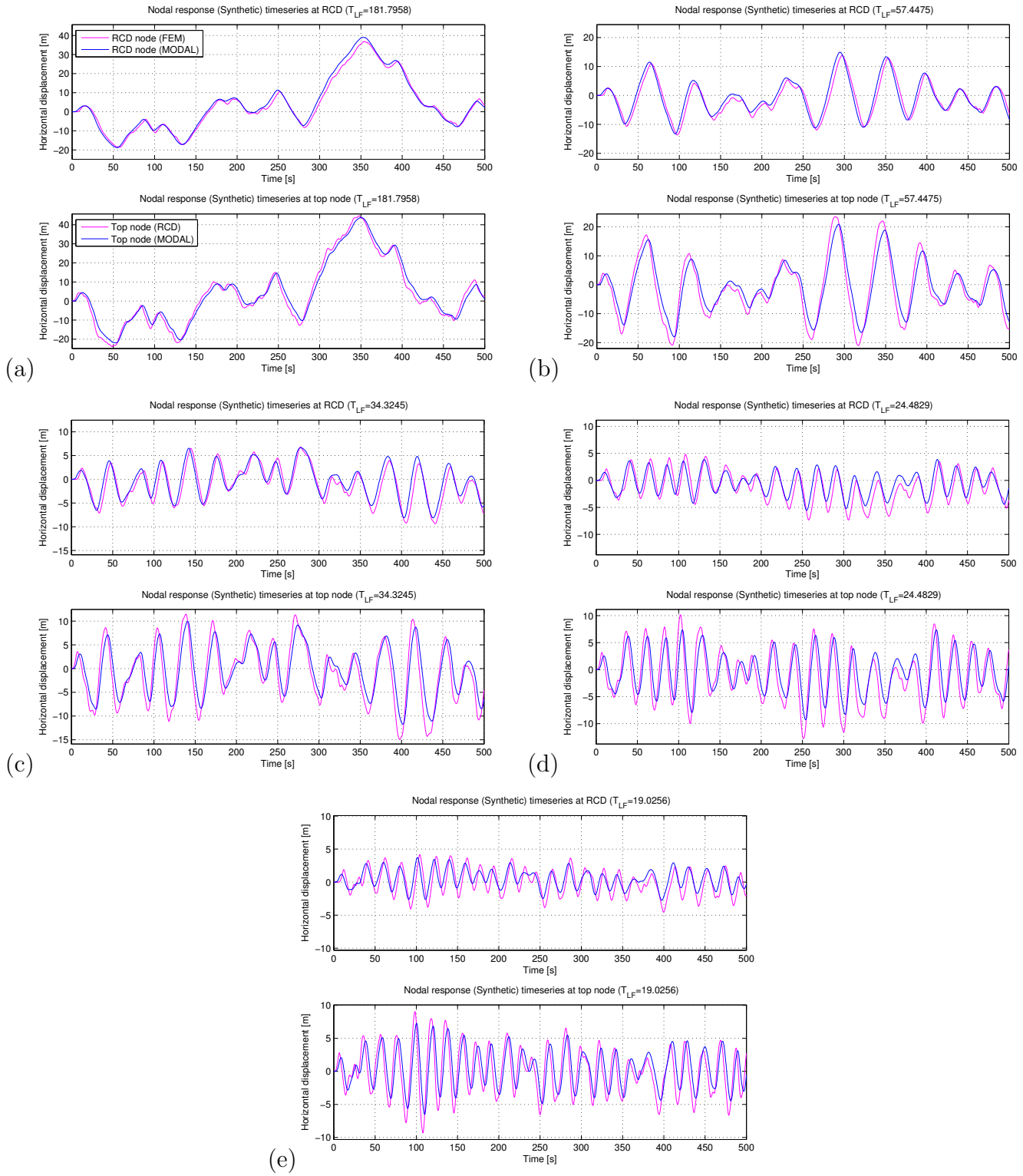

Figure 6.15: Nodal time series for the top node and the RCD for (a) $T_{LF} = 181s$, (b) $T_{LF} = 57s$, (c) $T_{LF} = 34s$, (d) $T_{LF} = 24s$ and (e) $T_{LF} = 19s$.

Harmonic motion results

Additional five simulations have been carried out with harmonic top motion to further investigate the physics properties of the riser system under "ideal" conditions. Furthermore the conceptualisation of a control system based on the riser modes can be easily developed using a more straightforward form of the problem as a basis. As the previous section the results are displayed in subfigures with the periods and corresponding figure in the caption. Only the harmonic results from Simulation 6 is provided here capturing the most important essentials from the analysis, the remaining simulations can be found in Appendix C.1. The harmonic simulation overview can be found in Table 6.3.

Simualtion	T_{LF}	**Mode**	Figure
6	181.8	1	Figures 6.16 and 6.17
7	57.4	2	Figure C.1
8	34.3	3	Figure C.2
9	24.4	4	Figure C.3
10	19.0	5	Figure C.4

Table 6.3: Harmonic simulation overview.

Simulation 6 corresponds to mode 1 which is easily identified in Figure 6.16. Compared to the synthetic motion the response is largely dominated by one frequency, verified by the modal composition graphs in Figure 6.17. The horizontal offset is about 4-6m, complying with the example of slow drift motion in surge, given in [11]. The modal model corresponds well with the FEM model, with only a minor deviation at the top point accounted for in the model verification, Chapter 4.

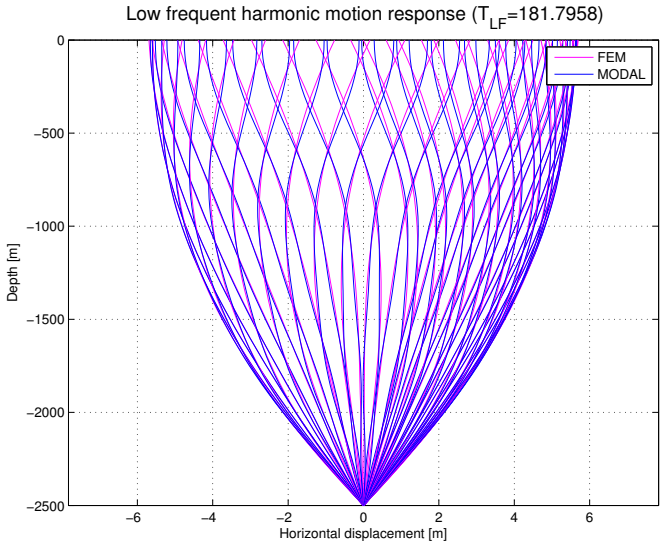

Figure 6.16: Harmonic motion snapshots for Simulation 6, $T_{LF} = 181s$.

The motion details in Figure 6.17 reveal that even for harmonic motion of this type, unimodal behaviour can be hard to obtain. Leading to the impression that due to the damping conditions for

deep water risers initiating a standing wave will require very special load conditions, which most likely never will occur. This idea have been pointed out by *Larsen et al.* in [30], where the altering current conditions excite numerous frequencies. The modal distribution in Figure 6.17 (d) suggest that the motion can be ascribed to mode 1, 2 and 3, with mode 4 and 5 only accounting for 3% for the motion. The curvature envelopes can be compared to the static curvature results obtained in the RIFLEX analysis, displayed in Figure 5.13. The curvature will however, deviate slightly from the static curvature in Figure 5.13, due to the dynamic motion of the top point, oscillating between mirrored and non-mirrored version of the mode shape.

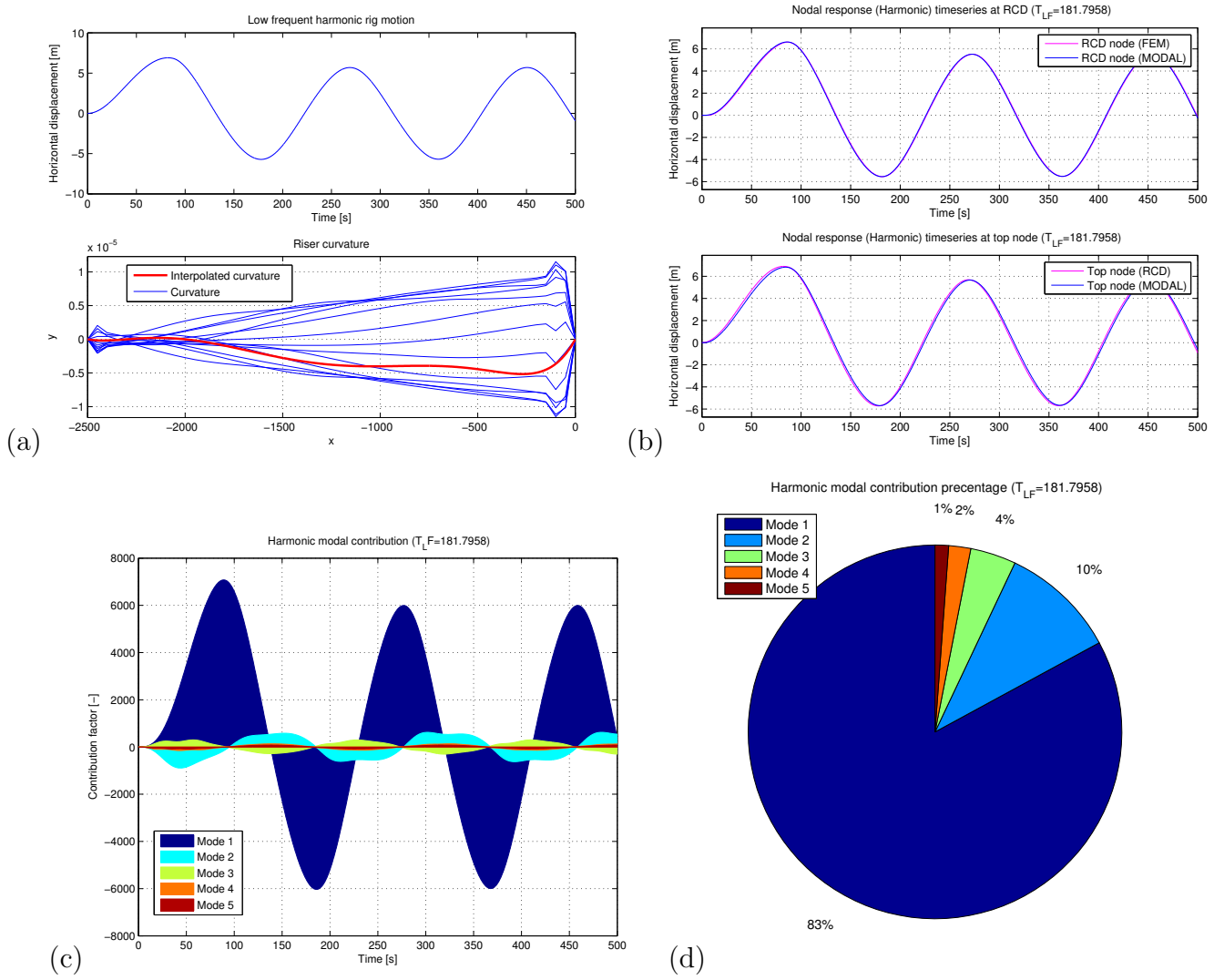

Figure 6.17: Harmonic motion results for Simulation 6, $T_{LF} = 181s$.

The harmonic results above and in Appendix C.1 bear clear evidence of resonance effects being excited by top motion. Compared to the synthetic motion the response intensity is increased for the distinct modes connected to the associated frequencies. The curvature propagation is now more efficient and covers the whole riser, resulting in larger curvature magnitudes further down.

6.4 Dynamic analysis review

The aim of the analysis was to confirm that motion comparable with slow drift motion experienced on rigs and vessels, with periods corresponding to the natural periods of the modes can lead to resonance responses, i.e. investigate the resonance sensitivity. Furthermore, can such responses be decomposed into separate modes and managed in a context where control mechanisms, supplied with this distribution information, attenuate the resonance dynamics?

The analysis shows how it is possible to deconstruct the riser behaviour into the fundamental modal components using the weighting information contained in the modal model. The nodal time series for the models indicate reasonably good correspondence between the modal and FEM model, which is vital for acquiring trustworthy estimations of the modal composition necessary in control applications. Due to the nature of the load distribution and damping, the synthetic and harmonic simulations provided results indicating difficulties obtaining unimodal behaviour, despite being tuned to the modal frequency. This is not to say that resonance is not likely to occur, but rather that resonance excited solely by top motion will be less formidable for deep water drilling risers than previously expected. However, there is a clear difference in resonance intensity between the synthetic motion and the more ideal harmonic motion indicating that the riser is sensitive in these frequency regions. This motivates the need to investigate the possible advantages of eliminating the resonance motion with manipulation of the resonance properties of the riser, and the practical aspects surrounding such a extension of a riser management system.

6.5 Riser control and guidelines

Results from the preceding section indicate that riser resonance response associated with top motions is likely to have significant damping, and trouble initiating standing waves and unimodal behaviour. However, comparison of the synthetic and harmonic results indicate an apparent resonance sensitivity connection between the rig/vessel and riser. Response dynamics at submerged riser locations, accommodating equipment vital for the drilling operation, will consequently benefit from a reduction in this sensitivity region. Attaching passive suppression systems directly on the riser can be a proactive solution, but will not account for all environmental loads/systems liable to contribute. E.g. resonance from thruster assisted position mooring systems (Posmoor) will not be diminished.

Negligence of such phenomena will result in larger motions and forces, which in turn reduces the lifetime of components such as the sealing element and well head. E.g. several well heads currently deployed in the North Sea are reaching the expected fatigue life and are therefore extra sensitive to resonance oscillations. Repairs and frequent exchanges of these parts will pose a significant economic expense and additionally add to the NPT. An extended version of existing riser management systems using "resonance property oriented" control strategies, can help reduce unwanted excitations. Avoiding riser damage and fatigue, and additionally increasing the safety and operational margins. This control approach will be referred to as *modal control*, due to the

utilisation of the modal properties of the riser. Motivated by the simulation results acquired in Section 6.3.4 an outline of the aspects related to the feasibility of extension of current riser management systems to incorporate such control will be presented.

In [44], T.R Stockton, presents a unofficial definition of riser management system formulated as: *" A real-time riser management system continuously monitors vessel, drilling, and riser parameters and processes this information in combination with vessel and riser mathematical models to present drilling personnel with information detailing the existing riser configuration and disconnect margins, and the margin remaining before a disconnect has to be initiated."*

Commercial riser control systems exists today. Kongsberg (Seaflex Riser Technologies) has developed Riser Management System (RMS) together with the Riser Position Reference (RPR) to facilitate riser integrity management and optimise operation and safety margins, e.g. limiting the flex joint angles [33]. Several other companies delivers similar RMS solutions for monitoring riser integrity and dynamics. There are three typical modes in which most RMS systems operate in:

- Drilling
- Non-drilling
- Disconnect

In drilling mode the main focus is on all operations related to drilling and monitoring of drillpipe and riser angles. Non-drilling mode will typically be associated with tripping, tool handling or other activity not related directly to drilling. Disconnect mode will include all activity associated building up to and during a disconnect from the BOP stack. For the purpose of exploring control the focus will be on activity related to drilling and non-drilling mode, since the forces on the RCD will involve the drill pipe being present. The most limiting operational factor in drilling is the tolerance for riser angle deviation relatively to the well head and at the top joint [48]. On account of ensuring that the angle magnitudes are within the operation envelopes for drilling, usually taken to be below $\pm 2^{\circ}$, RMS systems incorporate a control systems for calculation of the optimal rig/vessel position where both the upper and lower riser angles are as small as possible. In [47], Sørensen, Leira, Strand and Larsen propose a control system to minimize riser angles by finding an dynamic setpoint, optimal for the current modus operandi, referred to as *optimal setpoint chasing*. Using the idea of optimal setpoint chasing, the guidelines for a modal control system is explored.

6.5.1 Control strategies

The primary purpose of the modal control system is to avoid resonance sensitive regions by modifying the riser's resonance properties, so that the level of response is below the magnitude which there is no concern for the equipment or operations being conducted. The conceived control system would assist the RMS infrastructure, delivering setpoints used by the RMS in the operational visualization, to allow for the operator to attain the greatest possible situation awareness. By improving the intuitive overview and the correct perception of the current riser response. The

extended system would contribute to a safer and more optimal operation.

A key point for the modal control system to succeed, is the assumption that the riser can be instrumented to a degree where an accurate estimation of the riser shape can be obtained combining sensor data and mathematical model. The mathematical riser model should be able to replicate low frequency dynamic vessel displacement and resulting riser shape in response to forces acting on the vessel and riser. Acquiring comprehensive instrumentation can be extremely expensive and would require considerable assembly time when installing the riser. Following the recommended practices in DNV-RP-F206 and [8] for riser integrity management an idea of the number of measurement units can be assessed, based on VIV requirements:

"For VIV monitoring the spacing between adjacent instrumentation should be such that there are at least two instruments available to capture the quarter wave length of the highest mode expected."

VIV resonance frequencies are in general higher compared to rig/vessel eigenfrequency [9], moreover the VIV phenomena will exhibit different behaviour compared to resonance created by mooring lines and slow varying wave drift forces. The instrumentation requirements related to VIV will therefore be considered conservative in terms of riser response detection.

In the case of 2500m and mode 5 taken as the highest mode, this would entail about two units for per 250m and a total of 20 units, which is a considerable quantity. Overcoming this instrumentation problem would be subject for further research. Taken that the riser can be instrumented, a modal composition assessment can be done using the same approach as in Section 6.3.4 to supply the modal control system. Additionally an accurate representation of the current profile would allow for a better assessment of the prospective possibility for removing the riser out of the sensitive region. Based on this framework four main strategies developed for modal riser control, they are illustrated in Figure 6.18.

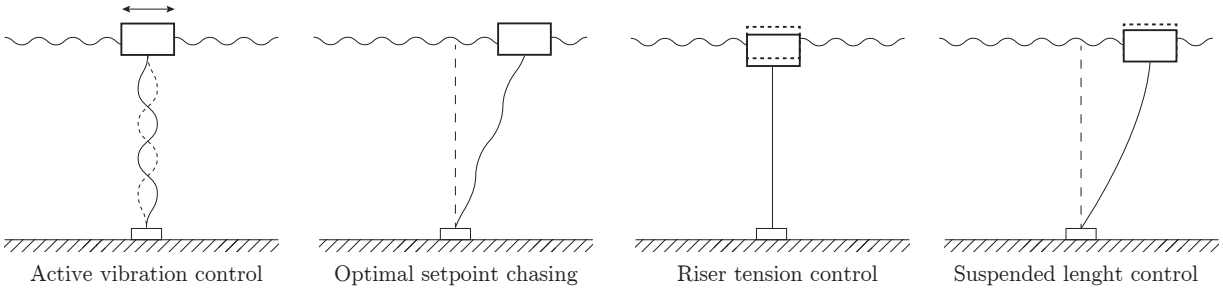

Figure 6.18: The four different control strategies.

Active vibration control

The active vibration control concept is based on active attenuation of the resonance frequencies by designated dynamical rig/vessel motion. The dictated motion would be tuned to the modal vi-

brations, but have phase difference 180° generating destructive interference between rig/vessel and the riser motion. The modal vibration would be based on the modal decomposition information supplied from the control systems internal riser analysis. The analysis must account for the influence from effective tension, leading to the modes evolving both in amplitude and wavelength along the riser. The timing of such a system would require precise estimates of the time required for the modal response to ascend and descend the riser, based structural and damping properties. Failure to cancel out the motions correctly could lead to additional response intensity and unfavourable results. The active control will produce a developing setpoint, similar to setpoint chasing used in [47], since the motion needs to be dynamic. A reference filter higher up in the control hierarchy must therefore preprocess the setpoint signal to avoid discontinuities.

Such a control strategy would require a powerful thrust system large enough to induce periods as low as 20s. Additionally the flex joint angles, specially the top flex joint, will be vulnerable to excessive angle magnitudes which would be the generated by the imposed rig/vessel motion. Additionally, deliberate resonant control is not structurally healthy considering fatigue factors. The feasibility of the control strategy and the practical considerations will be treated in more detail in the Section 6.5.2.

Optimal setpoint chasing

Motivated by the article by Sørensen et al. in [47], an extended version of the optimal setpoint chasing approach is proposed. In addition to minimize the top and bottom flex joint angle, local riser aspects are also considered. E.g. resonance oscillations and unwanted behaviour occurring in the intermediate region would also be considered in a optimisation criteria. The setpoint would be chosen so that the riser would avoid the resonance area, by shifting the eigenfrequency sensitivity up or down the frequency range, i.e. minimize the resonance sensitivity. Instead of active attenuation, the structural properties of the riser would indirectly be manipulated by changing eigenperiods with tension or position. The riser management system would use the information to generate an "resonance free" region. The idea is exemplified in Figure 6.19. The flex joint angles would typically be given more attention, but given sufficient safety margins for these, the focus can be shifted to local optimisation. The implementation complexity of such a system would rely on the existing control system infrastructure.

Riser tension control

Today's tension control systems are relatively simple and do not consider any input from the riser, the only job of the system is to keep the tension constant. There are several different ways of reducing the resonance sensitivity. The obvious one is of course to avoid the resonance area completely. The extended tension control system rely on passive attenuation of the resonance frequencies, by using top tension to manipulate the resonance properties of the riser. Based on the active modal components being excited, the tension control system deliberately increase or decreases the top tension. To move the modal properties above the frequency area can be problematic dealing with VIV, since there will always be a higher natural mode which correspond to the vortex shedding frequency [29]. It is therefore important to assess the periods of interest which can influence the

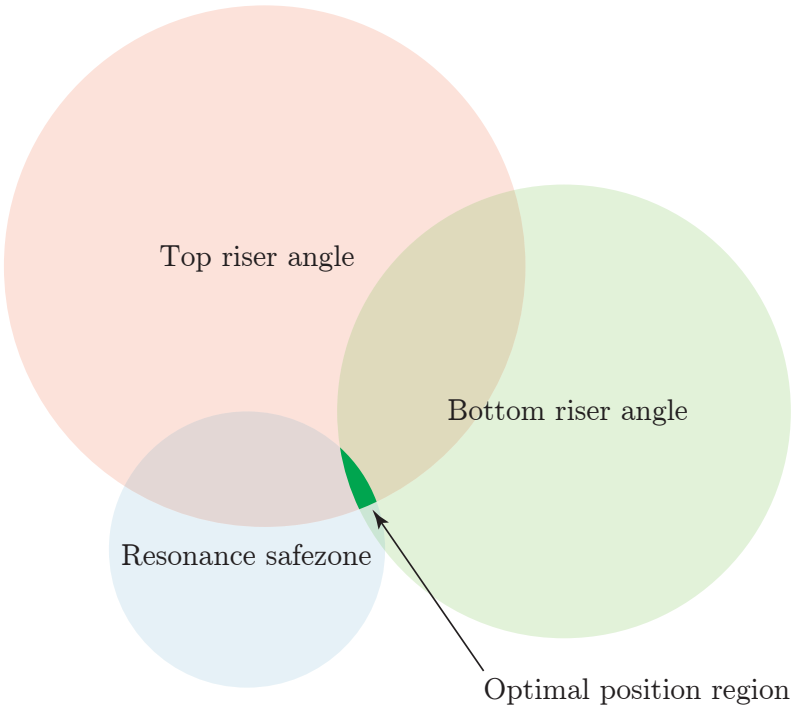

Figure 6.19: Optimal setpoint chasing with additional criteria from local riser aspects.

riser in the new configuration and use this proactively before finding a suitable tension. The top tension needs to be sufficiently high to avoid buckling, but the tension capacities of the rig/vessel and the riser axial stresses must be kept within certain limits to avoid plastic deformation.

Suspended length control

Suspended length control is similar to both setpoint chasing and tension control indirectly altering the structural properties of the riser to avoid to resonance area, but instead of just moving horizontally the tension is also kept constant. By doing this the length of the riser increase, but the tension distribution is the same leading to a change in the structural properties, which again affect the resonance region. Performed correctly this operation moves the sensitive frequency regions of the riser outside resonance regions for the loads. However, shifting of the riser natural periods does not remove the resonance problem, but rather redirects the riser sensitivity to other frequency regions less associated with local environmental loads. Lower and higher resonance frequencies need to be evaluated, so that interaction with new resonances does not occur. The allowable elongation will probably so small that the control strategy will be very ineffective, this is investigated in more detail in Section 6.5.2.

System architecture and guidance

The proposed system framework for modal riser control in Figure 6.20 use a supervisor and guidance block to evaluate the information received from the controllers, performing decision and guidance logic. The supervisor must take into account the operator, RMS system, operational parameters and control information in evaluation, making it the most complex component of the system. A typical task performed by the supervisor will be to find the control strategy with the best potential, supplied by instructions from the operator and the given operational limits. One critical operational parameters would the stroke available in the slip joint, calling for stoke related control strategies to be less usable. The RMS system will also interact with the supervisor, providing the optimal flex joint angles used in the controller setpoint evaluation. Depending on the control objective the supervisor must incorporate some form of weighting criteria to select the control strategy which best comply with the current and future state of the modal riser control system and RMS system. A trade-off between the various operational parameters and the prospects of utilizing the full capacity of the control system is inescapable. The details of which is beyond this thesis, but object for further research. However, some practical aspects surrounding this topic are discussed below.

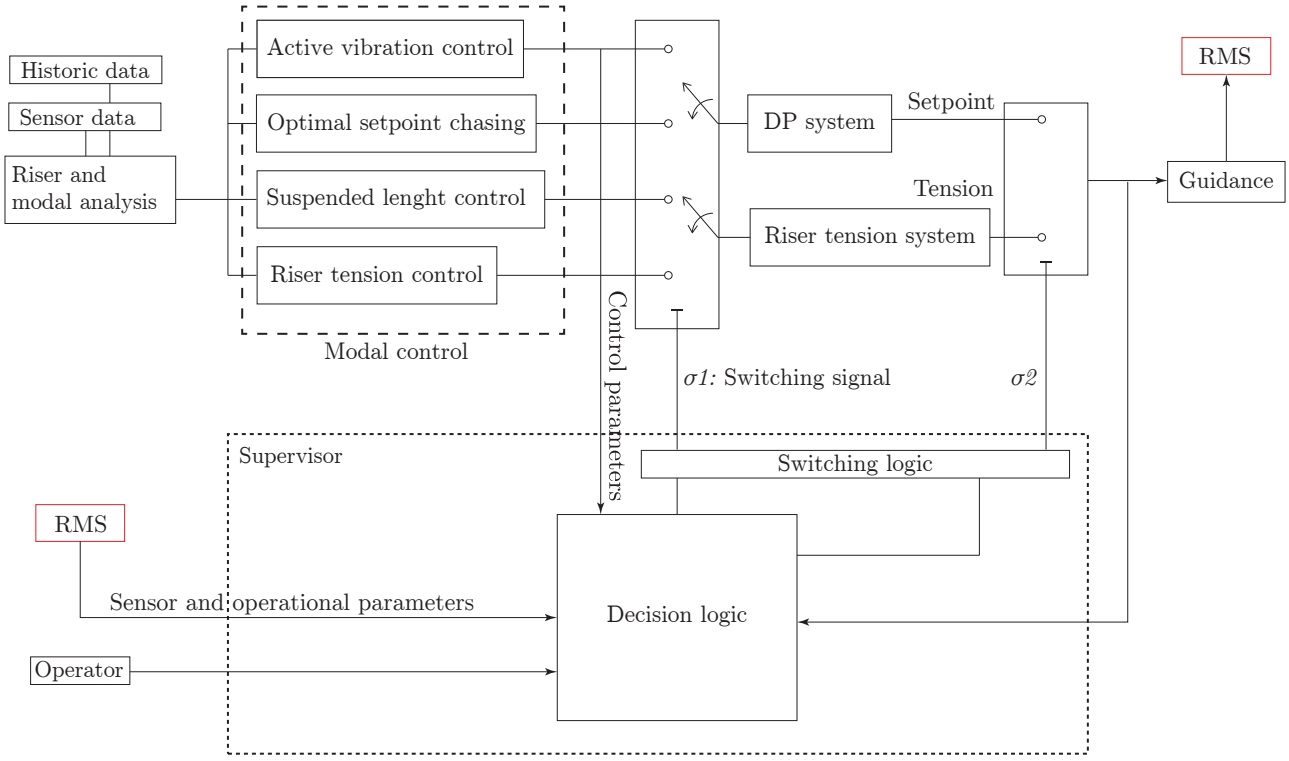

Figure 6.20: Principal control scheme.

6.5.2 Practical considerations and review of modal control

Extension and integration of a modal based control system must not conflict with the existing functions of the RMS system marginalizing operational safety. The purpose of modal control is rather to increase the safety margins and operational economy, e.g. by reducing the time spent suspended because of seal element exchange, the risk for well head fatigue. Additionally, the modal control system take aim at improvement of the operational visualization and decision support functions used by the operator. For deep water drilling RMS systems is subjected to physical limits and inherit properties of the riser system will confine the operating possibilities for dynamic control system. In [44] five limiting factors are listed for conventional RMS systems:

- Bottom joint / Flex joint angle
- Top riser angle
- Slip joint and tensioner strokeout (the available strokeout length)
- Riser / Moonpool contact (important in disconnect scenario)

Riser angles magnitudes influence all aspects in modal control limiting the accelerations and rig/vessel offset. E.g. a 2500m riser with a bottom angle of $\pm 2^\circ$ and no current will have a maximum offset of about 90m. From [11] the extreme horizontal offset is given as 10% of the water depth, leading to an extreme value of 250m. Based on this the normal operation would be within 90m, with an safety buffer of 160m. The control strategies based on setpoint and offset would be limited to an working region with radius 90m, consequently this also applies to the modal properties of the riser.

Slip joint and tensioner strokeout will be governed by the heave compensation system. Normally the slip joint / telescopic joint will have a stroke of about 15m, in calm waters. In hard weather all the available capacity can be used, leaving no accessible for the control system. The stoke will influence the tension and suspended length control directly by limiting the tensioner stroke and the slip joint stroke available to be used in control. A 100m completely horizontal offset on a 2500m riser will approximately give an additional length of 2m, which can be considered allowable if the weather is sufficiently calm. A quick assessment of the influence from 2m elongation will show that the change in eigenfrequency is insignificant, which in effect means the suspended length control will be very ineffective and most probably will need to be supplied by tension to achieve any detectable change in modal frequency. Riser / Moonpool contact is not considered to modify the control aspects, when drilling or non-drilling mode is assumed and riser is in place.

Already mentioned is the limiting factor of acceleration on exciting certain modal vibrations. Assuming a value of $0.01g_g$, where g_g is the gravitational constant, based on the general operating criteria for merchant ships in surge found in [11], modes with periods as small as about 20s is achievable, assuming a small $0 \pm 1m$ oscillation. Which for the 2500m example riser used in this thesis would be mode 1,2,3 and 4 can successfully be activated. This estimate will vary greatly with the thrust power available in surge motion, given specific for each drilling rig/vessel. The

inclusion of VIV suppression control in the modal control system can theoretically be feasible, but have several complications which limits what is practically achievable:

- Control actuators may need to cover large areas of the riser.
- Increased drag.
- Can be hard to predict.
- VIV oscillations change fast and is a multi frequency phenomenon.
- Marine growth can alter the VIV conditions.
- Theory is based on unidirectional current.

An brief evaluation of the control strategies, is found in Table 6.4.

Control type	**Advantages**	**Disadvantages**
Active vibration control	No increase in top tension is needed. Does not use available stoke capacity. Perfect and fast cancelation theoretically possible.	Rig/vessel motions and accelerations would increase fatigue and top riser angles. Failure to cancel out the motions correctly could lead to additional response intensity.
Setpoint chasing and Tension control	Practically easy to achieve and implement. No accelerations necessary. Can rely on historical data to assess the possible resonance regions and can therefore be used proactively.	Large offsets and tensions required, leading to increased risk for plastic deformations. Shifting the natural periods of the riser can cause resonances with new periods not accounted for. Needs to use available stoke capacity.
Suspended length control	Practically easy to achieve and implement. Can be used proactively.	Not very effective for manipulation structural properties. Needs to use available stoke capacity.

Table 6.4: Active and passive properties.

In view of the practical details discussed above, setpoint chasing and tension control are the most effective and practically attainable. They are also energy conservative, compared to active control. Suspended length control is not of current interest due to the marginal influence. One could consider an combination of these to exploit the best potential in the strategies. Implementation and simulation of setpoint chasing and tension control in Matlab and SIMULINK would be considered the next step in the development of these strategies.

Chapter 7

Concluding remarks

7.1 Conclusion

The work presented in this thesis has focused on modelling, simulation and control of a marine drilling riser. Following the development of modern drilling schemes, the utilisation of submerged equipment attached to the riser prompt the need for closer examination of the local dynamics in these regions. Analysis indicate that these forces are moderate with no or little impact on the operational conditions. A review of curvature and operational requirements deem the region 400m $\pm$50m suitable for accommodating for the equipment. Regional resonance oscillations will influence the drilling operation and reduce fatigue life. Simulations demonstrate that resonance excited solely by rig/vessel motion will be less prominent for deep water risers than previously expected, but at the same time be large enough to be considered vital for the riser integrity. To control the riser motion using offset and tension a qualitative assessment of control capabilities is conducted. This leads to the conclusion that tension and setpoint chasing control are the most effective and practical attainable strategies to handle resonance occurrences.

A pipe-in-pipe model, simulating the contact forces between the riser and drillpipe, was established in SIMA/RIFLEX to examine the internal forces influencing the seal element and the accommodating rotating control device. The system was simulated using typical metocean parameters for 100yr return current and wave loads in the Gulf of Mexico. A simulation time of 500s was deemed sufficient for conceptual work, due to the computational time associated with the pipe-in-pipe contact forces. The resulting lateral contact forces was discovered to be in the range from 2000N to 9000N. The magnitude of the force corresponds fairly well to simplified calculations, which indicate forces around 3400N. Accepting 9000N as the maximum force indicate that the lateral forces correspond to 4% of the sealing element's clamping force. The clamp force is around 260kN, applied to keep a tight seal around the drillpipe and segregate the fluid volumes in the dual gradient configuration. Even though the relative magnitude of the lateral forces acting on the seal element is limited, the combined effect of motion and forces can, over time, lead to considerable fatigue life reduction. Since these tools are attached to the drilling riser, considerations regarding the riser dynamics at these locations must be evaluated. Improvement of fatigue conditions calls for implementation and investigation of the potential benefits associated with control practice.

A FEM model is constructed and formulated in a state space representation using Matlab and SIMULINK. Subsequently, a modal decomposition model is developed based on the FEM model. Dynamic analyses of the riser are carried out using these two models. Investigating the resonance sensitivity of low frequent rig motion, indicates that the riser resonance response associated with top motions is likely to have significant damping. Due to the extensive damping, there will be trouble initiating standing waves and unimodal behaviour, suggesting high energy dissipation. However, comparison of the synthetic and harmonic results indicate an apparent res-

onance sensitivity connection between the rig/vessel and riser. Response dynamics at submerged riser locations, accommodating equipment vital for the drilling operation, will consequently benefit from a reduction in this sensitivity region. Motivated by the results the concept of modal control is suggested. By using the modal decomposition model of the FEM model, the response can be decomposed into modal components. This information can be used to detect resonance activity caused by environmental disturbances originating from rig/vessel motion, waves, current and vortex induced vibrations. Supplied with this information, control can be utilized to attenuate the unwanted excitations. Using the idea of controlling the modal properties, i.e. the resonance sensitive characteristics of the riser, four control strategies are proposed. A qualitative assessment of the capabilities manipulating the motion, offset and tension leads to the conclusion that tension and setpoint chasing control are the most effective and and practically attainable strategies available.

7.2 Proposals for further work

The SIMA/RIFLEX model has a comprehensive rig/vessel connection and pipe-in-pipe model, but more elaborate models could however be included for the rotating control device, blow out preventer and heave compensation system. Integration of auxiliary pipes could also be considered. A closer study of the life expectancy of the sealing element could be carried out in SIMA/RIFLEX including; multidirectional forces, rotating pipe, dynamic current speeds and internal flow effects. Future analysis of vortex induce vibrations using the SIMA/RIFLEX riser model could be conducted in conjecture with VIV software, like VIVANA developed by MARINTEK. There exist plans for integration of VIVANA in SIMA, which would make such an analysis feasible.

This work has focused on a two-dimensional drilling riser in the $xz-$plane. Extending the FEM model to cover three-dimensional space should be investigated further. As emphasised earlier, the extension of the model to account for non-constant geometric stiffness would be advised if more than conceptual evaluation is necessary. This would imply that the state space model would need to be time varying, which would need to be addressed if such a step is taken. A more realistic and frequency dependent damping model for the FEM model could be implemented to improve the physical accuracy of the response. The modal decomposition model used in this thesis is based on five modes. The effect of including more modes should be investigated further.

Prototypes of the control systems proposed should be implemented and simulated in Matlab/SIMULINK and the mathematical framework for the control strategies must be determined and demonstrated to fulfil stability requirements. Once functional, the verification and testing of the systems can be carried out, to further assess the individual efficiency of each strategy to attenuate riser resonance behaviour. This can potentially include exploration of vortex induced suppression control of the riser. Further studies of the riser control should include development of the logic architecture used in the supervisor and guidance systems, improving functional integration of the sub systems. The integration with the onboard control infrastructure, such as the DP system and riser management system is should be explored in more detail. The focus should be on functional integration and operational communication with the system operator.

Bibliography

[1] Bourgoyne, A. T.,Jr. *Rotating control head applications increasing.* Oil and Gas Journal, Vol. 93, pp.72-72, 1995.

[2] Brooks I.H. *A pragmatic approach to VIV on a drilling riser.* Offshore Tech. Conference, TX, ISBN 978-1-61399-080-3, 1987.

[3] Caughey, T.K. *Classical Normal Modes in Damped Linear Systems.* Journal of Applied Mechanics, Vol. 27, Trans. ASME, pp.269-271, 1960.

[4] Chen, C.T. *Linear System Theory and Design (3rd ed.)* Oxford University Press, ISBN 0-19-511777-8, 1999.

[5] Chen, Y., Y.H. Chai, X. Li, J. Zhou, *An extraction of the natural frequencies and mode shapes of marine risers by the method of differential transformation.* Computers & Structures, Vol. 87, pp. 1384-1393, ISSN 0045-7949, 2009.

[6] Dagens Næringsliv. *Staar foran store endringer.* DN.no, 2012.

[7] Dareing, D.W. *Natural frequency of marine drilling risers.* Journal of Petroleum Technology, Vol. 28, 1976.

[8] DNV. Recommended Practice for Riser Integrity Management. Det Norske Veritas, DNV-RP-F206, April, 2008.

[9] DNV. Recommended Practice, DNV-RP-F205 *Global performance analysis of deepwater floating structures.* October, 2010.

[10] Ervik, A.K. *Analysis and monitoring of drilling risers on DP vessels.* Norwegian University of Science and Technology, 2011.

[11] Faltinsen, O.M. *Sea Loads on Ships and Offshore Structures.* Department of Marine Technology, 1999.

[12] Farrant, T. and K. Javed. *Minimising the effect of deepwater currents on drilling riser operations.* Deepwater Drilling Technologies, Aberdeen Marriot, Aberdeen, 2001.

[13] Fredericks, P.D and D. Reitsma. *MPD automation addresses drilling challenges in conventional, unconventional resources.* Drilling Contractor, 2007.

[14] Furnes, G.K., T.Hassanein, K.H. Halse and M. Eriksen. *A filed study of flow induced vibrations on a deep water drilling riser.* Offshore tech. Conference, TX, ISBN 978-1-61399-093-3, 1998.

[15] Godhavn, S. *Control Requirements for High-End Automatic MPD Operations.* SPE/IADC Drilling Conference and Exhibition, 2009.

[16] Hatton, S. *The effects of deepwater current on drilling riser operations.* Latest Developments in Riser Design for Deep and Ultra Deep Water, IIR, Aberdeen, 2001.

[17] ISO, *Petroleum and natural gas industries. Specific requirements for offshore structures part 1: Metocean design and operating considerations.* International Organization for Standardization, ISO 19901-1, 2005.

[18] Hoen, C. and G.Moe, *Model decomposition of measured vortex induced response of drilling risers.* ISOPE, Brest, France, 1999.

[19] Hofmann, E.E. and S.J. Worley. *An investigation of the circulation of the Gulf of Mexico.* Journal of Geophysical Research, 1986.

[20] How, B.V.E., S.S. Ge and Y.S. Choo. *Active control of exible marine risers.* Journal of Sound and Vibration, doi:10.1016, 2008.

[21] Hsieh, L. and K. Scott. *The essentials of dual-gradient drilling: Several variations under development.* Drilling Contractor Magazine, March 27, 2012.

[22] Irani, M.B., V.J. Modi, F. Welf. *Riser dynamics with internal flow and nutation damping.* Proceedings of the 6th International Offshore Mech. and Arctic Engineering Conference, Vol. 3, pp. 119-125, 1987.

[23] Irgens, F. *Statikk (7th ed.),* Tapir Akademisk Forlag, ISBN 82-519-2067-1, 2005.

[24] Jazar, R.N. *Advanced Vibrations.* Springer Science and Business Media New York, 2013.

[25] Jin, Y, C.Liu, H.Liu, R.Xie and S. Cao. *Strength and stability analysis of deep sea drilling risers.* China University of Petroleum, Journal of Petroleum Science, Vol. 4, 2007.

[26] Jonathan, P. and K. Ewans. *Modelling the seasonality of extreme waves in the Gulf of Mexico.* Journal of Offshore Mechanics and Arctic Engineering, Vol. 133, May 2011.

[27] Kaasen, K.E. and H.Lie. *Analysis of Vortex Induced Vibrations of Marine Risers.* Journal of Modelling Identification and Control, Vol. 24, pp. 71-85, 2003.

[28] Langen, I. and R. Sigbjornsson. *Dynamic analysis of structures.* Tapir, ISBN 9-78-825190362-2, 1979.

[29] Larsen, C.M *A short and incomplete introduction to fundamental concepts in VIV.* Department of Marine Technology, 2010.

[30] Larsen C.M, Z. Zhao, H. Lie, *Frequency components of vortex induced vibrations in sheared current.* OMAE, 2012.

[31] Morooka, C.K., H. Y. Kubota, K. Nishimoto, J.R. Ferrari, J. A. Riberiro. *Dynamic behavior of a vertical production riser by a quase 3D calculation.* OMAE, 2003.

[32] Norwegian Petroleum Directorate, *Facts 2013,* March, ISSN 1504-3398, 2013.

[33] Osen, P and M. Høklie. *Marine Riser Management System for Deep-Water Drilling.* Dynamic Positioning Conference, 1999.

[34] RIFLEX, *RIFLEX user manual.* MARINTEK, 2010.

[35] Rustad, A.M. *Modeling and Control of Top Tensioned Risers.* Norwegian University of Science and Technology, 2007.

[36] Sexton, R.M., L.K. Agbezuge. *Random wave and vessel motion effects on drilling riser dynamics.* Offshore Technology Conference, TX, ISBN 971-1-5563-589-3, 1976.

[37] Sparks, C.P. *Fundamentals of Marine Riser Mechanics.* PennWell, 2007.

[38] Sparks, C.P. *Transverse modal vibration of vertical tensioned risers.* Oil and Gas Science Technology, Vol. 57, pp. 71-86, 2002.

[39] Stamnes, O.N., J. Zhou, G.O. Kaasa, O.M. Aamo, *Adaptive observer design for the bottomhole pressure of a managed pressure drilling system,* IEEE, Conference on Decision and Control, 2008.

[40] Stave, R. *Implementation of Dual Gradient Drilling.* SPE Bergen One Day Seminar, 2012.

[41] Stern, R.J., W.R. Dickinson, X. Li and K. McMillen. *Investigation of Oil-Trapping Mechanisms in Deepwater Gulf of Mexico.* SPE Annual Technical Conference and Exhibition, 19-22 September, 2010.

[42] Stern, R.J. and W.R. Dickinson. *The Gulf of Mexico is a Jurassic backarc basin.* Geosphere December, Vol. 6, No. 6, p. 739-754, 1986.

[43] Stensvold, T. *Gir kontroll over vanskelige brønner.* Teknisk Ukeblad, 2012.

[44] Stockton, T.R. *A Real-Time Riser Management System for DP Drilling Vessels.* MTS Dynamic Positioning Conference, 1998.

[45] Sui, P.C and S. Anderle. *Optimization of contact pressure profile for performance improvement of a rotary elastomeric seal operating in abrasive drilling environment.* Wear, Vol. 271, pp. 24662470, 2011.

[46] Sumer, B. M. and J. Fredsøe, *Hydrodynamics Around Cylindrical Structures,* World Scientifc Publishing, 1997.

[47] Sørensen, A.J., B.J. Leira, J. P. Strand and C.M. Larsen. *Optimal set point chasing in dynamic positioning of deep-water drilling and intervention vessels.* Journal of Robust Nonlinear Control. John Wiley & Sons Ltd., Chichester, UK, Vol. 11, pp.1187-1205, 2001.

[48] Sørensen, A.J. *Lecture Notes, Marine Control Systems,* Department of Marine Technology, Report UK-2012-76, 2012.

[49] Toellefsen, B.M. *Managed Pressure Drilling and its application on Mobile Offshore Drilling Units.* Norwegian University of Science and Technology, 2010.

[50] Wilson, E.L. *Three Dimensional Static and Dynamic Analysis of Structures.* University of California at Berkeley, Computers and Structures, 1995.

Appendix A

Simplified calculation

A.1 Simplified calculation of lateral contact force

In this section a quick hand calculation is carried out to check the if force magnitude from the SIMA/RIFLEX analysis is reasonable. First, an assumption of the horizontal offset likely to occur under strong weather conditions is taken to be roughly 0.17m. This is an educated guess based on the diameter of the pipes involved. Secondly the inclination rate $d\theta$ is found using the simple relation $tan(\theta) \approx \theta$ and assuming that $d\theta = (\Phi_1 + \Phi_2)$. Then a simple geometrical approximation is done, based on Figure A.1.

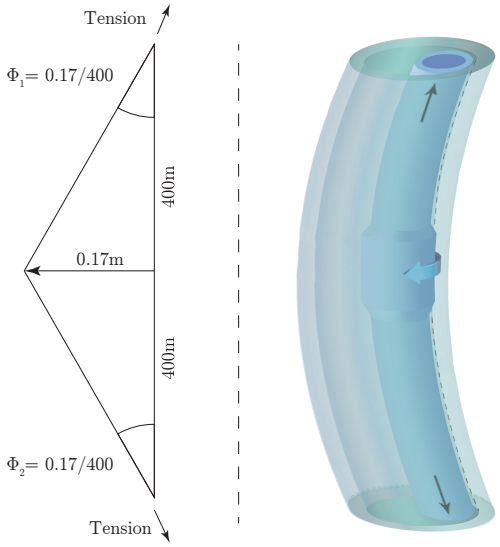

Figure A.1: Ideal representation for calculation of the lateral forces.

Assuming that the bending stiffness will have no influence, one can obtain this simplified formulation for the lateral force:

$$F = Td\theta,$$

usign $d\theta = (\Phi_1 + \Phi_2)$,

$$\begin{aligned} F =& T \cdot (\Phi_1 + \Phi_2) = 4000 \cdot 10^4 \cdot (\frac{0.17}{400} + \frac{0.17}{400}), \\ F =& 3400N \end{aligned}$$

Based on this, the lateral force magnitude should be around 3400N.

Appendix B

RIFLEX results

B.1 Scenario overview

Scenario	Mean force [N]	Maximum force [N]	Horizontal Displacement [m]
1.1	708	1557	1.13
1.2	1914	2010	4.38
1.3	2848	2994	9.67
1.4	3709	3986	16.57
1.5	4389	4595	24.53
2.1.E	5459	5707	11.68
2.2.E	4835	5038	12.40
2.3.E	4260	4431	12.97
2.4.E	3769	3924	13.57
2.5.E	3376	3517	14.0
2.1.N	1997	2141	1.81
2.2.N	1810	1939	1.97
2.3.N	1636	1800	2.08
2.4.N	1487	1665	2.27
2.5.N	1372	1425	2.44
3.1	4388	4420	24.53
3.2	3155	3212	3.32
3.3	3974	4035	10.93
3.4	4744	4786	14.44
3.5	8684	8700	17.67
4.1	4374	4492	24.53
4.2	3157	3431	3.32
4.3	3974	4191	10.93
4.4	4743	4905	14.44
4.5	8686	8800	17.67

Table B.1: Analysis results from SIMA/RIFLEX.

Appendix C

Dynamic analysis results

C.1 Harmonic motion

The upcoming pages contain the harmonic results from the dynamic analysis carried out in Section 6.3.4. Results are displayed in subfigures from (a) to (e), the periods and corresponding figure name can found in Table C.1.

Simualtion	T_{LF}	**Mode**	Figure
7	57.4	2	Figure C.1
8	34.3	3	Figure C.2
9	24.4	4	Figure C.3
10	19.0	5	Figure C.4

Table C.1: Harmonic simulation overview for Simulation 7,8,9 and 10.

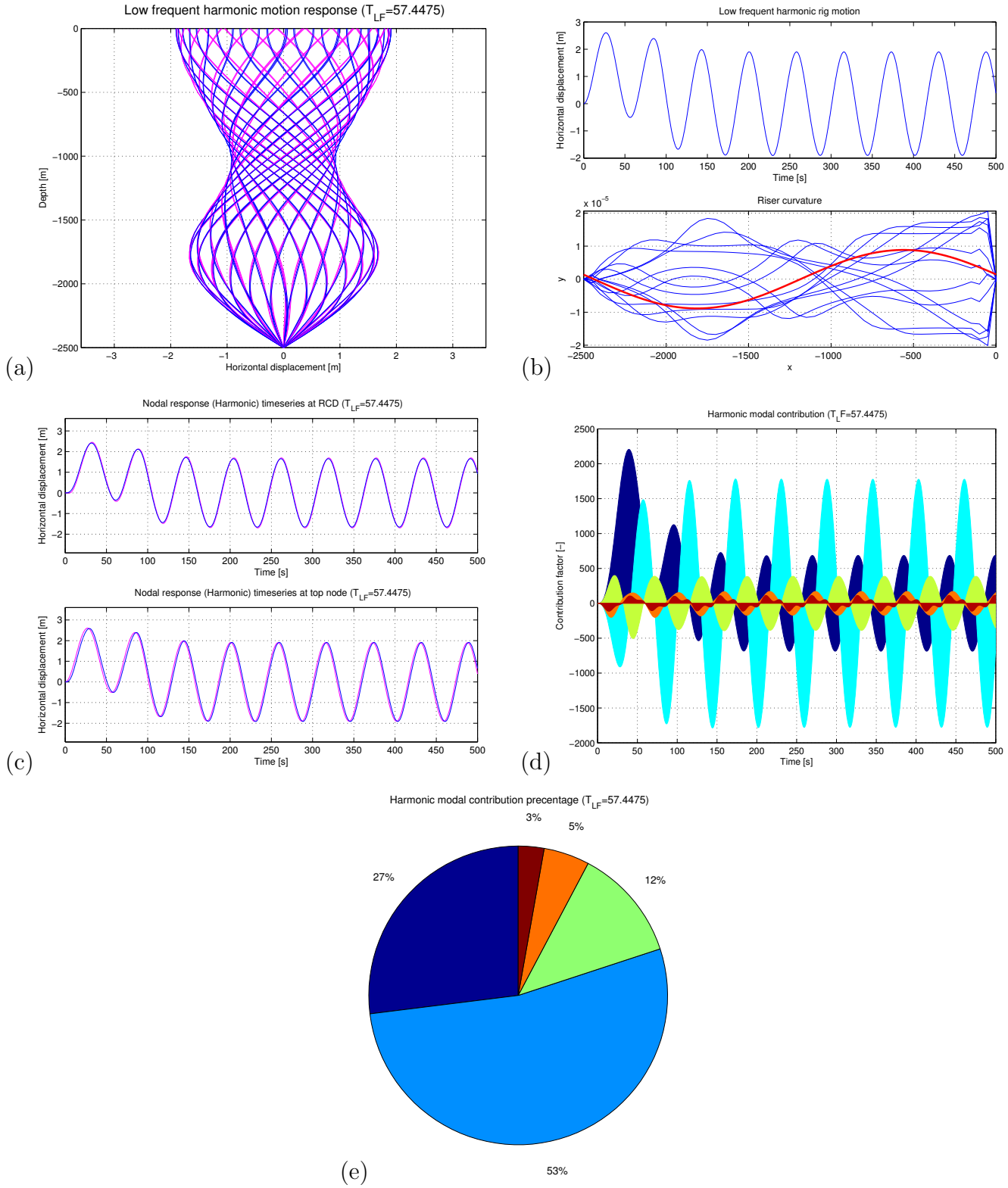

Figure C.1: Harmonic motion results for Simulation 7.

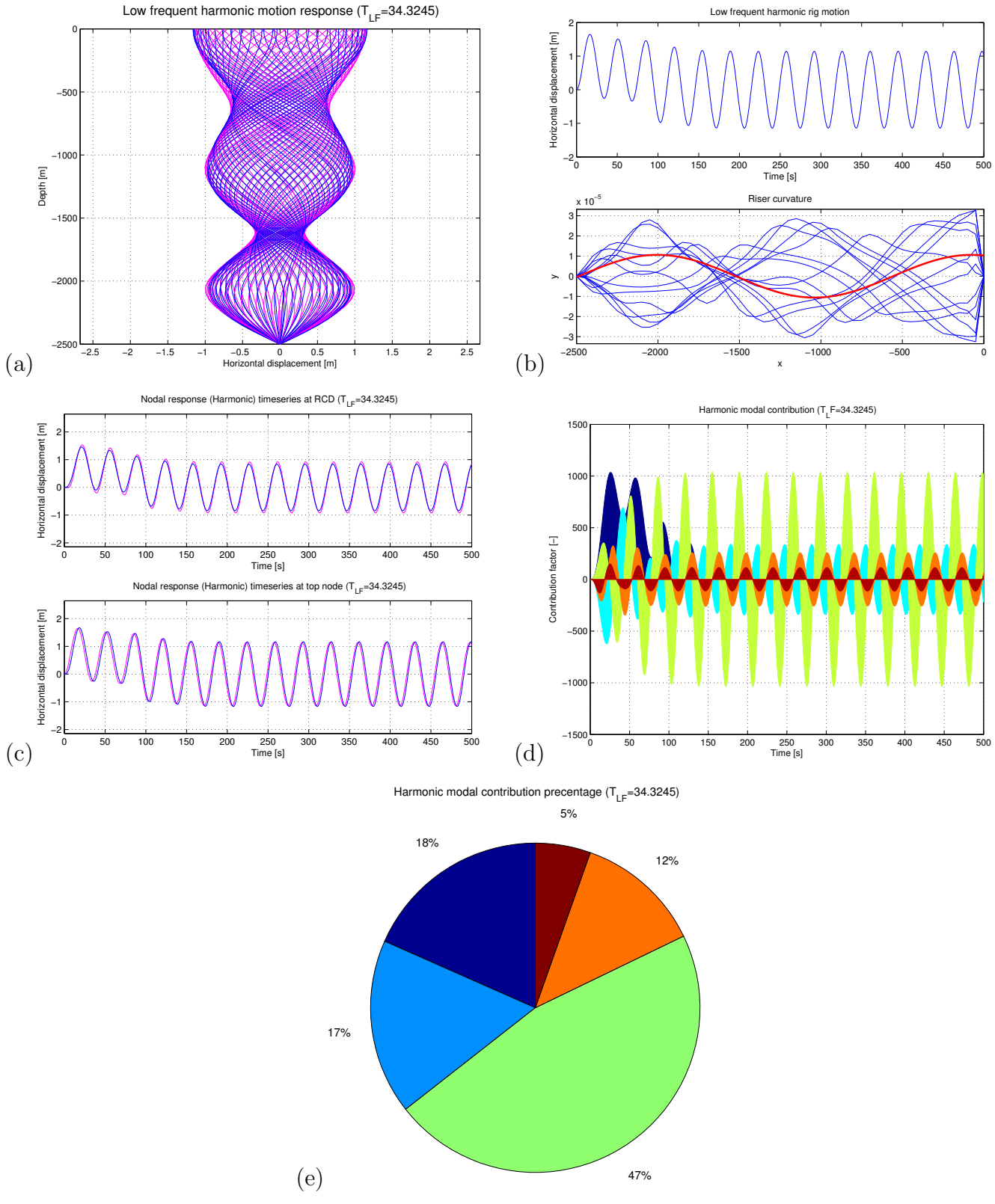

Figure C.2: Harmonic motion results for Simulation 8.

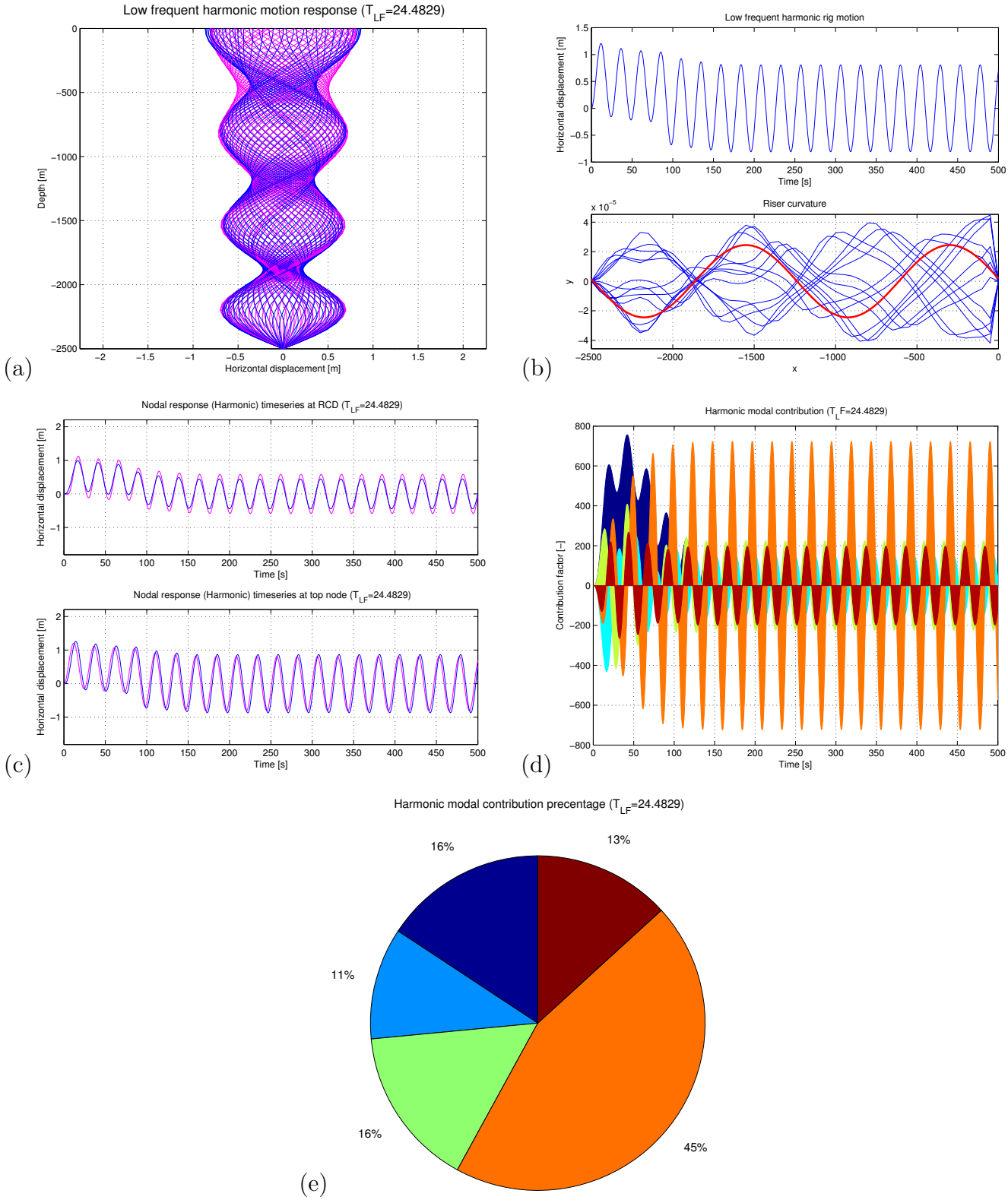

Figure C.3: Harmonic motion results for Simulation 9.

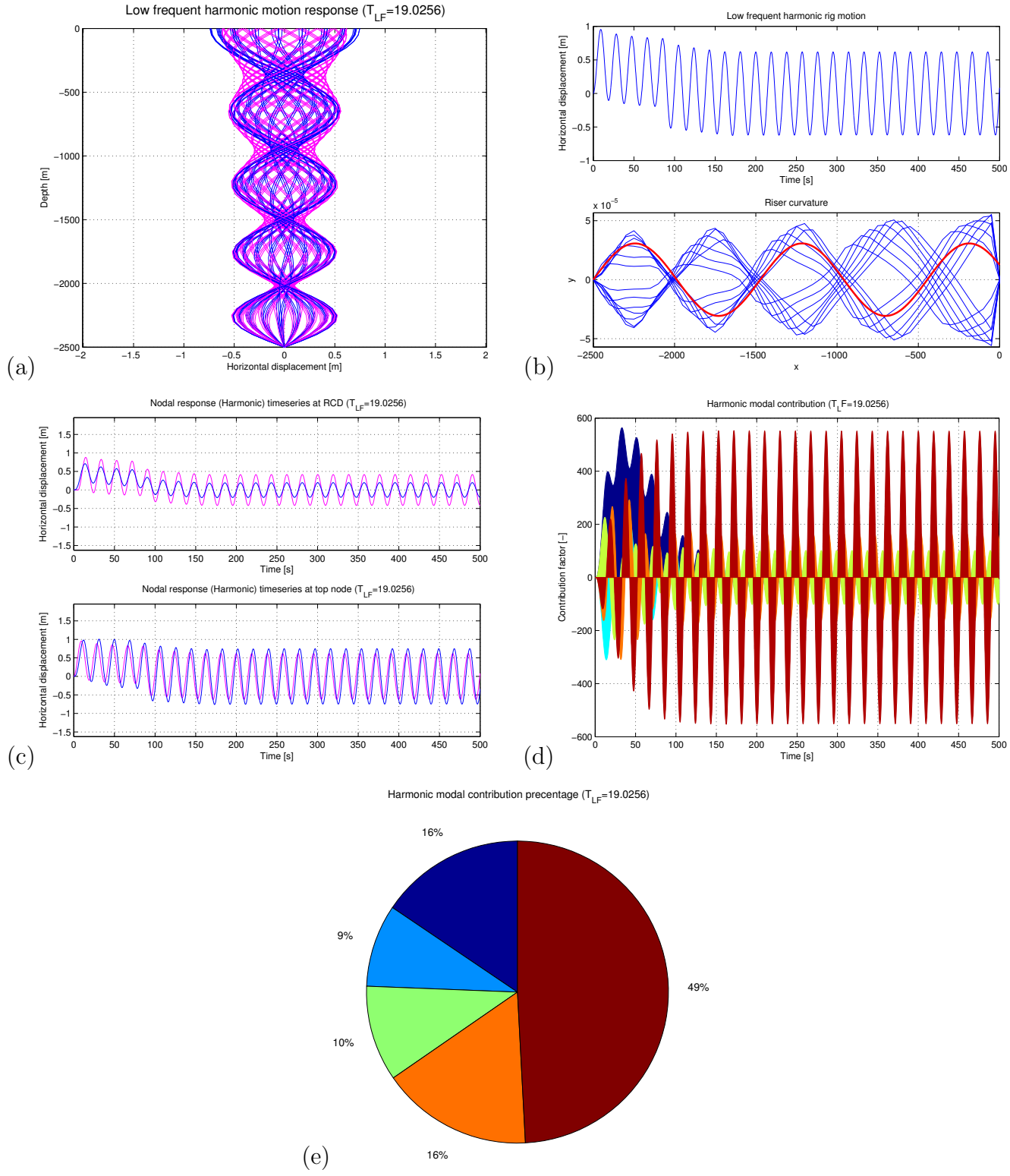

Figure C.4: Harmonic motion results for Simulation 10.

Appendix D

SIMA (RILEX) input files

D.1 Model and simulation files

The SIMA/RIFLEX model is comprehensive and contain a lot of data, the program files are therefore supplied electronically. They are found in the folder "Important_SIMA_RIFLEX_files", containing:

- Model and simulation files for simulation Scenario 1. File is titled "Simulation_1.zip"
- Simulation files for simulation Scenario 2. (extreme) File is titled "Simulation_2.zip"
- Simulation files for simulation Scenario 2. (normal) File is titled "Simulation_3.zip"
- Simulation files for simulation Scenario 3. File is titled "Simulation_4.zip"
- Simulation files for simulation Scenario 4. File is titled "Simulation_5.zip"

Contained in these compressed files is the following files:

- Model input (sima_inpmod.inp)
- Static calculation input (sima_stamod.inp)
- Dynamic calculation input (sima_dynmod.inp)

Additionally the SIMA model and preprocessor file is supplied. They are contained in a ".stask" file titled:

- "SIMA_2500_PIP.stask"

Appendix E

Matlab and SIMULINK files

Included electronically are the Matlab and SIMULINK files. The Matlab version used is: R2012b. All the files for the program can be found in the folder "Matlab_SIMULINK_files". A short description of how to use the riser program and the task description of each function is provided below.

E.1 How to run Matlab code

The main program is the Matlab script "Matlab_riser.m", which calls all the other sub functions and the SIMULINK simulation model. The script also contain the riser model. To run the riser program, open "Matlab_riser.m" and set the relevant model parameters. It is important that the number of elements, simulation time and sample time is set correctly. The preset is $n = 50$, $T_{sim} = 500s$ and sample time= $0.1s$. A uniform current with $0.2m/s$ applied to a 2500m drilling riser is the preset for the environmental loads and the riser. Finally make sure that the Matlab directory is in the same location as the files, before running the program.

E.2 Matlab & SIMULINK function description

- "Matlab_riser.m" - The main program. Runs the code and calls all other sub function.
- "riser_mass.m" - Calculates the riser mass per meter, accounting for buoyancy modules, mud density and riser steel.
- "eff_tension.m" - Calculates the tension distribution, given the mass, top tension and buoyancy module region.
- "fcn_decomp.m" - Using the FEM model, this function used modal decomposition to create the modal riser model.
- "current_profiles.m" - Can be toggled on/off. Plots the current profile used in the SIMULINK simulation.
- "Riser_environment_FEM_MODAL_RIG_MOTION.slx" - The SIMULINK riser model, called from "Matlab_riser.m".
- "Environmental_loads.m" - Used by SIMULINK to calculate the hydrodynamical loads, using the relative riser velocity.